







A new abelisaurid dinosaur from the end Cretaceous of Patagonia and evolutionary rates among the Ceratosauria

Diego Pol^{*a,b} , Mattia Antonio Baiano^{b,c,d,e} , David Černý^f , Fernando E. Novas^{a,b} , Ignacio A. Cerda^{b,e,g,h}  and Michael Pittman^{*c} 

^aMuseo Argentino de Ciencias Naturales Bernardino Rivadavia, Buenos Aires, Argentina; ^bConsejo Nacional de Investigaciones Científicas y Técnicas (CONICET), Buenos Aires, Argentina; ^cSchool of Life Sciences, The Chinese University of Hong Kong, Shatin, Hong Kong SAR, China; ^dÁrea Laboratorio e Investigación, Museo Municipal Ernesto Bachmann, Villa El Chocón, Neuquén, Argentina; ^eUniversidad Nacional de Río Negro (UNRN), General Roca, Río Negro, Argentina; ^fDepartment of the Geophysical Sciences, University of Chicago, Chicago, IL, USA; ^gInstituto de Investigación en Paleobiología y Geología (IIPG), General Roca, Río Negro, Argentina; ^hMuseo Provincial Carlos Ameghino, Cipolletti, Río Negro, Argentina

Received 5 January 2024; Revised 24 April 2024; Accepted 24 April 2024

Abstract

Gondwanan dinosaur faunae during the 20 Myr preceding the Cretaceous–Palaeogene (K/Pg) extinction included several lineages that were absent or poorly represented in Laurasian landmasses. Among these, the South American fossil record contains diverse abelisaurids, arguably the most successful groups of carnivorous dinosaurs from Gondwana in the Cretaceous, reaching their highest diversity towards the end of this period. Here we describe *Koleken inakayali* gen. et sp. n., a new abelisaurid from the La Colonia Formation (Maastrichtian, Upper Cretaceous) of Patagonia. *Koleken inakayali* is known from several skull bones, an almost complete dorsal series, complete sacrum, several caudal vertebrae, pelvic girdle and almost complete hind limbs. The new abelisaurid shows a unique set of features in the skull and several anatomical differences from *Carnotaurus sastrei* (the only other abelisaurid known from the La Colonia Formation). *Koleken inakayali* is retrieved as a brachyrostran abelisaurid, clustered with other South American abelisaurids from the latest Cretaceous (Campanian–Maastrichtian), such as *Aucasaurus*, *Niebla* and *Carnotaurus*. Leveraging our phylogeny estimates, we explore rates of morphological evolution across ceratosaurian lineages, finding them to be particularly high for elaphrosaurine noasaurids and around the base of Abelisauridae, before the Early Cretaceous radiation of the latter clade. The Noasauridae and their sister clade show contrasting patterns of morphological evolution, with noasaurids undergoing an early phase of accelerated evolution of the axial and hind limb skeleton in the Jurassic, and the abelisaurids exhibiting sustained high rates of cranial evolution during the Early Cretaceous. These results provide much needed context for the evolutionary dynamics of ceratosaurian theropods, contributing to broader understanding of macroevolutionary patterns across dinosaurs.

© 2024 The Author(s). *Cladistics* published by John Wiley & Sons Ltd on behalf of Willi Hennig Society.

Introduction

During the Late Cretaceous, Gondwanan dinosaur faunae comprised a number of different lineages. Especially in South America, the first stage of the Late Cretaceous saw the origin of several groups, some of which reached the Cretaceous–Palaeogene (K/Pg)

boundary, while others went extinct during the Cenomanian–Turonian interval (Apesteguía, 2002; Coria and Salgado, 2005; Bellardini et al., 2021; Baiano et al., 2022). The herbivorous South American faunae in the early stages of Late Cretaceous (Cenomanian–Turonian) were dominated by rebbachisaurid (e.g. *Rayososaurus*, *Cathartesaura*, *Limaysaurus*, *Katpensaurus*; Bonaparte, 1996; Salgado et al., 2004; Gallina and Apesteguía, 2005; Ibiricu et al., 2013) and titanosaurian sauropods (e.g. *Argentinosaurus*,

*Corresponding author: E-mail address: dpol@mef.org.ar (D.P.); mpittman@cuhk.edu.hk (M.P.)

Andesaurus, *Epachthosaurus*; Powell, 1990; Calvo and Bonaparte, 1991; Bonaparte and Coria, 1993), whereas ornithischians seem to be uncommon (e.g. *Jakapil*; Riguetti et al., 2022). The theropod fossil record is characterized mostly by the huge carcharodontosaurids (e.g. *Giganotosaurus*, *Mapusaurus*, *Meraxes*; Coria and Salgado, 1995; Coria and Currie, 2006; Canale et al., 2022), spinosaurids (e.g. *Oxalaia*; Kellner et al., 2011), abelisaurids (e.g. *Ekrixinatosaurus*, *Ilokelesia*, *Skorpiovenator*, and *Xenotarsosaurus*; Martínez et al., 1986; Coria and Salgado, 2000; Canale et al., 2009; Ibiricu et al., 2021), possible noasaurids (*Huinculsaurus*; Baiano et al., 2020), and small-sized maniraptoriforms such as *Buitreraptor* and *Alnashetri* (Makovicky et al., 2005, 2012).

After the Cenomanian–Turonian interval, there was faunal turnover with rebbachisaurids disappearing and titanosaurs replacing them in the principal role in ecosystems, and surviving until the end of the Maastrichtian. In fact, multiple titanosaur taxa are known from this age in South America (e.g. *Yamanasaurus*, *Neuquensaurus*, *Uberabatitan*, *Notocolossus*, *Baurutitan*, *Rocasaurus*, *Pelligrinisaurus*, *Saltasaurus*, *Arackar*; Bonaparte and Powell, 1980; Powell, 1992; Salgado, 1996; Salgado and Azpilicueta, 2000; Kellner et al., 2005; Salgado and de Souza Carvalho, 2008; González Riga et al., 2016; Apesteguía et al., 2020; Rubilar-Rogers et al., 2021). Ornithischian dinosaurs were more diverse compared to those from the first stages of the Late Cretaceous, encompassing ankylosaurs (e.g. *Stegouros*, *Antarctopelta*; Salgado and Gasparini, 2006; Soto-Acuña et al., 2021), early ornithopods (e.g. *Mahuidacursor*, *Talenkauen*, *Gasparinisaura*; Coria and Salgado, 1996; Novas et al., 2004; Cruzado-Caballero et al., 2019) and hadrosaurs (e.g. *Huallasaurus*, *Bonapartesaurus*, *Kelumapusaura*; Bonaparte et al., 1984; Cruzado-Caballero and Powell, 2017; Rozadilla et al., 2021). Theropod faunas also experienced a turnover during the Cenomanian–Turonian interval, as carcharodontosaurids and spinosaurids disappeared, and abelisaurids and megaraptorans became the predominant lineages (e.g. Coria and Salgado, 2005; Novas et al., 2005; Novas et al., 2013; Baiano et al., 2022; Baiano and Filippi, 2022). Late Turonian–Maastrichtian non-avian theropods include a high diversity of furileusaurian abelisaurids (e.g. *Elemgasem*, *Carnotaurus*, *Pycnonemosaurus*, *Quilmesaurus*, *Aucasaurus*, *Niebla*, *Guemesia*, *Llukalkan*, *Via-venator*, *Kurupi*; Bonaparte, 1985; Coria, 2001; Coria et al., 2002; Kellner and Campos, 2002; Filippi et al., 2016; Gianechini et al., 2020; Agnolín et al., 2021; Aranciaga Rolando et al., 2021; Iori et al., 2021; Baiano et al., 2022), noasaurids (e.g. *Velocisaurus*, *Noasaurus*, *Vespersaurus*; Bonaparte and Powell, 1980; Bonaparte, 1991; Langer et al., 2019), megaraptorids (e.g. *Aerosteon*, *Tratayenia*, *Maip*,

Megaraptor, *Murusraptor*; Novas, 1998; Sereno et al., 2008; Coria and Currie, 2016; Porfiri et al., 2018; Aranciaga Rolando et al., 2022), alvarezsaurids (e.g. *Patagonykus*, *Bonapartenykus*; Novas, 1996; Agnolín et al., 2012) and dromaeosaurids (e.g. *Unenlagia*, *Neuquenraptor*, *Pamparaptor*, *Austroraptor*, *Ypupiara*; Novas and Puerta, 1997; Calvo et al., 2004; Novas and Pol, 2005; Novas et al., 2009; Porfiri et al., 2011; Brum et al., 2021).

Abelisaurids were the most abundant theropods during the latest Cretaceous, occurring in all Gondwanan regions, except Antarctica and Australia where they remain unknown. They are known principally from South America (e.g. Novas et al., 2013), which has the best fossil record for this group, as well as from India (e.g. Wilson et al., 2003), northern Africa (e.g. Longrich et al., 2023), and Madagascar (e.g. Krause et al., 2007; Farke and Sertich, 2013). Incomplete abelisaurid specimens were also discovered in Europe (e.g. Accarie et al., 1995; Tortosa et al., 2014), adding evidence to the biogeographical link between southern Europe and Gondwana (Ezcurra and Agnolín, 2012). Despite the instability of some taxa (e.g. *Abelisaurus*, *Dahalokely*, *Genusaurus*), recent phylogenetic analyses typically agree that there are two principal clades within Abelisauridae, ‘majungasaurines’ and brachyrostrans (Canale et al., 2009; Tortosa et al., 2014). The clade recognized as ‘Majungasaurinae’ (*sensu* Baiano et al., 2022) mainly includes Indian and Malagasy forms, such as *Majungasaurus*, *Rahiolisaurus* and *Rajasaurus* (Sampson et al., 1998; Wilson et al., 2003; Novas et al., 2010), whereas Brachyrostra includes mainly, if not only, South American abelisaurids, such as *Carnotaurus*, *Aucasaurus*, *Elemgasem* and *Skorpiovenator* (Bonaparte, 1985; Coria et al., 2002; Canale et al., 2009; Baiano et al., 2022, 2023). Within Brachyrostra, an early diverging lineage is retrieved, which includes *Ekrixinatosaurus*, *Ilokelesia* and sometimes *Skorpiovenator*, and a more diverse clade, furileusaurian abelisaurids, that encompasses most South American abelisaurids known from the latest Cretaceous (e.g. Santonian–Maastrichtian; Filippi et al., 2016).

Here we present a new furileusaurian abelisaurid *Koleken inakayali* gen. et sp. n., from the Maastrichtian of Patagonia (La Colonia Formation) in Chubut Province, Argentina. The holotype is composed of a partial skeleton, including cranial, axial and appendicular elements, with a unique set of characters that distinguish it from all known theropods. In particular, *Koleken inakayali* shows several anatomical traits, especially in the skull bones, that differentiate it from *Carnotaurus sastrei*, the only other abelisaurid known from the La Colonia Formation. In order to determine the phylogenetic relationships between this new specimen and other abelisaurids, we carried out multiple phylogenetic analyses using a revised version of a

previously published dataset (Baiano et al., 2022). In addition to discussing the significance of the specimen, we used the newly inferred phylogenies to explore rates of morphological change among ceratosaurs to better understand their evolutionary dynamics.

Institutional Abbreviations: CCG, Chengdu College of Geology, Chengdu, China; MNN, Musée National Boubou Hama, Niamey, Niger; MPCN, Museo Patagónico de Ciencias Naturales, General Roca, Río Negro, Argentina; MPEF, Museo Paleontológico Egidio Feruglio, Trelew, Argentina; MPM, Museo Padre Molina, Río Gallegos, Santa Cruz, Argentina; UNPSJB, Universidad Nacional de Patagonia “San Juan Bosco,” Comodoro Rivadavia, Argentina.

Materials and methods

The specimen MPEF-PV 10826 is composed of cranial, axial and appendicular elements, including almost complete right and fragmented left maxillae, fragments of the left and right nasals, a partially preserved right postorbital, left and right squamosals, fragments of the left and right frontals, posterior portion of the left and right parietals (fused), an incomplete atlas, the fifth to twelfth dorsal vertebrae, a complete sacrum, the first to fifth caudal vertebrae and two middle and one posterior caudal vertebrae, both ilia, partially preserved right and left pubes and ischia, complete right and fragmented left femora, almost complete right tibia and fragments of the left one, complete right fibula, right astragalus, right distal tarsal IV, first to fourth right metatarsals and second and third left metatarsals (incomplete), left and right phalanges I-1, right phalanx II-1, left and right phalanges II-2, right ungual phalanx II-3, left and right phalanges III-1, right phalanx III-3, left ungual phalanx III-4 and right phalanx IV-5.

The specimen MPEF-PV 10826 was found in Maastrichtian layers of the Upper Cretaceous La Colonia Formation of Chubut Province, Argentina (Fig. 1). Chronostratigraphic data for the La Colonia Formation were provided by Clyde et al. (2021), who dated the underlying Puntudo Chico Formation. Through radioisotopic uranium–lead (U–Pb) dating, they found an age of ~71.7 Ma for this unit, suggesting a younger age for the La Colonia Formation. This result is also confirmed by palynological data owing to the presence of *Quadruplanus brossus*, which seems to be restricted to the Maastrichtian in several Gondwanan localities (e.g. Australia, New Zealand, Antarctica) (Clyde et al., 2021). Finally, magnetostratigraphic data confirmed that part of the La Colonia Formation unit was deposited during Chron C29r, an interval of reversed polarity, containing the K/Pg boundary (Clyde et al., 2021).

There are different hypotheses about the depositional environments for this lithostratigraphic unit (Clyde et al., 2021). It has been interpreted as a succession of facies from base to top, from fluvial, estuarine tidal flat or coastal plain to upper tidal flats (Pascual et al., 2000). Cúneo et al. (2013, 2014) suggested an origin related to clastic coastal plains bathed by shallow seas and development of barrier island/lagoon complexes. Gasparini et al. (2015) interpreted the area near where MPEF-PV 10826 was found as being part of a brackish to freshwater estuary.

The palaeontological record of the La Colonia Formation is rich in vertebrates and plants, and known since the 1980s. Indeed, the first vertebrate described from the La Colonia Formation was the iconic abelisaurid theropod *Carnotaurus sastrei* (Bonaparte, 1985). Yet, it was only in the last 20 years that periodic palaeontological expeditions yielded several discoveries that enriched the fauna and flora of this lithostratigraphic unit (Sterli et al., 2021). So far, the fauna of the La

Colonia Formation is composed of fishes (Apesteiguá et al., 2007); turtles (e.g. Sterli and de la Fuente, 2013; Gasparini et al., 2015; Orizobala et al., 2020); snakes (Albino, 2000; Gómez et al., 2019); plesiosaurs (e.g. O’Gorman et al., 2013a, 2013b; Gasparini et al., 2015); ornithischian (Gasparini et al., 2015), sauropod (Gasparini et al., 2015; Pérez-Moreno et al., 2024) and theropod (Bonaparte, 1985; Lawver et al., 2011; Gasparini et al., 2015) dinosaurs; and mammals (e.g. Rougier et al., 2009, 2021; Harper et al., 2019). The palaeontological record of the macro- and microflora includes especially aquatic ferns and angiosperms, but other plants as well as microphytes and dinoflagellate cysts have been reported also (e.g. Cúneo et al., 2014; Gallego et al., 2014; Gandolfo et al., 2014; Guler et al., 2014; Borel et al., 2016; De Benedetti et al., 2018).

Comparative anatomy

Vertebral laminae and fossae were described using the nomenclature proposed by Wilson (1999, 2012) and Wilson et al. (2011). We used terminology proposed by Hendrickx and Mateus (2014a) to describe the anatomical traits of the maxilla.

Bone histological evaluation

A histological analysis was conducted to determine the ontogenetic stage and minimum age of MPEF-PV 10826. A transverse section was obtained from the midshaft of the right tibia. The thin section was prepared at the Paleohistological Laboratory of the Museo Provincial Carlos Ameghino (Cipolletti, Argentina), using standard methods outlined by Cerda et al. (2020), and analysed using a petrographic polarizing microscope (Leica DM750P). The nomenclature and definitions of structures used in this study are derived from Francillon-Vieillot et al. (1990) and de Buffrénil and Quilhac (2021). For minimum age estimation, we counted the number of lines of arrested growth (LAGs). Double LAGs are here considered to represent a single annual growth cycle.

Phylogenetic dataset

The data matrix used for the analyses is composed of 245 characters and 47 taxa (after Carrano and Sampson, 2008; Pol and Rauhut, 2012; Rauhut and Carrano, 2016; Langer et al., 2019; Baiano et al., 2020, 2021, 2022; Ibricic et al., 2021; Cerroni et al., 2022). Characters 29, 30, 34, 116, 118, 141, 159, 170, 174, 185, 191, 204, 207 and 222 were treated as ordered. We deleted the character describing the orientation of ischial peduncle of ilium (ch. 172 in Pol and Rauhut, 2012) from the dataset, as its state 1 (vertically directed) is only present in *Carnotaurus* and *Genusaurus*; however, because the ischial peduncle was completely restored with plaster in the former taxon, the vertical condition could be an autapomorphy of the French abelisaurid (Supporting Information and *Koleken_data_matrix.nex* in Supplementary Data).

Parsimony analyses

In order to determine the phylogenetic relationships between *Koleken inakayali* and other abelisaurids, we carried out parsimony analyses using the program TNT v.1.6 (Goloboff et al., 2008; Goloboff and Morales, 2023). The heuristic search was performed under equally weighted parsimony, using new technology searches of up to 100 independent hits, followed by TBR branch swapping until the tree buffer was filled (at 100 000 trees). We carried out the IterPCR procedure (Pol and Escapa, 2009; see *iterper.out* in Supplementary Data) as implemented by Goloboff and Szumik (2015) in TNT in order to detect unstable taxa. Support values were evaluated in TNT using Bremer support, jackknife and nonparametric bootstrap (BS).

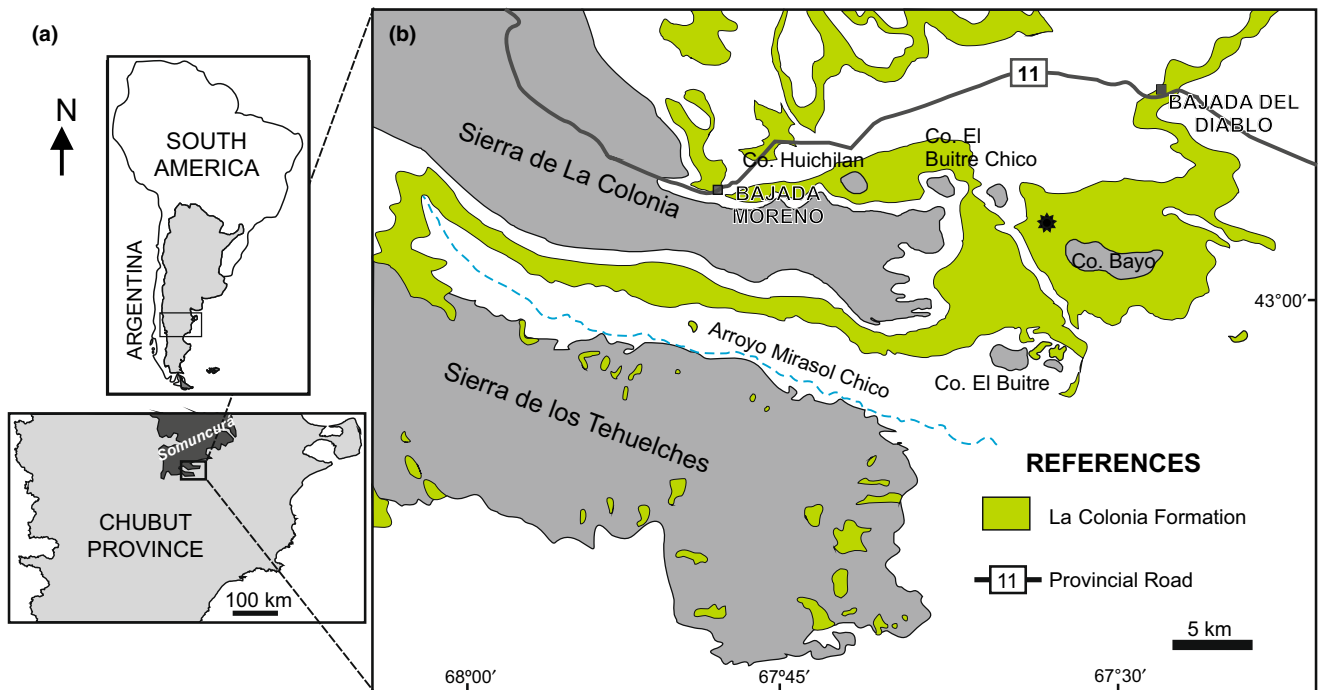


Fig. 1. Locality map showing where the type specimen of *Koleken inakayali* MPEF-PV 10826 was found (black star) within the La Colonia Formation of Chubut Province, Argentina. Figure modified from Sterli et al. (2021).

We also explored the use of the *pcrjak* script (Pol and Goloboff, 2020; see *pcrjak.run* and *pcrjak.out* in [Supplementary Data](#)) to detect taxa that decrease support values as a consequence of their instability in jackknife pseudoreplicates.

Parsimony analysis of evolutionary rates

We implemented a new custom TNT script (see *evolrates.run* in [Supplementary Data](#)) to assess rates of morphological change based on the parsimony optimization of characters. The TNT script uses all trees in memory and takes input from a simple text file named *fadlad* (see [Supplementary Data](#)) that contains the minimum age and maximum age for each terminal taxon (Table S2). Rates are calculated by evaluating optimization on trees that are calibrated against geological time by setting the minimum age of divergence for each node equal to the oldest maximum age of the terminal taxa descended from that node. All branches that are zero-length in temporal duration are assigned the minimum branch duration (1 Myr). Trees were evaluated individually but the output was also produced based on the strict consensus of these topologies. A random selection of 1000 MPTs was selected to calculate the evolutionary rates for this analysis. The parsimony optimization of characters is used to determine the number of changes occurring along each of the branches of the trees. The rate of morphological change was obtained by dividing the number of changes by the temporal duration of each branch. The script produces a text table output that includes the average rate of character change for each branch as well as a graphical output with a colour-coded scheme of rates scaled between the maximum and the minimum rate obtained for the branches of the tree (blue = low rate; red = high rate).

Ambiguous optimizations frequently occur in parsimony analyses, particularly when fossils contain large amounts of missing data and create uncertainty in the placement of character transformations on

the phylogenetic tree (Goloboff, 2022). As a result of the prevalence of these ambiguous optimizations, the script *evolrates.run* conducts iterative evaluations of alternative most parsimonious reconstructions for each character and calculates the average number of reconstructions that optimize a transformation along each branch for each character. For example, a typical instance of ambiguous optimization is the ACCTRAN/DELTRAN scenario (Swofford and Maddison, 1987), which presents just two alternative parsimony reconstructions. In such scenarios, each branch affected by an ambiguous transformation is assigned 0.5 steps for the rate analysis. The script *evolrates.run* also computes two stratigraphic fit measures, as outlined by Pol and Norell (2001; MSM*) and Wills (1999; GER).

Bayesian analyses used to estimate the relaxed clock priors

Using the program RevBayes v.1.2 (Höhna et al., 2016), we further conducted a Bayesian tip-dating analysis under the fossilized birth–death process (Stadler, 2010; Gavryushkina et al., 2014; Heath et al., 2014). Bayesian tip-dating combines both character data and stratigraphic age information to jointly infer tree topology, divergence times and evolutionary rates (Wright et al., 2022). Here, we used partitioned relaxed clocks to estimate the rate of morphological evolution separately for four different anatomical regions (the skull, axial skeleton, forelimb and the hind limb).

In order to derive informative hyperpriors for the relaxed clock model, we followed the protocol of Ronquist et al. (2012a) and performed a series of preparatory analyses, starting with the inference of a topologically unconstrained nonclock tree. To this end, we employed a hierarchical gamma-Dirichlet prior (Rannala et al., 2012; Zhang et al., 2012) on branch lengths, which first specifies a gamma hyperprior on overall tree length and then apports this total length

among individual branches according to a Dirichlet prior. Following the recommendations of Zhang et al. (2012), we set the shape (α) parameter of the gamma distribution to 1, and scaled the rate parameter (β) to obtain an expected prior mean length of 2.5 substitutions per character, close to the value suggested by the parsimony analysis (see Results and discussion). The concentration parameter of the Dirichlet distribution was set to 1 (flat prior), and no distinction was made between internal and terminal branches. The dataset was partitioned first into ordered and unordered characters as described above, and further by the number of observed states to ensure that each partition received an instantaneous rate matrix (Q) of appropriate dimensions. In total, four partitions were specified; for the three partitions comprised of unordered characters, the substitution process was modelled using the Mk model of Lewis (2001). Because all 245 characters included in the matrix were parsimony-informative, we applied the appropriate ascertainment bias correction (Allman et al., 2010); however, we note that this correction cannot be easily extended to multistate characters (Matzke and Irmis, 2018) and its implementation in RevBayes (*coding* = “informative”) should be regarded as experimental (Sebastian Höhna, pers. comm.). A single discrete gamma model with four rate categories (Yang, 1994) was linked across partitions to account for among-character rate variation (ACRV), with the shape parameter drawn from a diffuse Unif(0, 10^6) prior. Two Markov chain Monte Carlo (MCMC) runs were performed, with a burnin period of 80 000 iterations and a sampling period of 240 000 iterations. Under the default settings in RevBayes, each MCMC iteration consists of a number of moves (equal to the sum of move weights), as opposed to other Bayesian phylogenetic software packages such as MrBayes (Ronquist et al., 2012b) or BEAST 2 (Bouckaert et al., 2019), where each move is counted as a separate iteration (Turelli et al., 2018). Accordingly, our sampling period corresponded to 39 768 000 individual moves (= MrBayes or BEAST iterations).

Convergence of scalar parameters was assessed by visual inspection in the program Tracer v.1.7 (Rambaut et al., 2018). To assess topological convergence, we used the package *rwtv* (Warren et al., 2017) for the R statistical computing environment (R Core Team, 2022) to calculate the average standard deviation of split frequencies (ASDSF) and approximate topological effective sample size (Lanfear et al., 2016) based on path distances (Steel and Penny, 1993), ensuring that the former was <1.01 and the latter was >625 (Fabreti and Höhna, 2021). The pooled posterior sample from both runs was summarized using the maximum clade credibility (MCC) tree, which was then compared to the reduced consensus tree from the parsimony analysis using Robinson–Foulds (RF) distances (Robinson and Foulds, 1981) with a polytomy correction following Huerta-Cepas et al. (2016), as implemented in a custom R function employing the *TreeDist* package (Smith, 2020).

In order to obtain informative hyperpriors on the mean and variance of branch rates, we followed Ronquist et al. (2012a) and sampled nonclock as well as strict-clock branch lengths in units of expected substitutions per character (s/c) on a fixed topology corresponding to the MCC tree. In contrast to the scenario explored by Ronquist et al. (2012a), in which these analyses were restricted to the extant portion of the tree, our taxon sample consists exclusively of fossils, and the strict-clock analysis therefore had to account for the different ages of individual tips in order to yield interpretable results. Accordingly, instead of using arbitrary time units, we first estimated branch durations in units of Myr and subsequently multiplied them by the mean posterior clock rate (in units of expected substitutions per character per Ma, s/c/Ma) to recover branch lengths in units of s/c, directly comparable to the nonclock estimates. This approach required conducting a full tip-dating analysis under the fossilized birth–death (FBD) tree prior (Gavryushkina et al., 2014), which only differed from the final analysis by employing a fixed topology and a strict rather than relaxed clock.

The rates of speciation (λ), extinction (μ) and fossil sampling (ψ) were assumed to be constant through time and reparameterized in terms of the net diversification rate $d = \lambda - \mu$, extinction fraction $r = \mu/\lambda$ and fossil recovery probability $s = \psi/(\mu + \psi)$. We placed an Exp(10) prior on d , a Beta(2, 1) prior on r , which favoured high values in accordance with Marshall’s (2017) “third law of paleobiology” (λ tends to equal μ when averaged over time), and a Unif(0, 1) prior on s . The extant sampling fraction (ρ) was fixed to 0. The root age was drawn from an exponential prior with an offset of 197.5 Ma (the minimum plausible age of *Saltriovenator*, which represents the oldest currently known ceratosaur; Dal Sasso et al., 2018) and a rate of 0.06623. This ensured that 95% of the total probability mass was placed on ages younger than 212.6 Ma, the maximum age of the Hayden Quarry (Petrified Forest Member, Chinle Formation) at Ghost Ranch according to Irmis et al. (2011). The Hayden Quarry represents the youngest assemblage containing a diverse theropod fauna but no ceratosaurs, suggesting that the clade’s origin postdates its deposition. Following Barido-Sottani et al. (2019), tip dates were assigned uniform priors spanning their respective uncertainty ranges.

The topology was fixed to that of the 47-tip nonclock MCC tree after stripping it of the four outgroups (*Herrerasaurus*, “*Syntarsus*”, *Dilophosaurus*, *Allosaurus*). Outgroups tend to be sampled less densely than the ingroup, and as such may result in bias in the estimates of d , r and s , which could propagate downstream to the parameters of interest (topology, divergence times, evolutionary rates). The removal of outgroups rendered 33 of the original 245 characters constant; we chose to remove these from the dataset. Another 42 characters were rendered parsimony-uninformative, motivating a change in the ascertainment bias correction (from *coding* = “informative” to *coding* = “variable”). The global clock rate was drawn from a lognormal prior with a mean of 0.005 s/c/Ma and σ set to 1.17481 so as to ensure that the 95% highest prior density interval would span exactly two orders of magnitude. Two runs were performed, each with a burnin period of 90 000 iterations (12 510 000 moves) and a sampling period of 287 500 iterations (39 962 500 moves). The pooled posterior sample was summarized as an MCC tree with mean node heights (Fig. S6).

The fixed-topology nonclock analysis was performed on the full MCC tree (including the outgroups) to ensure that the ingroup topology was rooted, and thus directly comparable to the rooted strict-clock tree. We used the same gamma-Dirichlet branch length prior as in the unconstrained analysis. Two runs were carried out, each with a burnin period of 112 500 iterations (12 498 750 moves) and a sampling period of 360 000 iterations (39 996 000 moves).

After verifying that the effective sample sizes (ESS) of all scalar parameters exceeded 625, we summarized the posteriors yielded by the strict-clock and nonclock fixed-topology analyses using MCC trees. After pruning the outgroups from the nonclock tree, we regressed the nonclock branch lengths against the strict-clock branch durations, obtaining a slope of 7.5×10^{-4} s/c/Ma. This value was used as the mean of a diffuse lognormal hyperprior on the mean clock rate, again parameterized so that the 95% highest prior density interval spanned exactly two orders of magnitude. Next, we multiplied the strict-clock branch durations by the estimated clock rate to convert them into branch lengths, calculated the squared differences between the strict-clock and nonclock branch lengths, and regressed these against the strict-clock branch lengths. Following Ronquist et al. (2012a), we used the slope of the resulting regression line as the median of an exponential hyperprior on the variance-scaling hyperparameter of the relaxed clock model (Fig. S7).

Tip-dating analyses

The main tip-dating analysis was conducted on the same dataset as the strict-clock analysis (43 taxa and 212 characters; i.e. without outgroups or constant characters) and under the same FBD prior.

We chose to run the main analysis without sampled ancestors, which are unlikely to occur in datasets such as ours with a sparse sampling of temporally and geographically disparate taxa (Simões et al., 2020; Černý et al., 2022). However, we also performed a sensitivity analysis that allowed for sampled ancestors (Table S5 and Fig. S9). The analysis employed the white noise clock model of Lepage et al. (2007), as parameterized by Zhang and Wang (2019) and previously implemented in RevBayes by Szöllösi et al. (2022). For the purposes of the clock model, we defined four anatomy-based partitions: the skull (ch. 1–95), axial skeleton (ch. 96–150, 235–245), forelimb (ch. 151–178) and the hind limb (ch. 179–234). All four partitions drew their respective branch rates from gamma distributions with a shared mean c and (potentially distinct) variances $\sigma_1^2, \dots, \sigma_4^2$, and individual branch rates were reparameterized as products of the mean clock rate c and relative rates (multipliers) r_1, \dots, r_{2n-2} . The relative rate r_{ij} for the i -th branch and the j -th partition then follows a new $\Gamma(\alpha, \beta)$ distribution with $\alpha = \beta = \frac{ct_i}{\sigma_i^2}$, where t_i is the duration of the i -th branch in calendar time, so that the mean $\frac{\alpha}{\beta} = 1$ and variance $\frac{\alpha}{\beta^2} = \frac{\sigma_i^2}{ct_i}$.

We explored two different variations on this basic model: one in which the variance scalars were linked across partitions ($\sigma_1^2 = \sigma_2^2 = \sigma_3^2 = \sigma_4^2$) and a single set of branch rates was applied to all four anatomical regions, and another one in which the variance scalars were unlinked (that is, treated as i.i.d. draws from a common hyperprior) and each partition received a separate set of branch rates. In both cases, the clock model hyperparameters were drawn from the following hyperpriors, derived using the approach described above: $c \sim \text{LogNorm}(\mu = -7.88553, \sigma = 1.17481)$; $\sigma_1^2, \sigma_2^2, \sigma_3^2, \sigma_4^2 \sim \text{Exp}(3.24339)$. We compared the linked and unlinked clock models using Bayes factors (BF; Kass and Raftery, 1995), computed from marginal likelihoods estimated using the stepping-stone approach of Xie et al. (2011). This method samples from a series of unnormalized “power posterior” distributions of the form $f_\beta = (\text{prior}) \times (\text{likelihood})^\beta$, constructed along the path between the prior ($\beta = 0$) and the posterior ($\beta = 1$). After a pre-burnin period of 200 000 (linked model; 50 400 000 moves) or 100 000 (unlinked model; 51 600 000 moves) iterations, we initialized 128 β values, taking advantage of a recently introduced RevBayes routine for fully parallelized power posterior sampling (Höhna et al., 2021). Each power posterior was run for 6200 (linked model; 1 562 400 moves) or 3050 (unlinked model; 1 573 800 moves) iterations, with a burnin fraction of 50%. The results were summarized using the 2 log BF statistic (twice the difference of the log marginal likelihoods) and interpreted following the guidelines of Kass and Raftery (1995).

The final tip-dating analysis was conducted under the preferred clock model. Because the clock-model partitions based on anatomy intersected with the substitution-model partitions based on character type and state number, the overall model consisted of 12 distinct phylogenetic continuous-time Markov chains. We performed four MCMC runs, each with a burnin period of 100 000 iterations (51 600 000 moves) and a sampling period of 400 000 iterations (206 400 000 moves). Throughout the analysis, the partition-specific branch rates were logged on each sampled tree. After checking for convergence (scalar ESS > 350, approximate topological ESS > 625, ASDSF < 0.01), we processed the pooled posterior sample using TreeAnnotator v.2.7.6 (Bouckaert et al., 2019) to generate an MCC tree with median node heights and annotations for branch rate summary statistics.

Systematic palaeontology

DINOSAURIA Owen, 1842.
THEROPODA Marsh, 1881.
CERATOSAURIA Marsh, 1884.
ABELISAUURIDAE Bonaparte and Novas, 1985

BRACHYROSTRA Canale et al., 2009
FURILEUSAURIA Filippi et al., 2016

Koleken gen. n.

(LSID urn:lsid:zoobank.org:act:8E384B7B-6731-40DF-B65B-035AD7DB753B)

Type species. Koleken inakayali, by monotypy.

Derivation of name. Adapted from Kóleken, a name in Teushen language spoken by the native population of central Patagonia that means “coming from clay and water”, given the specimen was found in a sedimentary section dominated by claystone representing an estuarine environment.

Diagnosis. As for the type and only species.

Koleken inakayali sp. n.

(LSID urn:lsid:zoobank.org:act:A147BAD3-87F0-403F-A1C0-2067D0B11169)

Derivation of name. Honouring Inakayal, one of the last chiefs of Tehuelches, native people from central Patagonia. He is known for his resistance against Argentina’s Conquest of the Desert military campaign, which resulted in the decimation and displacement of native communities from Patagonia. After his capture and eventual death in 1888, Inakayal’s skeleton was stored at the La Plata Museum Anthropology collection but in 1994 his skeleton was respectfully restituted in its native place and buried by his people near the town of Tecka, in central Patagonia (Chubut Province, Argentina).

Holotype. MPEF-PV 10826. The specimen includes closely associated (but disarticulated) remains of the skull and atlas, as well as the articulated postcranial skeleton composed of the posteriormost eight dorsal vertebrae, a complete sacrum, eight caudal vertebrae, an almost complete pelvis and hind limbs. Select measurements are provided in Table S1.

Locality and horizon. The specimen was found at the Cerro Bayo Norte area, east of the Sierra de La Colonia, centre north of Chubut Province, Argentina (Fig. 1). Precise geographical provenance is deposited at the MPEF collection. The specimen was found close to the base of the stratigraphic section of the La Colonia Formation that crops out in this region (see Gasparini et al., 2015: Fig. 2). The age of the base of this unit has been recently restricted to the early Maastrichtian (Clyde et al., 2021), constraining the age of the new taxon to the Maastrichtian.

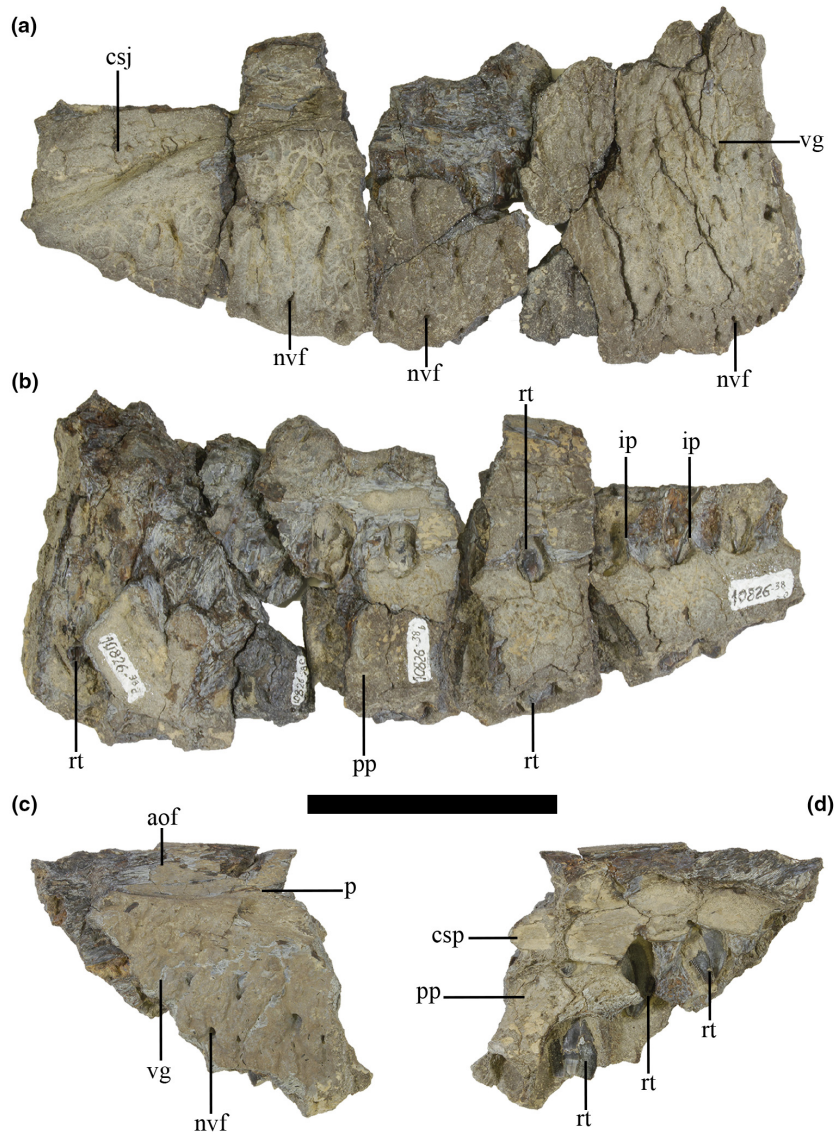


Fig. 2. Right and left maxillae of *Koleken inakayali* MPEF-PV 10826. Right (a, b) and left (c, d) elements in (a, c) lateral and (b, d) medial views. aof, antorbital fossa; csj, contact surface for the jugal; csp, contact surface for the palatine; ip, interdentary plate; nvf, neurovascular foramen; p, protuberance; pp, paradental plate; rt, replacement tooth. Scale bar: 5 cm.

Diagnosis. *Koleken inakayali* is a brachyrostran abelisaurid different from other theropods in having the following set of autapomorphies (marked with a *): (i) medially smooth paradental plates; (ii) dorsal surface of the nasal with a row of foramina orientated obliquely with respect to the longitudinal skull axis; (iii) *anterior ramus of the postorbital lacking the lateral wall reflected by a dorsoventral height less than half of its anteroposterior length, which makes the orbital surface face ventrally instead ventromedially; (iv) *dorsal surface of the postorbital with a shallow depression facing dorsolaterally, located at the junction between anterior and posterior rami, and bounded anteriorly by a well-defined ridge; (v) parietal with a mediolaterally concave dorsal surface and

lacking a knob-like dorsal projection and; (vi) ventral process of the squamosal slender and thorn-like, lacking a kink on the anterior margin; (vii) *dorsal neural spines in lateral view bearing an elevated rim along the anterior, dorsal and posterior margins of the neural spine; (viii) margin of the proximal articular surface of tibia connecting lateral and medial condyles obliquely orientated, facing posterolaterally.

Differential diagnosis. MPEF-PV 10826 shows further anatomical differences from several Cretaceous abelisauroids, especially the sympatric *Carnotaurus sastrei* Bonaparte, 1985. The angle between the premaxilla and maxilla rami of the nasal is lower than in *Carnotaurus*, *Majungasaurus* and *Aucasaurus*. The

proximal tip of the lesser trochanter ends proximally to the ventral margin of the femoral head (ends below in *Carnotaurus*, *Ekrixinosaurus* and *Aucasaurus*), the distal femur lacks a well-defined transverse ridge across the infrapopliteal fossa (present in *Carnotaurus*, *Aucasaurus*, *Eoabelisaurus*, *Xenotarsosaurus* and *Quilmesaurus*), the distal end of metatarsal II has a faintly marked extensor fossa in which the distal margin is poorly developed (more conspicuous in *Eoabelisaurus*, *Aucasaurus*, *Majungasaurus*, *Masiakasaurus* and *Skorpiovenator*), metatarsal III has a poorly developed ventrolateral corner of the proximal articular surface (prominent in *Aucasaurus* or *Elaphrosaurus*), metatarsal IV is slightly shorter than metatarsal II, curving laterally (almost straight or barely curved in noasaurids and in *Aucasaurus* and *Skorpiovenator*).

Description

Skull

General information. The skull is represented by six bones: partially preserved right maxilla, fragmentary left maxilla, fragmentary left and right nasals, partial right postorbital, partial right frontal, partially preserved left and right squamosals, and fragmentary fused parietals (Figs 2–4).

Maxilla. *Koleken* includes the partially preserved right and left maxillae that represent the entire morphology of the maxilla, except for the ascending ramus and the posteriormost tip of the bone (Fig. 2a–d). A bone fragment with an L-shaped cross-section, rugose lateral surface and a broken ventral surface is probably from the left maxilla. The left maxilla is preserved as the ventral rim of the antorbital fossa, which is missing in the right maxilla. The ventral rim of the body is slightly convex, as in all abelisaurids and in most theropods (Fig. 2a,b). The lateral surface is flat and ornamented with a dendritic pattern of vascular grooves orientated dorsoventrally, with some containing ventrally directed foramina (Fig. 2a,c). This pattern of ornamentation is observed in all abelisaurids where the maxilla is known (e.g. *Aucasaurus*, *Carnotaurus*, *Majungasaurus*, *Skorpiovenator* and *Spectrovenator*). However, *Koleken* lacks the curved grooves observed in the middle and posterior portion of the maxillary body present in *Rugops*, *Tralkasaurus* and the indeterminate abelisaurid UNPSJB-PV247. Two small fragments with a similar lateral surface that medially preserve the broken rim of alveoli are probably from the left maxilla. The anterior rim of the right maxilla preserves a notch for the articulation of the maxillary ramus of the nasal, just below the base of the anterior ramus which is distally

broken as in *Carnotaurus*, *Kryptops*, *Majungasaurus*, *Rugops* and the indeterminate abelisaurid UNPSJB-PV247. The left maxilla is represented by a portion of the ventral margin of the antorbital fossa (Fig. 2c). Laterally, this margin is smooth but punctuated with a small pointed protuberance that marks the anterior end of the contact surface for the jugal. The contact surface for the jugal forms a shelf, which is smooth and inclined dorsally at almost 45°, as in *Carnotaurus* and *Skorpiovenator* (Fig. 2a). Medially, the ventral margin of the antorbital fenestra is smooth, rounded and stepped above the ventral surface of the antorbital fossa.

The medial surface of the maxilla is relatively smooth with only a faint texture and a very small number of posteroventrally directed foramina (Fig. 2b,d). By contrast, most abelisaurids have a rugose texture in this region comprising dorsoventrally-orientated ridges, many of which contain ventrally directed foramina (e.g. *Carnotaurus*, *Llukalkan*, *Majungasaurus*, *Rugops*, *Tralkasaurus* and the indeterminate abelisaurid UNPSJB-PV247). The absence of these ridges and of a rugose surface is here considered as an autapomorphic trait of *Koleken* within the context of Abelisauridae. Posteriorly, the contact surface for the palatine is poorly preserved. There are at least 12 maxillary teeth based on preserved alveoli. The distalmost preserved alveolus is partially broken, but given its small size it probably represents the last maxillary tooth position equating to a maxillary tooth count of 12. This number of teeth is shared with *Carnotaurus*, while *Aucasaurus* (14 or 15), *Ekrixinosaurus* (16+), *Majungasaurus* (17) and *Skorpiovenator* (16+) have a higher number of teeth. The maxillary teeth of *Koleken* are replacement teeth and have the general form typical of abelisaurids, showing moderately laterally compressed crowns with curved serrated mesial carina and a tooth apex close to the level of the straight serrated distal carina (Hendrickx and Mateus, 2014b; Hendrickx et al., 2020; Meso et al., 2021). There is a longitudinal row of pits on the medial surface of the maxilla. These pits are associated with tooth development (Carrano and Sampson, 2008), and replacement teeth are visible within them. The parietal and the interdental plates are all fused, forming a medial wall and the separation among the alveolus.

Nasal. The nasals are preserved as fragments of the left and right anterior rami, a large fragment of the posterior portion of the right nasal and a smaller fragment of the posterior portion of the left nasal (Fig. 3a–d). The preserved surface of the anterior rami is ornamented with a dendritic pattern of vascular grooves weakly orientated mediolaterally and seemingly randomly placed small foramina. The anterior ramus of the left nasal has a rugose posterior end covered with large subcircular blind pits and

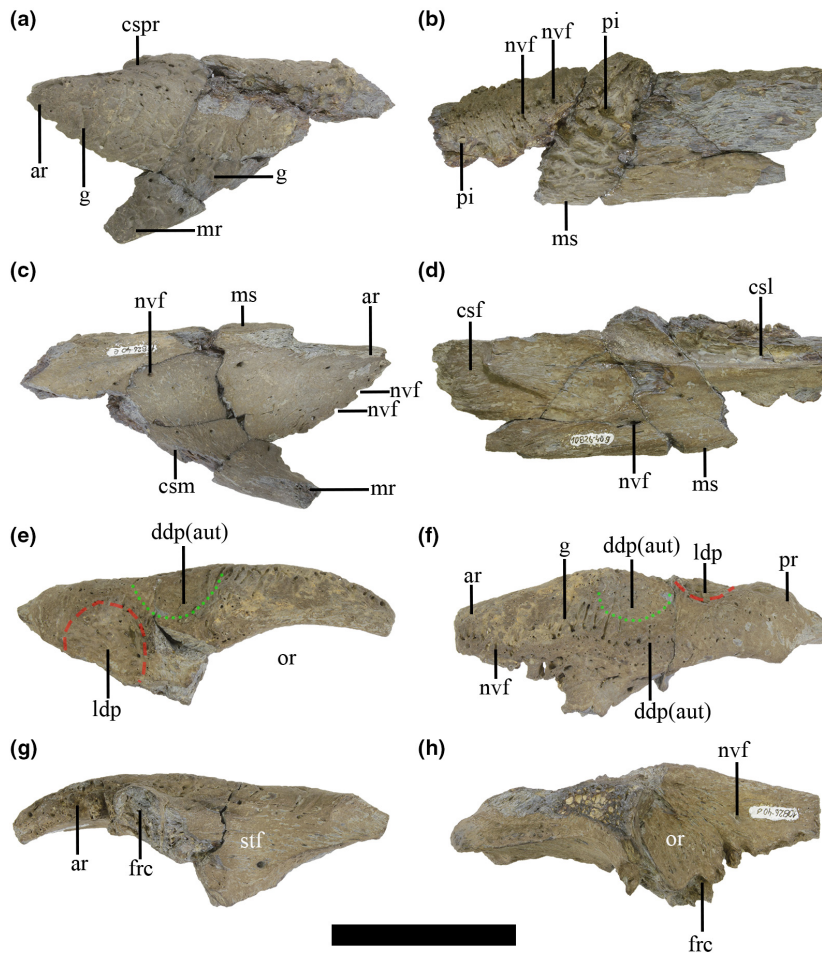


Fig. 3. Right and left nasals and right postorbital of *Koleken inakayali* MPEF-PV 10826. Right (b, d, e–h) and left (a, c) elements in (a, e) lateral, (b, f) dorsal, (c, g) medial and (d, h) ventral views. ar, anterior ramus; aut, autapomorphy; csf, contact surface for the frontal; cs, contact surface for the lacrimal; csm, contact surface for the maxilla; cspr, contact surface for the nasal process of the premaxilla; ddp, dorsal depression of the postorbital; frc, frontal contact; g, groove; ldp, lateral depression of the postorbital; mr, maxillary ramus; ms, medial symphysis; nvf, neurovascular foramen; or, orbit; pi, pit; pr, posterior ramus; stf, supratemporal fenestra. The dashed line indicates the outline of the lateral depression, whereas the dotted line indicates the outline of the dorsolateral depression. Scale bar: 5 cm.

multiple small foramina (which is likely to represent the anterior end of the lateral crest of the nasal; see below) (Fig. 3a). The maxillary ramus is isosceles triangle-shaped, but the distal tip of the maxillary ramus is broken. The contact surface for the nasal process of the premaxilla is finger-shaped, and ends dorsally at the level of the acute, triangular bifurcation of the premaxillary and maxillary rami. The contact surface for nasal process of the premaxilla is delimited medially by a raised projection, implying that the posterior tip of this process was not in contact with its counterpart. This condition differs from *Carnotaurus*, where both nasal processes of the premaxillae are in contact along the whole length. Furthermore, in *Koleken*, the angle between the premaxilla and maxilla rami is $\sim 80^\circ$, whereas in *Carnotaurus* this value is higher, being $\sim 105^\circ$, and between $\sim 85^\circ$ and $\sim 90^\circ$ in *Aucasaurus* and *Majungasaurus*.

The larger posterior fragment of the right nasal preserves an unfused suture with the left nasal (Fig. 3b). Among abelisaurids there is a complex pattern of nasal fusion: the smaller, subadult *Majungasaurus* specimen FMNH PR 2100 has fused nasals, whereas the larger, adult *Aucasaurus* (Baiano and Cerda, 2023) and *Carnotaurus* have separate nasals. The preserved posterior region of the nasal is flat overall, as in *Rugops*, *Spectrovenator* and *Skorpiovenator*, but conversely *Koleken* lacks the high lateral ridge present in these abelisaurids (Fig. 3b). Furthermore, this condition in *Koleken* contrasts with the dorsally convex nasal surface of *Carnotaurus*, *Aucasaurus*, *Llukalkan* and *Majungasaurus*. The preserved posterior portion of the right nasal has three distinct textures on its dorsal surface (Fig. 3b). The posteriormost region is flat and smooth, close to its contact with the frontal. The central portion is flat and has large subcircular pits. Some of these pits

contain tiny foramina. The anterior region is more complex and has a convex lateral half and a slightly concave medial half. The convex dorsal portion of the lateral surface bears numerous neurovascular foramina that extend into mediolaterally orientated vascular grooves (Fig. 3b). This convex and rugose area would have formed a low ridge close to the lateral margin of the nasal, which is likely to have extended anteriorly up to the level of the posterior end of the external nares (based on the rugose elevated surface with neurovascular foramina preserved on the anterior ramus of the left nasal). The neurovascular foramina of this region are roughly aligned along an anteromedial-posterolateral axis. This condition differs from the anteroposterior orientation of other abelisaurids (e.g. *Carnotaurus*, *Spectrovenator*, *Rugops* and *Skorpiovenator*). In *Skorpiovenator*, *Spectrovenator* and *Rugops* there are fewer foramina but these seem to be relatively larger (Cerroni et al., 2020). In *Koleken*, the surface medial to the row of dorsal foramina is concave. This region of the nasal markedly differs from the condition of *Carnotaurus*, which has an evenly convex dorsal surface of the nasal and foramina that lack associated grooves projecting medially.

The ventrolateral surface of the left anterior ramus and posterior portion of the right nasal are smooth and have seemingly randomly positioned small foramina that are mainly directed anteriorly (Fig. 3c). However, some aligned foramina are located along the dorsal rim of the naris, whereas abundant small randomly positioned foramina are situated near the contact surface for the nasal process of the premaxilla (Fig. 3c). The contact surface for the right nasal is smooth. The posterior portion of the ventral surface of the right nasal preserves the contact with the frontal, which is shallow, W-shaped, and has faint anteroposteriorly orientated ridges (Fig. 3d). The anterolateral end of the posterior portion of the nasal has an anteroposteriorly long and mediolaterally narrow concave facet for the articulation of the anterior process of the lacrimal, which is medially bounded by a conspicuous ridge. The facet slightly curves laterally and broadens towards its posterior end and has a generally smooth surface with a few scattered foramina and associated shallow anteroposteriorly aligned grooves (Fig. 3d).

Postorbital. The right postorbital is partially complete, missing the ventral ramus, the medial articular surface for the frontal, and the distalmost portion of the posterior ramus (Fig. 3e–h; see also *Postorbital.ply* in [Supplementary Data](#)). In lateral view, there is a distinct fossa at the anterodorsal corner of the infratemporal fenestra, where the anterior, posterior and ventral rami meet (Fig. 3e). A similar fossa is present in *Eoabelisaurus*, *Abelisaurus*, *Arcovenator* and *Spectrovenator*, but is absent in *Carnotaurus* and *Aucasaurus*. This fossa has a

rugose texture that contrasts with the smooth surface of the fossa of *Eoabelisaurus* and *Arcovenator*. In *Abelisaurus* this fossa also has a rugose surface but less developed than in *Koleken*. Also in lateral view, the dorsal rim of the anterior ramus (= dorsal brow of the orbit) is convex.

In dorsal view (Fig. 3f), the anterior ramus of the postorbital is lateromedially broad at its origin and gradually narrows along a straight lateral edge and rugose medial edge to a small and flat articular surface for the lacrimal. In *Carnotaurus*, the anterior ramus of the postorbital is also lateromedially broad at its origin, but only gradually narrows along a straight medial margin with the lateral margin remaining parallel to the postorbital body axis. Although the distal tip of the ramus is missing, it is possible to infer from the flat and relatively small size of this broken cross-section that the bone probably tapered to a flat and relatively small articulation as well. The dorsal surface is generally rugose but lacks the dorsal bulge present in *Arcovenator*, *Ekrixinatosaurus*, *Ilokelesia* and *Skorpiovenator*. It also bears scattered small foramina mostly directed dorsoventrally and with the central portion containing the highest concentration of foramina including the largest ones. On the dorsolateral surface, there are mediolaterally orientated grooves that contain foramina, concentrated at the base of the anterior ramus. A shallow dorsolaterally facing depression is present on the dorsal surface of the postorbital, at the junction between anterior and posterior rami. This depression is bounded anteriorly by a conspicuous ridge that delimits this depression from the anterior ramus. This rounded depression is likely to be an autapomorphic trait of *Koleken* as it is not present in other abelisaurids. In *Carnotaurus* there is a faint depression on the same area of the postorbital, but this faint depression is exposed laterally rather than dorsally given that *Carnotaurus* has a narrow dorsal surface of the postorbital rather than the mediolaterally broad dorsal surface present in the postorbital of *Koleken*.

In medial view, the margin of the anterior ramus is heavily rugose with a sponge-like structure and has a marked interdigitated sutural surface for the frontal (Fig. 3g). By contrast, this margin is not rugose in *Carnotaurus*. The anterior portion of the supratemporal fossa is only slightly inclined and has a smoother surface than the remaining bone.

The posterior ramus is shorter than the anterior ramus, as in other derived abelisaurids (e.g. *Carnotaurus* and *Majungasaurus*), and has a smooth medial surface that defines the anterolateral margin of the supratemporal fenestra. The anterodorsal corner of the supratemporal fenestra has an anteroposteriorly orientated canal for a neurovascular foramen. The posterior end of the ramus preserves the two sutural contacts for the squamosal; one of them is much

longer and located on the ventral surface and the other facet is shorter, rectangular and located on the dorsomedial surface of the posterior ramus. The dorsal margin of the dorsomedial facet for the squamosal forms a sharp well-defined ridge that in lateral view is only slightly raised, whereas in *Carnotaurus* it is more dorsally elevated. The ventral facet for the squamosal has a well-defined anteroventrally curving dorsal edge that is flush with the medial surface of the supratemporal fenestra. The lateral surface of the ventral facet is inset laterally and has a set of small foramina. The ventral facet forms a well-defined groove in ventral view.

The ventral surface of the anterior ramus of the postorbital of *Koleken* forms the posterodorsal corner of the orbit (Fig. 3h). This surface is smooth and bears fine vascular grooves and foramina. Furthermore, the anterior ramus is dorsoventrally low and lacks a lateral wall, consequently resulting in a ventrally faced ventral surface. Conversely, the postorbital of other

abelisaurids, especially *Carnotaurus*, have a dorsoventrally deeper lateral surface, contributing to the lateral and dorsal borders of the orbit. This makes this portion of the orbital surface face ventromedially instead. Indeed, in *Koleken* the ratio between the dorsoventral height and the anteroposterior length of the anterior ramus is the lowest among abelisaurids (0.44), with some abelisaurids such as *Ilokelesia*, *Aucasaurus* and *Arcovenator* having ratios between 0.52 and 0.65, and other abelisaurids such as *Carnotaurus* and *Skorpiovenator* having ratios >0.80 . The peculiar morphology of the anterior ramus of the postorbital in *Koleken* is here considered as autapomorphic for this species.

Squamosal. The left and right bones are partially preserved. Their anterior end is partially broken and they do not preserve the dorsomedial ramus (= parietal process) (Fig. 4a–c). Without the dorsomedial ramus, it is not possible to determine whether the ramus was

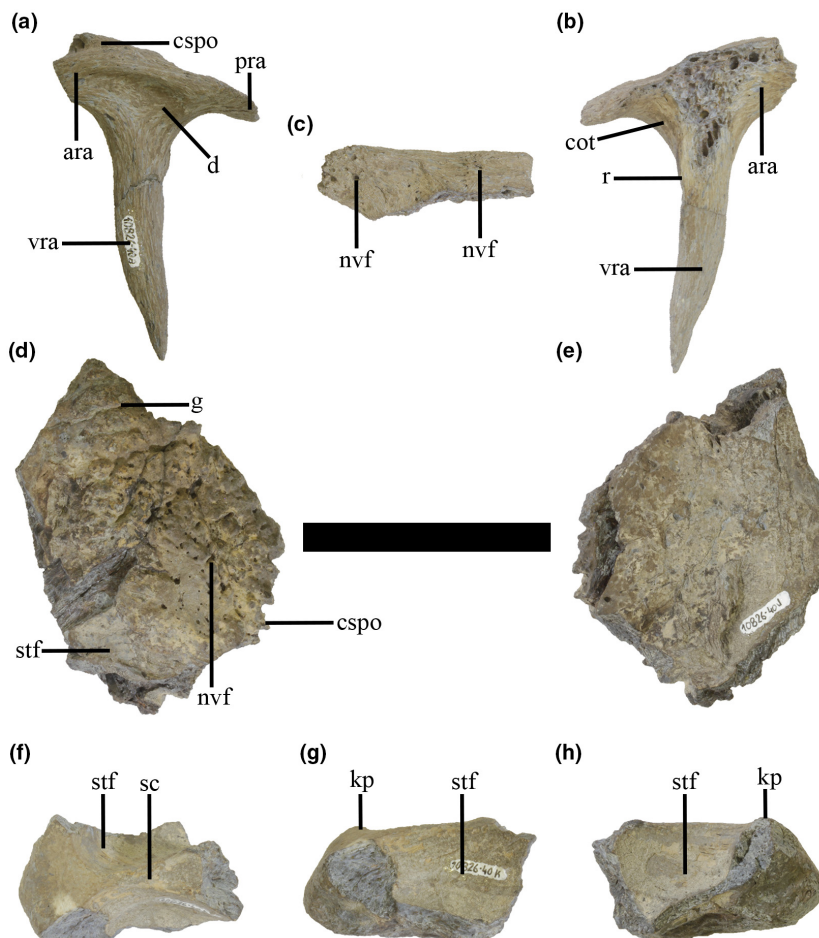


Fig. 4. Left squamosal, right frontal and fused parietals of *Koleken inakayali* MPEF-PV 10826. In (a, g, h) lateral, (b) medial, (c, d, f) dorsal and (e) ventral views. ara, anterior ramus; cot, cotyle; cspo, contact surface for the postorbital; d, depression; g, groove; kp, knob-like projection; nvf, neurovascular foramen; pra, posterior ramus; r, ridge; sc, sagittal crest; stf, supratemporal fenestra; vra, ventral ramus. Scale bar: 5 cm.

dorsoventrally high as in *Carnotaurus* and *Majungasaurus* or dorsoventrally low as in *Spectrovenator*. The entire surface of the squamosal is smooth.

In lateral view, the squamosal is T-shaped (Fig. 4a). The anterior ramus (= postorbital ramus) is dorsoventrally low, lateromedially broad, with a missing tip and a flat and rounded dorsal surface (Fig. 4b,c). Medially, a dorsal ridge separates the frontal process from the infratemporal fenestra. The dorsal surface shows a portion of the articular surface for the postorbital anteriorly, whereas it is flat posteriorly with a poorly developed rugosity but pierced by several foramina (Fig. 4c). The posterior ramus (= quadrate ramus) is finger-shaped and posteroventrally directed. On the ventral surface of the posterior ramus there is a deep cotyle for the quadrate condyle. Furthermore, the posterior ramus doesn't wrap the head of the quadrate as in other abelisaurids. The ventral ramus (= quadratojugal ramus) is slender as in the indeterminate abelisaurid MAU-Pv-LI-582, but is different from the more robust ventral ramus of other abelisaurids (e.g. *Abelisaurus*, *Majungasaurus* and *Llukalkan*). The ventral ramus is slightly curved in the posteroventral direction and tapers to a fine point. Compared to *Carnotaurus*, the ventral ramus of *Koleken* differs in being more slender and thorn-like, although the distal tip of the ramus is missing in *Carnotaurus*. The anterior margin of the ventral process is kinked in *Majungasaurus*, *Viavenator*, *Abelisaurus*, *Llukalkan* and *Skorpiovenator*, whereas this is smooth in *Koleken*, *Carnotaurus* and *Spectrovenator*. The combination of slender, thorn-like shape (subcircular cross-section and tapering to a fine point) and kinked anterior margin in the ventral process of *Koleken* is possibly an autapomorphic feature. The lateral surface bears a triangular-shaped fossa bounded by well-developed dorsal and anterior rims. A similar lateral fossa is present in *Skorpiovenator*, *Abelisaurus*, *Llukalkan*, *Viavenator* and *Carnotaurus* (as noted by Cerroni et al., 2021), but is absent in *Spectrovenator*, *Majungasaurus* and *Arcovenator*. The anterior margin of the ventral ramus is slightly sinusoidal as in *Spectrovenator*, *Carnotaurus* and the indeterminate abelisaurid MAU-Pv-LI-582, lacking the anterior swelling observed in *Abelisaurus* and *Majungasaurus*, and possibly in *Llukalkan* and *Skorpiovenator*. The posterior margin of the ventral end of the squamosal is straight (Fig. 4b).

Frontal. The main body of the right frontal and a fragment of the left one are preserved (Fig. 4d,e). The dorsal surface is slightly domed and has a rugose texture, as in *Guemesia*, *Aucasaurus* and *Abelisaurus* (Fig. 4d). The dorsal surface corresponds to the position of the lateral frontal horns in *Carnotaurus*, so *Koleken* lacks this feature. In *Koleken*, this surface has small foramina and neurovascular canals as in *Aucasaurus* and *Abelisaurus*,

but lacks the two large foramina present in *Guemesia*. The postorbital and prefrontal contacts for the frontal have a sponge-like texture and meet at an angle of around 130° (Fig. 4d). The right frontal preserves part of the lacrimal suture which is dorsoventrally deep and weakly interdigitates. The bone surface is smoother close to the lacrimal suture. The supratemporal fossa is partially preserved but clearly defined, showing a smooth surface and facing posterodorsally. Ventrally, the bone surface is not preserved in either the left or right frontals (Fig. 4e).

Parietal. The parietals are represented by its fused medioposterior portion (Fig. 4f–h). The sagittal crest forms a posterior transversely narrow bar, widening anteriorly to form a triangular plate. In this way, the sagittal crest narrows the anteromedial corner of the supratemporal fenestra in dorsal view (Fig. 4f). A sagittal crest is a condition shared by most abelisaurids (e.g. *Carnotaurus*, *Majungasaurus*, *Skorpiovenator* and *Viavenator*), and incipiently developed in *Ceratosaurus*. The triangular plate has a mediolaterally orientated shallowly concave dorsal surface. The medial surface of the preserved supratemporal fenestra portion is steep and smooth (Fig. 4g,h). The dorsal elevation of the nuchal wedge and parietal alae is low in *Koleken* and *Aucasaurus* when compared to most abelisaurids (e.g. *Carnotaurus*, *Majungasaurus* and *Viavenator*). This relates to the horizontal orientation of the sagittal crest which is posterodorsally-anteroventrally-orientated in other abelisaurids. The parietal lacks the pronounced knob-like dorsal projection of some derived abelisaurids such as *Arcovenator*, *Carnotaurus*, *Majungasaurus* and *Viavenator*, but instead has a mediolaterally orientated shallowly concave dorsal margin (Fig. 4g,h) as in *Aucasaurus*. The posteriorly projecting supraoccipital tuberosity seems to be significantly reduced, unlike other abelisaurids including *Carnotaurus* and *Viavenator*. The combination of these two parietal characteristics in *Koleken* is possibly an automorphic feature.

Axial skeleton

Atlas. Only the intercentrum of the atlas is preserved, which is anteriorly bowed and has a subtrapezoidal outline (Fig. 5a–f), different from a more circular outline present in *Aucasaurus* (Baiano et al., 2023), whilst in *Carnotaurus* the intercentrum is transversely rectangular. Anteriorly, the articular surface is strongly concave (Fig. 5a). The posterior articular surface is convex, and holds a dorsally concave transversal step that separates it from the articular facet of the first cervical rib (Fig. 5b). In both lateral views, the surfaces have rectangular outlines and the contact surfaces for the first cervical ribs are ventrally directed (Fig. 5c,d). The dorsal rim is concave, due to the articular projections for the neuroapophyses (Fig. 5e). The ventral rim is slightly

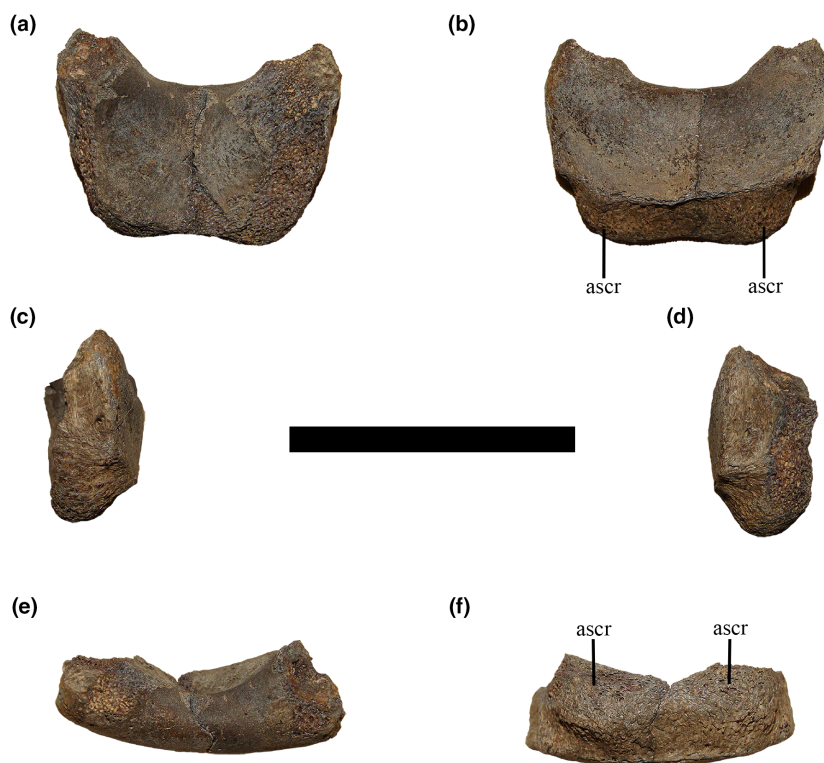


Fig. 5. Atlas of *Koleken inakayali* MPEF-PV 10826. In (a) anterior, (b) posterior, (c) left lateral, (d) right lateral, (e) dorsal and (f) ventral views. ascr, articular surface for the cervical rib. Scale bar: 5 cm.

W-shaped due to the articular facets for the first cervical ribs (Fig. 5f).

Dorsal vertebrae. The preserved dorsal series includes eight vertebrae and was found articulated with the pelvis, caudal vertebrae and hind limb. Some vertebrae are laterally crushed, showing breakage and missing portions on the left side of the neural arches. Based on comparisons with *Carnotaurus*, we consider the anteriormost preserved vertebra to be the fifth to the twelfth dorsal vertebra (Figs 6 and 7). This is because the parapophyses are completely positioned on the neural arch, whereas they are only positioned between the centrum and neural arch on the fourth dorsal vertebra as in all known abelisaurids. They have a conspicuous prezygapophyseal ventral process that constitute the lateral walls of the hypantrum, which is shared with other abelisaurids (e.g. *Huinculsaurus*, *Masiakasaurus*, *Majungasaurus*, *Skorpiovenator* and *Viavenator*), but different from the absent or reduced process in *Aucasaurus* and other theropods (e.g. *Allosaurus*, *Ceratosaurus*, *Eoabelisaurus* and *Elaphrosaurus*) (Baiano et al., 2020, 2023). All right transverse processes have experienced medial rotational deformation causing them to be almost vertical rather than laterally directed. The preserved dorsals increase in size posteriorly along the series. All preserved dorsal vertebrae have

amphycoelic spool-shaped centra with an unfused neurocentral suture indicating subadult ontogenetic development (Brochu, 1996). All dorsal vertebrae in *Koleken* have laterally projecting parapophyses that almost reach the lateral extent of the transverse processes, as in all abelisaurids where they are known (e.g. *Elaphrosaurus*, *Huinculsaurus*, *Masiakasaurus*, *Majungasaurus*, *Carnotaurus* and *Viavenator*; Bonaparte et al., 1990; O'Connor, 2007; Carrano et al., 2011; Rauhut and Carrano, 2016; Filippi et al., 2018; Baiano et al., 2020, 2023). Consequently, the well laterally projected parapophyses of *Koleken* are connected with transverse processes through a robust paradiapophyseal lamina, a feature also shared by several abelisaurids (e.g. O'Connor, 2007; Carrano and Sampson, 2008; Carrano et al., 2011; Farke and Sertich, 2013; Rauhut and Carrano, 2016; Baiano et al., 2020, 2023; Cerroni et al., 2020). The parapophyses, when well-preserved, show a teardrop-shaped outline pointing dorsally. The transverse processes have a D-shaped outline in dorsal view as in most abelisaurids, and have an anteroposterior length approximately two-thirds the length of the neural arch. The spinopostzygapophyseal laminae (spol) are robust especially at their bases, except in the last dorsal vertebra where they almost disappear. The postzygapophyseal centrodiapophyseal fossa (pocdf) is transversely wide, occupying the whole posterior

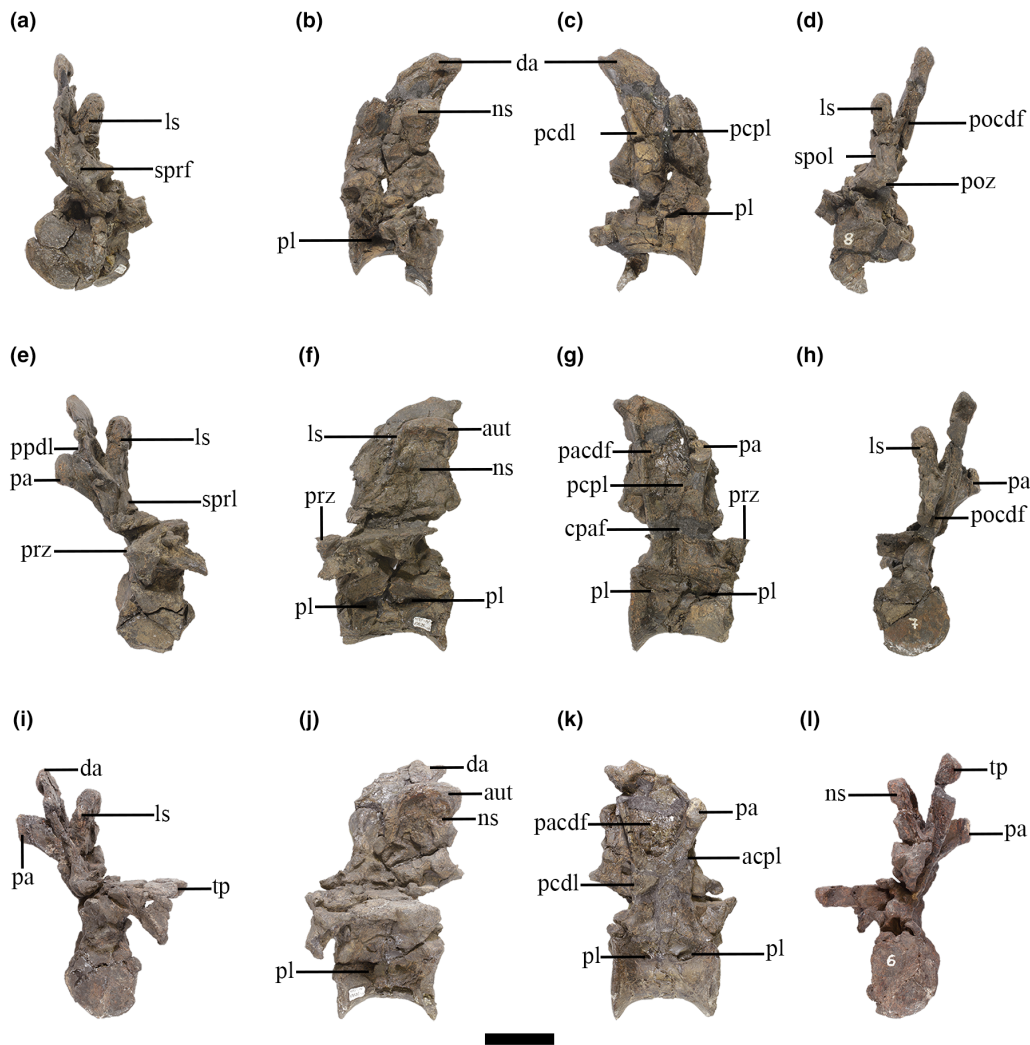


Fig. 6. Fifth, sixth and seventh dorsal vertebrae of *Koleken inakayali* MPEF-PV 10826. In (a, e, i) anterior, (b, c, f, g, j, k) lateral and (d, h, l) posterior views. acpl, anterior centroparapophyseal lamina; aut, autapomorphy; cpaf, centroparapophyseal fossa; da, diapophysis; ls, ligamental scar; ns, neural spine; pa, parapophysis; pacdf, parapophyseal centriadiapophyseal fossa; pcdl, posterior centriadiapophyseal lamina; pcpl, posterior centroparapophyseal lamina; pl, pleurocoel; pocdf, postzygapophyseal centriadiapophyseal fossa; ppdl, paradiapophyseal lamina; prz, prezygapophysis; spol, spinopostzygapophyseal lamina; sprf, spinoprezygapophyseal fossa; sprl, spinoprezygapophyseal lamina; tp, transverse process. Scale bar: 5 cm.

surface of the transverse process. Where preserved, the postzygapophyses and hyposphene project over the posterior articular surface of the centrum, except for the seventh dorsal vertebra where the ventral portion of the hyposphene does not seem to surpass the posterior edge of the centrum. Moreover, the hyposphene, preserved from the ninth dorsal vertebra, is dorsoventrally tall and slightly wider ventrally, forming a stout structure below the postzygapophyses. The neural spine occupies at least half of the length of the neural arch and is dorsally directed. Furthermore, all preserved dorsal neural spines have lateral surfaces with a sunken central portion, forming a flange around its entire outline and considered an autapomorphic trait of *Koleken*.

The fifth dorsal vertebra is strongly damaged and deformed, preserving the centrum, right transverse

process and neural spine (Fig. 6a–d). The anterior articular surface of the centrum is transversely oval (Fig. 6a). On the lateral sides, there are deep depressions with at least an anterior pleurocoel that has an anteriorly pointing teardrop-shaped contour (Fig. 6b, c). The presence of a posterior pleurocoel cannot be evaluated as a consequence of the deformation of the preserved vertebra. The posterior articular surface is partially worn, but it seems to be wider than high and deeper than the anterior articular surface (Fig. 6d). The ventral surface has a faint anteroposteriorly directed ridge, but in *Carnotaurus* this ridge is more pronounced.

The anterior portion of the neural arch is poorly preserved. It is missing the prezygapophyses and spinoprezygapophyseal laminae (sprl), but a triangular

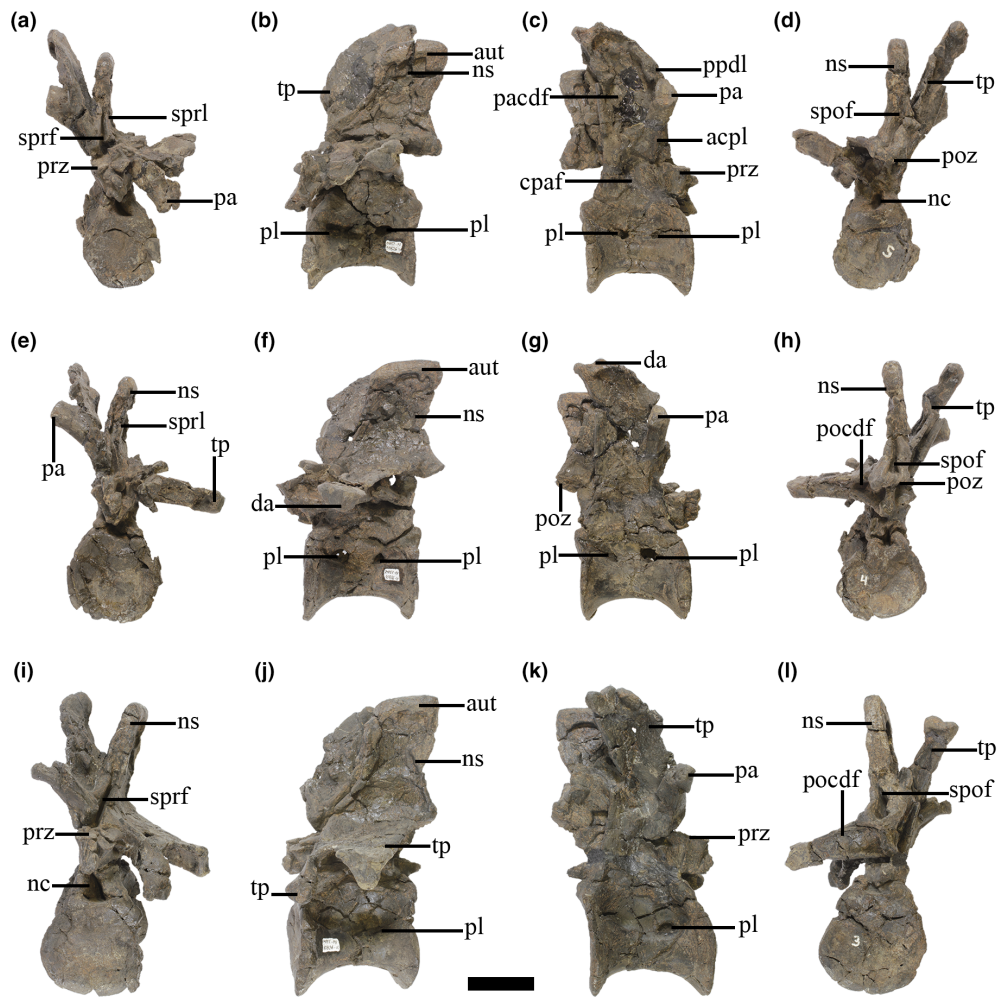


Fig. 7. Eighth, ninth and tenth dorsal vertebrae of *Koleken inakayali* MPEF-PV 10826. In (a, e, I) anterior, (b, c, f, g, j, k) lateral and (d, h, I) posterior views. acpl, anterior centroparapophyseal lamina; aut, autapomorphy; cpaf, centroparapophyseal fossa; da, diapophysis; nc, neural canal; ns, neural spine; pa, parapophysis; pacdf, parapophyseal centrodiapophyseal fossa; pl, pleurocoel; pocdf, postzygapophyseal centrodiapophyseal fossa; poz, postzygapophysis; ppdl, paradiapophyseal lamina; prz, prezygapophysis; spof, spinopostzygapophyseal fossa; sprf, spinoprezygapophyseal fossa; sprl, spinoprezygapophyseal lamina; tp, transverse process. Scale bar: 5 cm.

and deep spinoprezygapophyseal fossa (sprf) is discernible (Fig. 6a), a feature present in most subsequent dorsal vertebrae. The prezygapophyseal centrodiapophyseal fossa (prcdf) is partially deformed; but it probably had a triangular outline originally and was bounded at least by the prezygodiapophyseal lamina (prdl) and the anterior centroparapophyseal lamina (acpl). The anterior surface of the neural spine has a reduced rugose ligamental scar that is separated from the neural spine by two V-shaped grooves. In lateral view (Fig. 6b,c), the parapophyses are missing on both sides, although the acpl is conspicuous, and remaining robust in all subsequent neural arches. Moreover, an anterior portion of the posterior centroparapophyseal lamina (pcpl) was preserved, which ventrally intersects an accessory lamina, producing a small fossa. The posterior centrodiapophyseal lamina (pcdl)

is stout and is developed along the ventrolateral rim of the transverse process ending ventral to the diapophysis. The diapophyseal articular facet has an anteroposteriorly concave surface and a teardrop-shaped outline pointing anteriorly. The neural spine is low with a rectangular outline, being taller than long. In this view, the dorsal rim of the neural spine is markedly convex, more than in the other preserved dorsal vertebrae. In posterior view (Fig. 6d), the surface of the neural arch is also poorly preserved and few structures are recognizable. The postzygapophyses are slightly ventrolaterally directed. The pocdf is visible on the right transverse process, but is highly crushed. However, it seems anteroposteriorly deep. Despite the spinopostzygapophyseal fossa (spof) being transversely deformed, it is shallow and bounded laterally by low spinopostzygapophyseal laminae (spol). The posterior

surface of the neural spine also has a ligamental scar separated dorsally from the dorsal edge by a pair of V-shaped grooves. In posterior view, the dorsal rim of the neural spine is transversely convex. In dorsal view, the right transverse process has a slight posterior inclination and the lateral rim of the diapophysis is concave.

The sixth dorsal vertebra is preserved as a centrum and neural arch that has experienced deformation and breakage (Fig. 6e–h). The anterior articular surface of the centrum has an eroded rim but seems to have a circular outline (Fig. 6e). The lateral surfaces have a deep depression with two oval pleurocoels positioned anteriorly and posteriorly (Fig. 6f,g). The anterior pleurocoel is bigger than the posterior one and both are anteroposteriorly longer than dorsoventrally tall. The posterior articular surface has a subcircular outline (Fig. 6h). The anteroposteriorly ventral ridge is more prominent anteriorly, disappearing on the posterior portion of the ventral surface.

In anterior view (Fig. 6e), the prezygapophyses have dorsolaterally inclined articular facets, as in almost all dorsal vertebrae in *Koleken*, and seem to be separated by a reduced hypantrum, although this morphology could be affected by lateral crushing. Similarly laterally inclined prezygapophyseal articular surfaces are found in the last few dorsals of abelisaurids such as *Majungasaurus*, *Viavenator* and *Carnotaurus*, but no-saurids and several non-ceratosaur theropods have dorsomedially inclined prezygapophyses instead (e.g. Filippi et al., 2016; Baiano et al., 2020, 2023). The sprl are stout and anteroventrally-posterodorsally inclined, as in the remaining dorsal vertebrae, and frame a high sprf, but unfortunately, we cannot estimate the depth of the latter owing to lateral deformation. The prcdf is deformed, and it is delimited by the prezygodiapophyseal lamina and the paradiapophyseal lamina (ppdl) in addition to the acpl and the prdl. On the dorsal portion of the neural spine, the ligamental scar is more conspicuous than in the preceding vertebra. In lateral view (Fig. 6f,g), the conspicuous prezygapophyseal ventral process overhangs the anterior margin of the centrum. The parapophysis is concave and shows an oval surface that is directed dorsoventrally. The ppdl is reduced and connects the parapophysis to the ventral surface of the transverse process, whereas the pcpl is long and stout. The pcpl separates the ventral surface of the transverse process into two fossae, the parapophyseal centrodiaepophyseal fossa (pacdf) dorsally and the centroparapophyseal fossa (cpaf) ventrally. Despite the deformation and weathering in the dorsal vertebrae in *Koleken*, the posterior centrodiaepophyseal lamina is well-developed, a trait shared with other abelisauroids (e.g. O'Connor, 2007; Farke and Sertich, 2013; Filippi et al., 2018; Baiano et al., 2020, 2023). The neural spine is anteroposterior long,

occupying more than two-thirds of the anteroposterior length of the neural arch as in *Aucasaurus*, *Carnotaurus* and *Skorpiovenator* (Baiano et al., 2023). This feature is present up to at least the eleventh dorsal vertebra. The dorsal rim of the neural spine is less convex than the previous vertebra. In posterior view (Fig. 6h), the postzygapophyses and hyposphene are not preserved. The spof is transversely compressed. The posterior ligamental scar is reduced when compared with the previous vertebra. The pocdf is delimited by a prominent pdcl and a thin postzygodiaepophyseal lamina (podl). In dorsal view, the prezygapophyses show a rectangular outline along their long axis. The D-shaped transverse process is slightly anteroposteriorly longer than the previous vertebra, occupying almost the whole length of the neural arch.

The centrum of the seventh dorsal vertebra has articular surfaces with a subcircular outline (Fig. 6i–l), although they are partially weathered. On the right lateral surface (Fig. 6j,k), the longitudinal depressions still holds two oval pleurocoels with the long axis of the anterior one being anterodorsally directed and the long axis of the posterior one being posterodorsally directed, as in the previous vertebra. In the corresponding vertebrae of *Carnotaurus*, there is only one anterior pleurocoel present on the left lateral surface whilst the right one is not preserved. The ventral surface of the centrum loses the ridge of previous vertebrae, remaining smooth in all subsequent dorsal vertebrae.

The anterior portion of the neural arch is poorly preserved so it is not possible to comment on most of its structures. The only discernible features are a right parapophysis that is more robust and more laterally projected than in the previous dorsal vertebrae, and a conspicuous ligamental scar on the dorsal end of the neural spine located between the two sprl (Fig. 6i). Laterally (Fig. 6j,k), there are two foramina situated in the pacdf and near the pdcl. These foramina are separated from each other by a robust lamina and are distinct in size. In *Carnotaurus*, the relevant portion of the neural arch is only preserved on the left lateral side, but the exact portion of the pacdf is still preserved under matrix. Thus, the presence or absence of foramina there cannot be evaluated. In MPEF-PV 1082 the posterior portion of the neural arch is badly damaged (Fig. 6l). The pocdf is deformed; however, it is possible to see that there are two pneumatic foramina separated by a lamina. Dorsally, a step among the dorsal end of the neural spine and the anterior ligamental scar is visible.

The morphology of the centrum of the eighth dorsal vertebra is similar to the seventh one (Fig. 7a–d). On the lateral surfaces of the centrum (Fig. 7b,c), the depressions remain deep and hold a small anterior and posterior pleurocoel, although these are now subequal

in size. In the corresponding vertebra of *Carnotaurus*, the right lateral surface has only an anterior pleurocoel with a small associated dorsoposteriorly positioned foramina. On the left lateral surface of the same vertebra of *Carnotaurus* there is a posterior pleurocoel, whereas we cannot confirm the presence of an anterior pleurocoel as this area is obscured by matrix.

In anterior view (Fig. 7a), the prezygapophyses maintain a dorsolateral inclination and they do not surpass the anterior rim of the centrum. A crushed hypantrum is present. The sprf is anteroposteriorly deep and framed by anteroventrally-posterodorsally inclined sprl. These laminae end dorsally on the poorly developed ligamental scar, which remain reduced in subsequent dorsal vertebrae. The ppdl is mediolaterally wider than in the previous vertebrae. The pacdf is wide and deep (Fig. 7b,c), whereas the cpaf is reduced in size with respect to the former fossa. In posterior view (Fig. 7d), the postzygapophyseal facets are slightly ventrolaterally directed. In *Carnotaurus*, these structures are ventromedially directed in comparable dorsal vertebra. The hyposphene is not preserved. The spof has a more triangular outline. In dorsal view, we cannot evaluate the morphology of the prezygapophyseal facets as they are incomplete. The transverse processes are here slightly wider transversally than the previous vertebra.

The ninth dorsal vertebra has the anterior and posterior articular surfaces wider than tall (Fig. 7e–h). The lateral depressions still hold two pleurocoels (Fig. 7f,g), which in this vertebra returns to being larger for the anterior one compared to the posterior one. In the corresponding vertebra of *Carnotaurus*, the right lateral surface also has two teardrop-shaped pleurocoels, a larger, anterior dorsoanteriorly-ventroposteriorly aligned one and a smaller, posterior ventroanteriorly-dorsoposteriorly aligned one. Both contain matrix that obscures their depth. On the left lateral surface of the same vertebra of *Carnotaurus*, there appears to be only an anterior horizontally-aligned pleurocoel but its form is obscured by encrustation on the fossil.

Laterally (Fig. 7f,g), the parapophyses are dorsally displaced when compared with previous vertebrae, causing a reduction of the ppdl. The diapophysis is bean-shaped. The neural spine has an almost flat dorsal rim. In posterior view (Fig. 7h), the hyposphene is broken, but it may have been prominent originally owing to the presence of a ridge among the postzygapophyses and because of a robust preserved fragment of hyposphene articulated with the hypantrum in the next vertebra. The postzygapophyses are longer than wide and are slightly medioventrally directed.

The tenth dorsal centrum differs from the previous vertebra in having only an anterior pleurocoel on the lateral surface, which has an anteroposteriorly oval outline (Fig. 7i–l). In anterior view (Fig. 7i), the prezygapophyses delimit a deep hypantrum that is hidden

by a fragment of the previous hyposphene. In lateral view (Fig. 7j,k), we cannot determine whether the ventral process of the prezygapophyses surpassed the anterior margin of the centrum as a consequence of its state of deformation. The pocdf is shallow and delimited dorsally by a thin podl and ventrally by a stout pcld (Fig. 7l). The spol now are dorsoventrally low.

The eleventh dorsal vertebra is tightly articulated with the following vertebra and partially bordered between the iliac blades, with the transverse processes directly articulating with the medial surface of the blades. The vertebra is the biggest of the preserved dorsal vertebrae, and has oval anterior and posterior articular surfaces. Although the lateral surfaces conserve lateral depressions, they lack pleurocoels or any other sign of external pneumaticity. By contrast, the equivalent vertebra in *Carnotaurus* has an anterior, horizontally-orientated pleurocoel on each lateral surface, with the right one larger than the left one.

The prezygapophyses are partially broken. The transverse processes and the associated laminae and fossae are almost entirely hidden by the iliac blades but seem to have similar morphology to the previous vertebra. A unique difference with the preceding vertebra is the position of its parapophyses which are now included in the prdl, at the same elevation as the diapophyses. We cannot elucidate the posterior morphology of the neural spine as a result of its articulation with the next vertebra.

The morphology of the twelfth vertebra is difficult to fully appraise as it is completely bordered by the iliac blades and articulates with the previous dorsal vertebra and the sacrum. The centrum is completely apneumatic, although lateral depressions are still present; this same condition is present in the equivalent vertebra of *Carnotaurus*. The anterior articular surface remains transversely wider than tall, but the posterior one is now dorsoventrally elliptical. The neural spine is anteroposteriorly reduced when compared to the previous vertebrae. The sprl and spol have become vestigial, whilst the sprf and spof have now completely disappeared.

Sacrum. The sacrum is composed of six vertebrae, which were preserved in articulation and fused to the medial surface of the blades of both ilia (Fig. 8a–c). Thus, some anatomical traits were not discernible. Six sacral vertebrae are also observed in most other ceratosaurs such as *Ceratopsaurus*, *Eoabelisaurus*, *Aucasaurus* and *Carnotaurus*, but not in *Majungasaurus* (e.g. O'Connor, 2007; Baiano et al., 2023) and most non-maniraptoran neotheropods which have a sacrum composed of five vertebrae (Carrano and Sampson, 2008; Carrano et al., 2012). All sacral centra are apneumatic. The first centrum has a slightly concave and dorsoventrally elliptical, anterior articular surface. The centra of the second to fifth sacral vertebra are fused

together and are transversely thinner than the first and last sacral centra as in several ceratosaurs. All of the sacral neural spines except the first one are fused to each other forming a midline wall (Fig. 8b), as in several abelisaurids (e.g. Baiano et al., 2023). The dorsal end of the neural spine table is only slightly transversely expanded, whereas it is transversely wider in *Aucasaurus* and *Carnotaurus* (Baiano et al., 2023). The transverse processes of the third and fourth sacrals are anteroposteriorly longer than the other sacral transverse processes.

The transverse constriction of the mid-sacral centra observed in *Koleken* (Fig. 8c) is a condition shared with several ceratosaurs, but unlike *Masiakasaurus* in which the centra have a similar width (Carrano et al., 2002, 2011). The anteroposteriorly arched sacrum of *Koleken* is a widespread trait within

Abelisauroida (e.g. *Masiakasaurus*, *Eoabelisaurus*, *Majungasaurus*, *Aucasaurus* and *Carnotaurus*; Baiano et al., 2023) and found in *Elaphrosaurus*, unlike the more horizontal sacrum of *Rajasaurus* (Wilson et al., 2003), basal ceratosaurs (e.g. *Ceratopsaurus*), and most non-avian tetanurans (e.g. *Allosaurus*, *Sinraptor*; Madsen, 1976; Currie and Zhao, 1993). Despite the dorsal edge of the sacral neural spines of *Koleken* being not as transversely wide as in *Aucasaurus* and *Carnotaurus*, they are thickened as in several abelisauroids (e.g. *Elaphrosaurus*, *Eoabelisaurus* and *Majungasaurus*; O'Connor, 2007; Pol and Rauhut, 2012; Rauhut and Carrano, 2016; Baiano et al., 2023).

Caudal vertebrae. The preserved anterior caudals include the first five vertebrae, being the first and the second elements still articulated with the sacrum (Figs 8

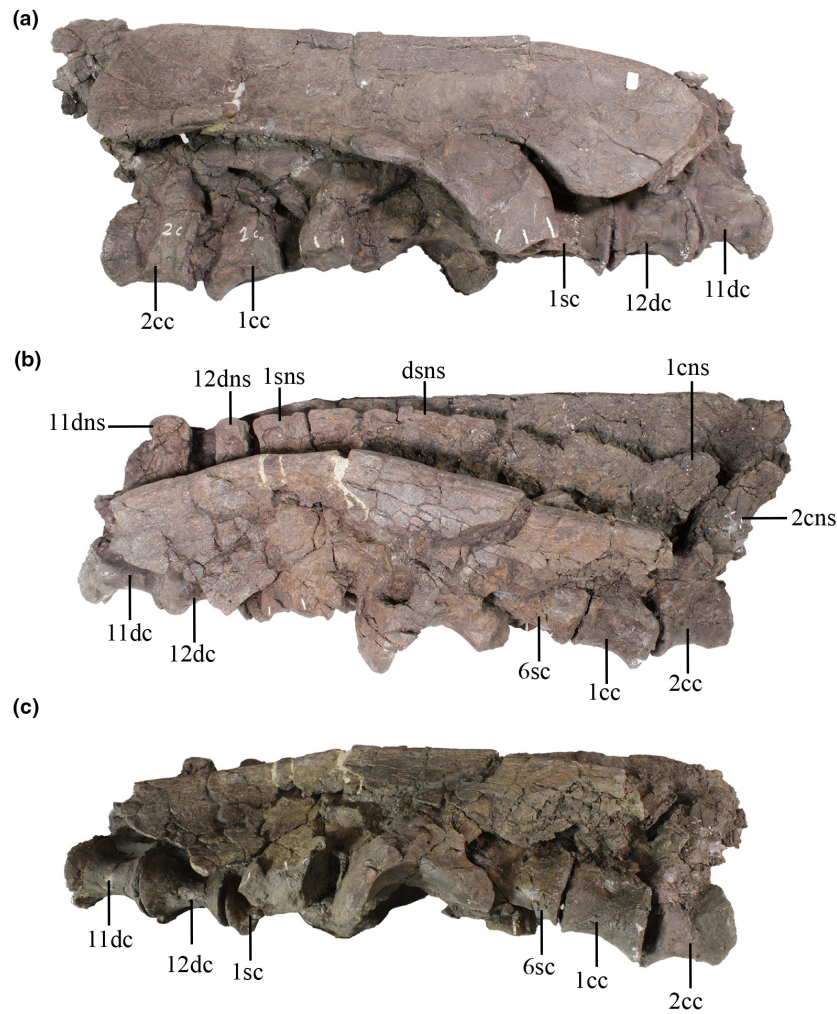


Fig. 8. Sacrum of *Koleken inakayali* MPEF-PV 10826. In (a) lateral, (b) dorsolateral and (c) ventrolateral views. 11dc, eleventh dorsal centrum; 11dns, eleventh dorsal neural spine; 12dc, twelfth dorsal centrum; 12dns, twelfth dorsal neural spine; 1cc, first caudal centrum; 1cns, first caudal neural spine; 1sc, first sacral centrum; 1sns, first sacral neural spine; 2cc, second caudal centrum; 2cns, second caudal neural spine; 6sc, sixth sacral centrum; dsns, dorsal table of the fused sacral neural spines. Scale bar: 10 cm.

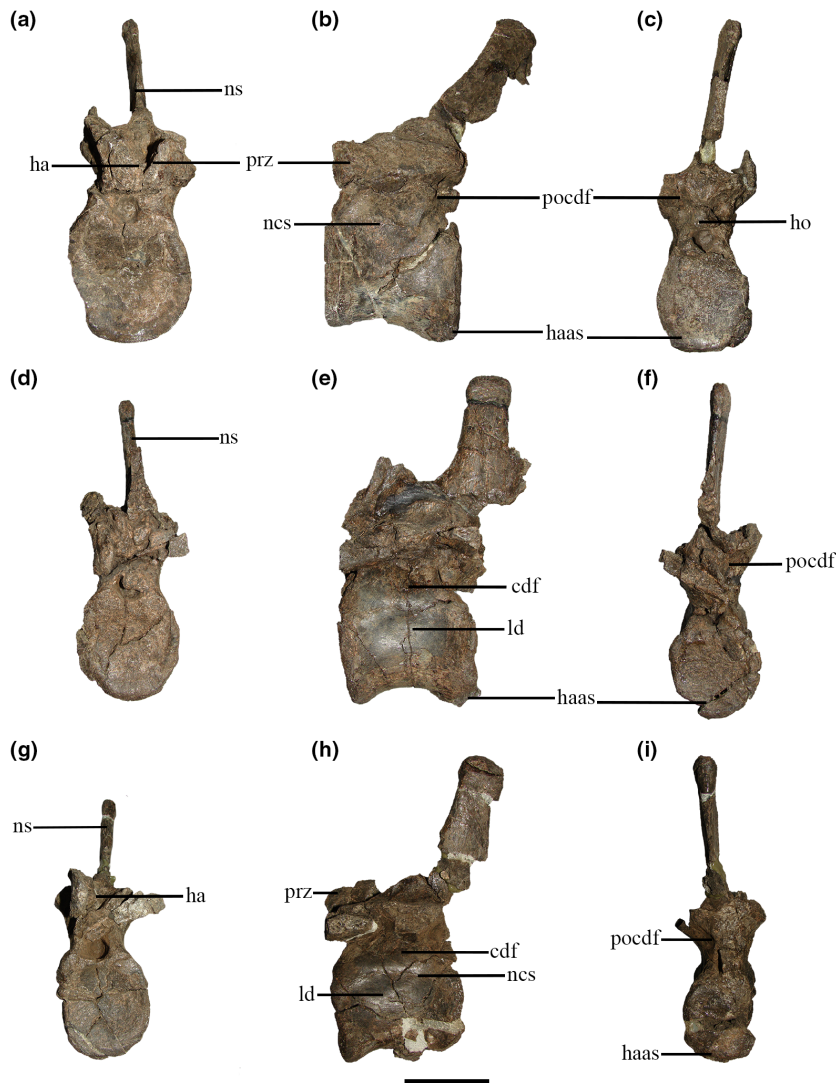


Fig. 9. Third, fourth and fifth caudal vertebrae of *Koleken inakayali* MPEF-PV 10826. In (a, d, g) anterior, (b, e, h) lateral and (c, f, i) posterior views. cdf, centrodiapophyseal fossa; ha, hypantrum; haas, haemal arch articular surface; ld, lateral depression; ncs, neurocentral suture; ho, hyposphene; ns, neural spine; pocdf, postzygapophyseal centrodiapophyseal fossa; prz, prezygapophysis. Scale bar: 5 cm.

and 9). All caudal centra are apneumatic, but they have shallow lateral depressions. The neurocentral suture is still visible in all vertebrae (Fig. 9a–i). The anterior and posterior articular surfaces are dorsoventrally taller than transversely wide, although in the first and second centrum the articular surfaces are almost flat (Fig. 9a–i). In all centra, the posterioventral articular facet for the haemal arch is wider and deeper than the anteroventral one, and there are no grooves or ridges on the ventral surface. An anteroposteriorly directed ventral groove is also absent in *Elaphrosaurus*, *Eoabelisaurus*, *Pycnonemosaurus*, *Rahiolisaurus* and *Carnotaurus*, but is present in *Majungasaurus*, *Aucasaurus* and *Viavenator* (e.g. O'Connor, 2007; Rauhut and Carrano, 2016; Delcourt, 2017; Filippi et al., 2018; Baiano et al., 2023).

The prezygapophyses are dorsomedially directed and dorsoventrally high, at least from the second neural arch, implying a well-developed hypantrum-hyposphene articulation that also is found in several neotheropods (Fig. 9a,d,g) (e.g. Canale et al., 2009; Rauhut and Carrano, 2016; Baiano et al., 2023). The sprl are low, whereas the sprf is deep anteroposteriorly; however, the size of this fossa reduces along the caudal series. All transverse processes are almost entirely missing. A fragment of the distal portion of a transverse process is in contact with the dorsolateral rim of the right ilium. This fragment resembles the anterior awl-like process present in several brachyros-tran abelisaurids such as *Aucasaurus*, *Carnotaurus*, *Ilokelesia*, *Kurupi*, *Pycnonemosaurus*, *Skorpiovenator*,

Tralkasaurus and *Viavenator* (Bonaparte et al., 1990; Coria and Salgado, 2000; Coria et al., 2002; Canale et al., 2009; Filippi et al., 2016; Delcourt, 2017; Cerro et al., 2020; Iori et al., 2021; Baiano et al., 2023).

At the bases of the transverse processes, the centrodiapophyseal fossa (cdf) is shallow (Fig. 9b,e,h) and framed anteriorly and posteriorly by low acdl and pcld laminae that are also present in several abelisaurids such as *Aucasaurus*, *Carnotaurus*, *Pycnonemosaurus*, *Viavenator* and the indeterminate abelisaurid MPCN PV 69 (Rauhut et al., 2003; Méndez, 2012; Filippi et al., 2016; Delcourt, 2017; Baiano et al., 2021, 2023). Both laminae join distally to form a robust centrodiapophyseal lamina (cdl). The precdf and the pocdf are reduced in size and shallow when compared with the dorsal neural arches. Up to the fourth caudal vertebra the pocdf holds a small pneumatic foramen. This foramen is present up to at least the sixth caudal vertebra of *Carnotaurus* and up to the ninth caudal vertebra of

Aucasaurus. The neural spines show the same changes in size and morphology along the series. The first caudal neural spine is the tallest, even taller than the preserved dorsal neural spines. However, it is anteroposteriorly shorter than the posteriormost dorsal vertebrae, a characteristic found only among abelisaurids, such as *Majungasaurus*, *Aucasaurus* and *Carnotaurus*; (and possibly in some material referred to *Ceratosaurus*; Madsen and Welles, 2000). Along with the second and third caudal neural spines, they are posteriorly inclined and surpass the posterior margin of the centrum, whereas the fourth and fifth are almost vertical (Fig. 9b,e,h). From the third to fifth vertebra, the anteroposterior reduction in the length of the neural spines causes the presence of a lamina connected with the sprl. The dorsal portion of the neural spines are slightly transversely swollen and have faint longitudinal ridges. The postzygapophyseal facets are longer than wide and are lateroventrally orientated. The

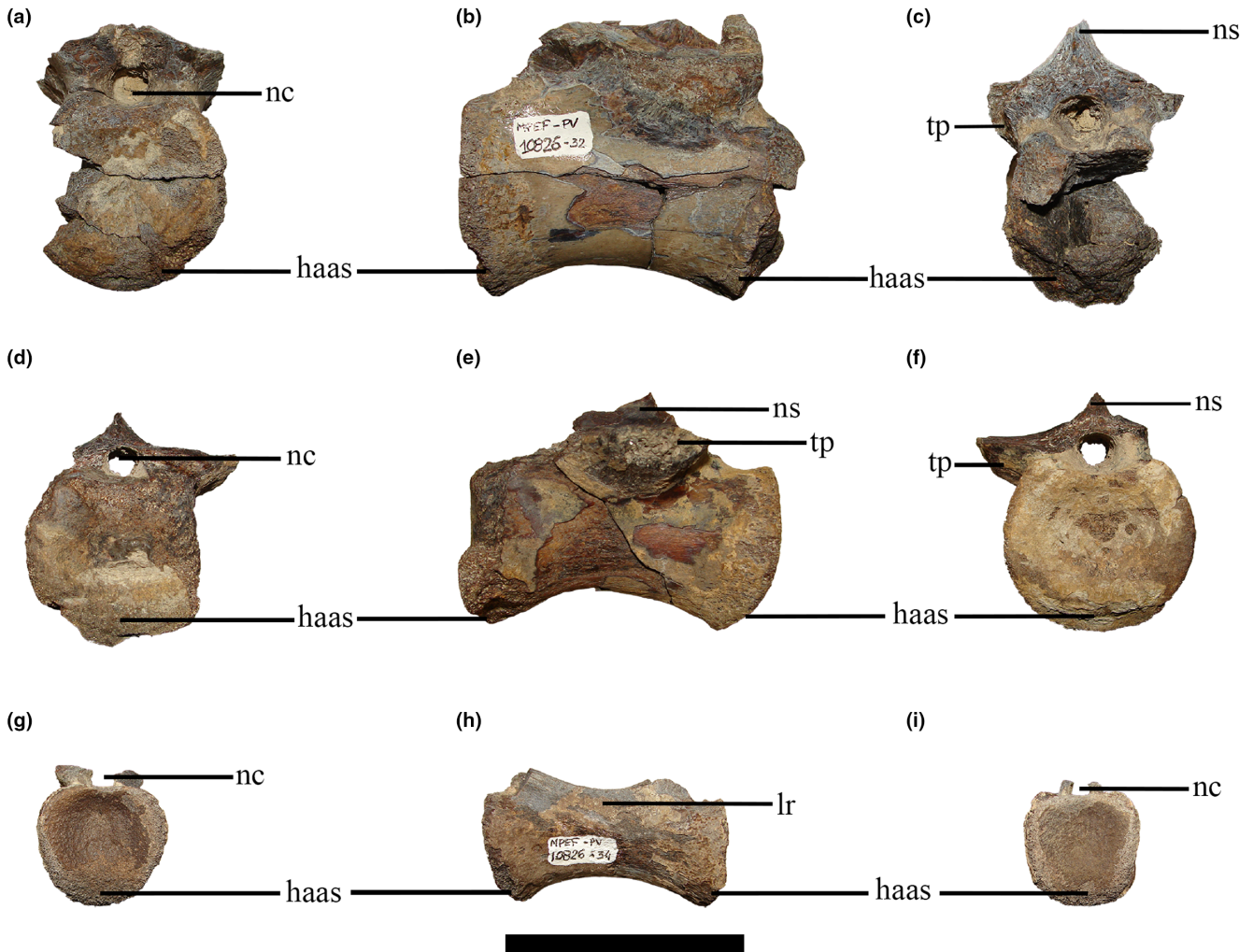


Fig. 10. Middle and posterior caudal vertebrae of *Koleken inakayali* MPEF-PV 10826. In (a, d, g) anterior, (b, e, h) lateral and (c, f, i) posterior views. haas, haemal arch articular surface; lr, lateral ridge; nc, neural canal; ns, neural spine; tp, transverse process. Scale bar: 5 cm.

hyposphene is conspicuous, at least in the vertebrae where it is preserved (Fig. 9c,f,i).

The middle caudal vertebrae have concave and sub-circular articular surfaces (Fig. 10a–f). The lateral surfaces are smooth, lacking any pneumatic features (Fig. 10b,e). As in the anterior caudal vertebrae, the posterior articular facet for the haemal arch is wider and deeper than the anterior one. A very faint depression is present on the anterior portion of the ventral surface of the centrum. The neural arches are poorly preserved, because the pre- and postzygapophyses, transverse processes and neural spines are almost all missing. The neural canal has a circular outline. The base of the transverse processes are situated slightly posteriorly with respect to the midline of the centrum, and lack any ventral fossae or laminae. The bases of the neural spines are located on the posterior half of their neural arches, and anteriorly to them there is a low and longitudinal ridge that is probably connected with the prezygapophyseal processes.

The only distal caudal vertebra preserved has a centrum with a heart-shaped anterior articular surface and a subquadrangular posterior articular surface (Fig. 10g–i), unlike the transversely oval articular surfaces present in *Vespersaurus* and *Elemgasem* (Langer et al., 2019; Baiano et al., 2022). The lateral surfaces are apneumatic, and have an anteroposteriorly longitudinal ridge that is more prominent on the middle of the lateral surfaces and close to the rims of the anterior and posterior articular surfaces (Fig. 10h). The neural arch preserves the lateral walls of the neural canal which are wider posteriorly than anteriorly. It also preserves the bases of the prezygapophyses, which are dorsally directed.

Appendicular skeleton

Pelvis. Pelvic elements are incomplete and seem to be partially fused around the acetabulum as most of their margins are still discernible. In *Carnotaurus*, these elements appear separate but closer inspection shows that respective articular surfaces are broken so fusion cannot be ruled out. In other ceratosaurs, the pelvic bones are at least partially fused around the acetabulum (e.g. Pol and Rauhut, 2012; Rauhut and Carrano, 2016; Cerroni et al., 2022).

Ilium. Both ilia are preserved, the right one being complete (Fig. 11a). The ilium is anteroposteriorly longer than the femur length (1.1 times), as in some ceratosaurs but unlike *Elaphrosaurus* and *Limusaurus* where the femur is longer. In *Koleken*, the anterior margin of the preacetabular process faces anteroventrally, as in other abelisauroids but unlike the anteriorly facing margin of most early-diverging tetanurans. This implies a tight angle between the anterior edge of the pubic

peduncle and the distal margin of the preacetabular process of the ilium. The anterior margin of the preacetabular process is slightly undulated, as in some ceratosaurs such as *Elaphrosaurus*, *Carnotaurus* and *Majungasaurus*. The posterior margin of postacetabular blade has an undulating shape, as in other abelisauroids, forming a prominent posteriorly directed process as in *Carnotaurus*, *Majungasaurus*, *Skorpiovenator* and the indeterminate abelisaurid MCF-PVPH-237 (also found in *Elaphrosaurus*). This posterodorsal process of the ilium has a rugose lateral surface. The ilium of *Koleken* has raised dorsal, posterior and posteroventral edges whereas the anterior and anteroventral edges show only a slight change in rim texture in *Aucasaurus* and *Carnotaurus*. The ventral margins of the brevis shelf slightly diverge posteriorly with respect to the dorsal rim, as in other ceratosaurs and other early-diverging theropods. The lateral brevis shelf faces laterally, as in other abelisaurids but different from noasaurids where it faces dorsolaterally. The morphology of the lateral surface between the supraacetabular crest and the lateral margin of brevis shelf is continuous as in other abelisauroids (in *Carnotaurus* the area above the ischial peduncle is reconstructed but it still appears to transition from a ridge to an inflected margin as in *Koleken* and *Aucasaurus*). The brevis fossa is deep, widening posteriorly. The supraacetabular crest is located anterior to the ischial peduncle and posteroventrally directed as in *Aucasaurus*, *Eoabelisaurus*, *Genusaurus*, *Majungasaurus* and *Skorpiovenator*. The dorsal margin of the central blade is straight, as in *Genusaurus*, *Majungasaurus*, *Masiakasaurus*, *Carnotaurus*, *Spectrovenator* and the indeterminate abelisaurid MCF-PVPH-237, but different from the convex dorsal margin found in *Ceratosaurs*, *Elaphrosaurus*, *Eoabelisaurus* and *Skorpiovenator*. The iliac–pubic articulation is anteroposteriorly larger than the iliac–ischial articulation, as in other ceratosaurs and tetanurans (Carrano and Sampson, 2008). Furthermore, the pubic peduncle is considerably longer than the ischial peduncle, as in most abelisauroids except *Majungasaurus* where both peduncles have a similar length (neither is preserved in *Carnotaurus*). The ischial peduncle is posteroventrally inclined, as in other theropods and different from the autapomorphic condition observed in *Genusaurus* that has a vertical orientation. The vertical orientation observed in *Carnotaurus* in the left ischial peduncle is a consequence of plaster reconstruction and the right one is completely missing; thus, the orientation of its peduncle cannot be established.

Pubis. Both pubes are preserved up to half of the shaft length (Fig. 11b). A portion of the iliac peduncle of the right pubis was preserved partially fused to the pubic peduncle of the right ilium as the suture is still visible. The anteroventral edge of the iliac peduncle in *Koleken* is anteriorly pinched. This condition appears

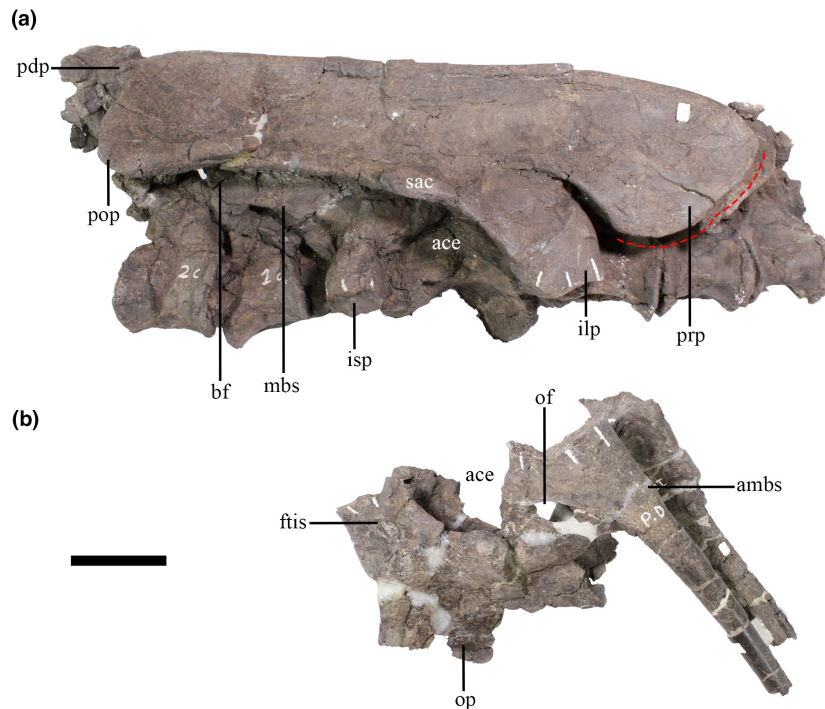


Fig. 11. Right ilium, pubis and ischium of *Koleken inakayali* MPEF-PV 10826. In (a, b) lateral view. ace, acetabulum; ambs, m. ambiens scar; bf, brevis fossa; ftis, m. flexor tibialis internus scar; ilp, iliac peduncle of the ilium; isp, ischial peduncle of the ilium; mbs, medial brevis shelf; of, obturator foramen; op, obturator process; pdp, posterodorsal process; pop, postacetabular process; prp, preacetabular process; sac, supraacetabular crest. Scale bar: 10 cm.

to be the same in the right iliac peduncle of *Carnotaurus*, but this is equivocal because part of the anteroventral edge has been reconstructed. However, the anteroventral edge is more tightly curved than in *Koleken* and its anteroposterior length is twice the mediolateral width of the pubic shaft compared to three times in *Carnotaurus*. The posteroventral edge of the iliac peduncle is straight in both *Koleken* and in *Carnotaurus*. On the anterolateral surface, the oval obturator foramen is subhorizontally-aligned as in *Aucasaurus*, *Carnotaurus* and *Skorpiovenator* (with a slight variation in the shape and orientation of the foramen between the pubes of *Carnotaurus*). The origin of the m. ambiens is represented by a rugose tubercle on the anterolateral surface of the proximal shaft. The ischial peduncle is poorly preserved to discern the morphology. The shaft is straight and anteroventrally directed.

Ischium. The ischium is represented by the proximal portions of both elements (Fig. 11b). The process for the origin of the m. flexor tibialis internus, located on the posteroventral rim of the iliac peduncle, is subtle in *Koleken*, whereas it is more pronounced in *Carnotaurus*. The iliac peduncle has a flange that is similar in width to the ischial shaft whereas this flange is narrower in *Carnotaurus* and transitions from a convex-margined apron that is absent in *Koleken*. The

rectangular-shaped flange in *Koleken* has a slightly concave anterior margin and a slightly convex ventral margin that forms a slightly dorsally upturned distal tip. In *Carnotaurus*, the anterior margin is strongly convex, creating a narrower anteroposterior length anteriorly than posteriorly. The sharper angle between the ventral margin of the flange and the ischial shaft creates a ventrally downturned distal tip. There appears to be a peg-and-socket contact between the ischium and ilium in *Koleken*, as found in other abelisaurids. The relatively flat and damaged contacts on the right and left ischia and left and right ilia of *Carnotaurus* makes the nature of the contact morphology impossible to determine. We also cannot estimate the dimension and shape of the obturator process, as a consequence of the poor preservation of the bone in this area. The pubic peduncle is also badly preserved, though seems to be fused to the ischial peduncle of the pubis.

Femur. The femur is represented by a complete right femur and the distal articular end of the left femur (Fig. 12a–f). The femur is similar to other abelisaurids in being robust, having an anteromedially-orientated femoral head, a scar-like trochanteric crest (as in other averostrans), and a pronounced epicondylar medial crest. The femur is 56.2 cm long from the top of the femoral head to the base of the medial condyle,



Fig. 12. Right femur of *Koleken inakayali* MPEF-PV 10826. In (a) proximal, (b) lateral, (c) medial, (d) anterior, (e) posterior and (f) distal views. ail, anterior intermuscular line; at, accessory trochanter; fc, fibular condyle; ft, fourth trochanter; gt, greater trochanter; lt, lesser trochanter; mec, medial epicondylar crest; pil, posterior intermuscular line; tc, tibial condyle; tfc, tibiofibular crest; ts, trochanteric shelf. Scale bar: 10 cm.

similar to the anteroposterior length of the ilium. This is similar to other ceratosaurs, except *Limusaurus* and *Elaphrosaurus* which have noticeably longer femora. The femoral head is triangular in proximal view (Fig. 12a), with sinusoidal anterior and posterior rims. The greater trochanter is conspicuous and rugose. The posterior surface of the femoral head is sinuous and slightly concave, as in *Skorpiovenator*. In this region we cannot determine the presence of an oblique ligament groove on the posterior side that occurs in other theropods.

The lesser trochanter is a distinct structure and has a marked rugosity on its lateral surface for the m. ilio-trochantericus caudalis (Carrano and Hutchinson, 2002) (Fig. 12b–d). It has a less developed and more horizontal ridge separating the areas of insertion for puboischiofemorales 1 and 2 (PIF1 and PIF2) when compared to *Skorpiovenator*. The proximal tip of the lesser trochanter ends proximally to the ventral margin of the femoral head, a feature also present in *Skorpiovenator* but different from *Ekrixinatosaurus*, *Carnotaurus* and *Aucasaurus*, in which the lesser trochanter is located at the same level or slightly distal to the femoral head. The lesser trochanter of *Koleken* is broad and more medially positioned on the femur than

the narrower trochanter of *Skorpiovenator* and *Carnotaurus* (in the latter the lateral margin extends past the lateral extent of the femoral shaft), and has a narrower and more pointed proximal end. Furthermore, this structure is relatively short and proximomedially directed in *Koleken* (Fig. 12a–d), as in *Aucasaurus*, but different from the higher and more vertically-orientated trochanter of *Skorpiovenator* and *Carnotaurus*. In proximal view, the lateral end of the lesser trochanter is orientated in line with the femoral shaft. The lateral surface of the distal end of the lesser trochanter of *Koleken* is concave and bound by an elongated bulge (= accessory trochanter) (Fig. 12b–d), for the m. puboischiofemorales internus 2 (Carrano and Hutchinson, 2002), as in *Aucasaurus* and *Skorpiovenator*. The anterodistal end of the lesser trochanter bears a small bulge that marks the insertion of the m. ilio-trochantericus caudalis, as in *Xenotarsosaurus*, *Skorpiovenator* and *Carnotaurus*. A small nutrient foramen is present on this surface, which is also present in *Masiakasaurus*, *Velocisaurus*, *Eoabelisaurus* and *Ceratosaurs*.

The fourth trochanter is present as a low crest (Fig. 12c), similar to the condition of some ceratosaurs such as *Aucasaurus*, *Carnotaurus*, *Majungasaurus*

and *Berberosaurus*. By contrast, most ceratosaurs have a more developed fourth trochanter forming a high ridge (e.g. *Ceratosauros*, *Skorpiovenator*, *Spectrovenator*, *Xenotarsosaurus* and *Ekrixinatosaurus*). The femoral shaft has two rugose intermuscular lines, the anterior intermuscular line running distal to the medial end of the lesser trochanter and marking the separation among Mm. femorotibiales components (Carrano and Hutchinson, 2002) (Fig. 12d), and the posterior intermuscular line running along the midshaft in between the level of the lesser trochanter and the fourth trochanter, separating the m. femorotibialis externus origin from the Mm. caudofemoralis brevis and m. adductor femoris 2 insertions (Carrano and Hutchinson, 2002) (Fig. 12e). The latter intermuscular line ends distally in an oblique rugose band. The proximal half of the medial epicondyle of the femur is preserved but its distal portion has been damaged (Fig. 12c,d). Its development in the preserved portion is similar to that of other abelisaurids (including *Carnotaurus*), but different from the hypertrophied structure observed in some noasaurids such as *Masiakasaurus*.

In posterior view, the longitudinal femoral tibiofibular crest is broad as in *Carnotaurus* (Fig. 12e). It is obliquely-orientated as in most ceratosaurs, but in *Koleken* it is also located close to the lateral margin of the femur as in *Carnotaurus*, whereas in *Aucasaurus* it is more medially located creating a narrower popliteal fossa. No well-defined transverse ridge is present across the fossa (infrapopliteal ridge between medial distal condyle and tibiofibular crest) as in *Skorpiovenator*, *Rajasaurus*, *Genusaurus* and *Ekrixinatosaurus*, but it is present in *Carnotaurus*, *Aucasaurus*, *Eoabelisaurus*, *Xenotarsosaurus* and *Quilmesaurus*. Interestingly, the presence of the infrapopliteal ridge seems to be variable among coelophysoids (e.g. *Coelophysus*, “*Syntarsus*”; M. Ezcurra pers. comm.). However, there is no record of intraspecific variability among abelisaurids up to now, owing to the limited number of specimens. The distal end of the fibular condyle is positioned dorsoventrally higher on the femur than the distal end of the tibial condyle. In distal view, the distal end of the tibial condyle is anteroposteriorly deeper than the fibular condyle as in *Carnotaurus*, due to a conspicuous medial epicondylar crest. In both abelisaurids, the tibiofibular crest is more anteriorly projected than the tibial and fibular condyles. Moreover, the tibial condyle has a rectangular outline, different from a more oval outline of the fibular condyle (Fig. 12f).

Tibia. Part of the shaft and the proximal end of the right tibia is preserved in *Koleken* as well as the proximal and distal end of the left tibia (Fig. 13a–h). Most of the cnemial crest is preserved, which is anteroproximally expanded and occupies more than half of the proximal surface of the tibia, as in most

ceratosaurs (Fig. 13a). In proximal view (Fig. 13a), the articular surface is lateromedially narrow and the cnemial crest curves laterally at its anterior end. This curvature, however, is not as developed as in some abelisaurids such as *Aucasaurus*, *Ekrixinatosaurus*, *Quilmesaurus*, *Skorpiovenator* and *Xenotarsosaurus*. The posterior medial condyle is approximately half the mediolateral width of the lateral condyle, different from a more reduced lateral condyle in *Skorpiovenator*. *Koleken* also differs from the latter in having a more rounded lateral condyle. Moreover, the posterior rim of the proximal articular surface shows a marked posteromedial-anterolateral direction, different from the more transversal rim of other abelisaurids. In medial view (Fig. 13b), the proximal margin of the cnemial crest is elevated above the level of the proximal articular condyles of the tibia, a condition observed in several ceratosaurs and many early-diverging tetanurans. The medial surface of the cnemial crest is smooth and evenly convex but the lateral surface is concave and bears a ridge (= lateral ridge). On the posterior portion of the proximomedial surface there is a shallow depression.

The lateral ridge is proximodistally directed on the lateral surface of the cnemial crest (Fig. 13c), as in *Xenotarsosaurus*, *Skorpiovenator*, *Ekrixinatosaurus*, *Aucasaurus* and *Eoabelisaurus*. This feature is absent in *Elaphrosaurus*. The distal end of the cnemial crest is expanded proximodistally, but we are unable to estimate whether it has a rectangular or axe-like outline because the distalmost portion is broken (Fig. 13b,c). *Ekrixinatosaurus*, *Eoabelisaurus*, *Majungasaurus*, *Rahiolisaurus*, *Spectrovenator*, *Velocisaurus*, *Xenotarsosaurus*, *Masiakasaurus* and *Ceratosauros* have a cnemial crest with a proximodistally expanded distal end and rectangular outline. By contrast, the proximodistally expanded distal end of the cnemial crest of *Aucasaurus*, *Genusaurus*, *Pycnonemosaurus*, *Quilmesaurus*, *Skorpiovenator* and *Elemgasem* has an axe-like outline owing to the presence of a ventral process. The fibular crest is only partially preserved but appears to be positioned proximally (Fig. 13c,d) as in other ceratosaurs, and it is vertically orientated towards the shaft. Moreover, the fibular crest joins the lateral ridge, ending in the lateral bulge for the attachment of the Mm. ambiens, femorotibiales and ilioltibiales. Only part of the tibial shaft has been preserved, which is robust and ovoid in cross-section. In lateromedial view (Fig. 13b,c), the shaft is curved with the distal portion positioned more posteriorly than the proximal one. This morphology differs from an almost vertical shaft observed in several ceratosaurs, from *Quilmesaurus* that only has a posteriorly bent distal articular surface, and from *Arcovenator* that has an anterior bent of the proximal articular surface. In posterior view (Fig. 13e), there is a triangular fossa between the proximal condyles. The medial condyle is triangular, ending distally

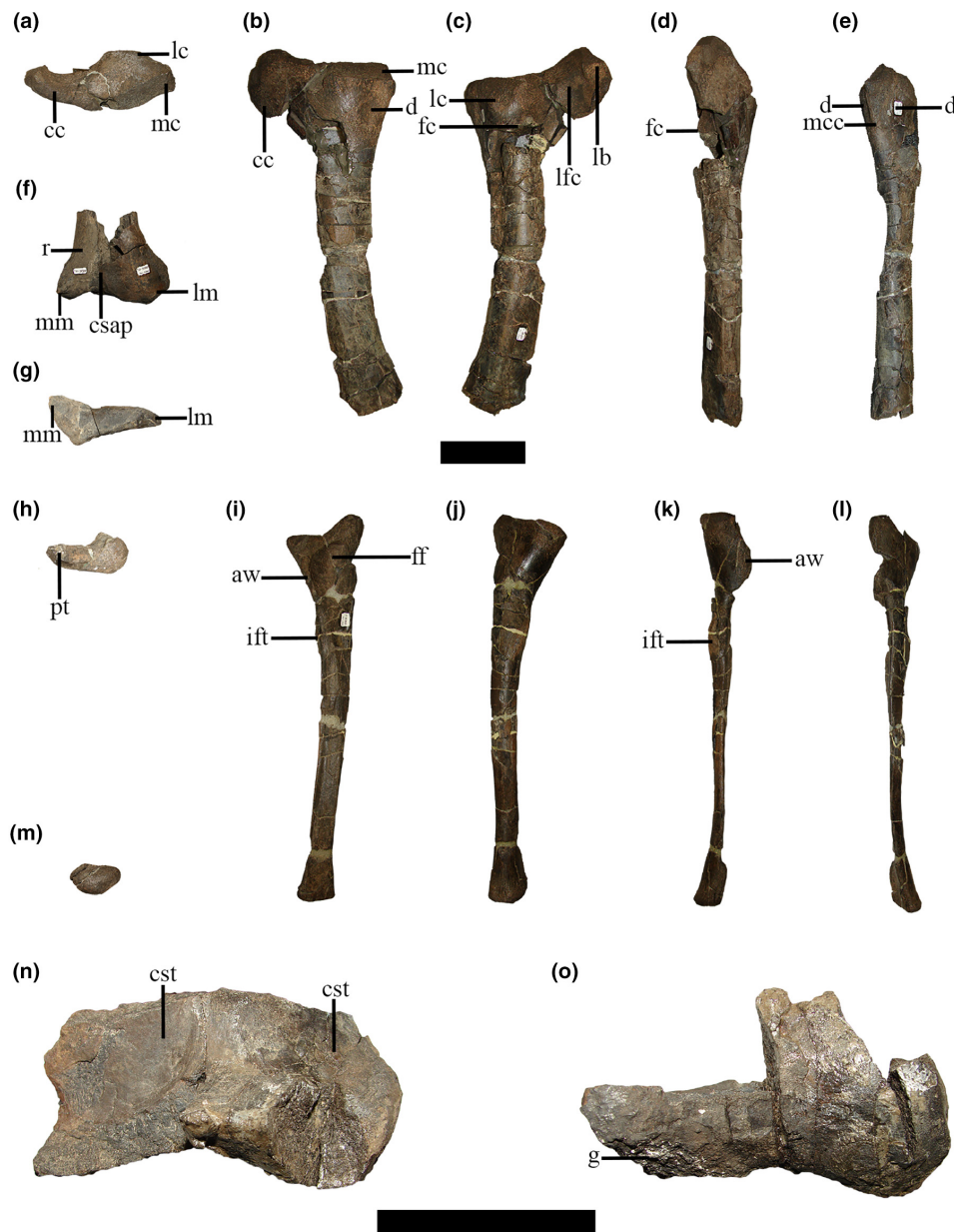


Fig. 13. Right and left tibiae, right fibula and astragalus of *Koleken inakayali* MPEF-PV 10826. In (a, h, n) proximal, (b, i) medial, (c, j) lateral, (d, f, k, o) anterior, (e, l) posterior and (g, m) distal views. aw, anterior wall; cc, cnemial crest; csap, contact surface for the ascending process; cst, contact surface for the tibia; d, depression; fc, fibular crest; ff, fibular fossa; g, groove; ift, iliofibular tubercle; lb, lateral bulge; lc, lateral condyle; lfc, lateral fibular crest; lm, lateral malleolus; mc, medial condyle; mcc, medial condyle crest; mm, medial malleolus; pt, posterior tubercle; r, ridge. Scale bars: 10 cm (a–m); 5 cm (n, o).

with a vertical crest, whereas the lateral condyle is rounded.

In *Koleken*, the distal end is expanded mediolaterally forming two asymmetrical malleoli in anterior view (Fig. 13f). The medial malleolus is mediolaterally narrower than the lateral one that has a flange-like shape. This mediolaterally elongated morphology of the distal articular surface is shared with several neotheropods. The articular surface for the ascending process is

concave and rectangular in outline, being higher than wide and possibly reflecting the morphology of the latter. However, this surface is not sufficiently preserved to comment on its stepped condition. There is a faint ridge on the medial malleolus directed sub-horizontally as in *Aucasaurus*, *Ekrixinatosaurus*, *Eoabelisaurus*, *Pycnonemosaurus*, *Skorpiovenator* and *Xenotarsosaurus*, but different from *Elaphrosaurus*, *Velocisaurus* and *Quilmesaurus* where this surface is smooth. The lateral

malleolus has a textured surface where the fibula would have articulated. The ventral margin is sinusoidal with a small protuberance in its posterior corner for the articulation with the astragalus. In ventral view, the medial malleolus is anteroposteriorly deeper than the lateral one in distal view as in other ceratosaurs, giving the distal end of the tibia a triangular shape (Fig. 13g). It is unclear if there is a groove incised into the distal articular surface because the distal surface is imperfectly preserved.

Fibula. The fibula is a slender bone with an anteroposteriorly expanded proximal end, as in most theropods (Fig. 13h–m). In proximal view (Fig. 13h), the articular surface is anteroposteriorly concave and kidney-shaped with a comparatively broader anterior end. On the posterior portion there is a tubercle projected proximally. In medial view (Fig. 13i), the fibular fossa is located close to the proximal end of the fibula and is deep and opens posteriorly. The fibular fossa is bounded anteriorly by a prominent wall and has a smaller rim along its posterior end. Despite a well-developed anterior wall, the fibular fossa in *Koleken* is medially open as in *Aucasaurus* and *Elaphrosaurus*, although in the latter the anterior wall is more reduced. A posteriorly open fibular fossa is present in most ceratosaurs preserving this portion of the fibula (e.g. *Elengasem*, *Skorpiovenator*, *Rajasaurus*, *Rahiolisaurus*, *Majungasaurus*, *Eoabelisaurus*, *Genusaurus*, *Arcovenator* and

Berberosaurus) and is probably a neotheropod plesiomorphy. The fibular fossa becomes gradually shallower and disappears at the level of the iliofibular tubercle. Different from a flat medial surface, the lateral surface of the fibula is gently convex (Fig. 13j). In this view, an anterior bending of the fibular shaft is visible. The proximolateral surface of *Koleken* lacks the rugose pattern present in the abelisaurid *Elengasem*, although a rugose scar is present on the anterior portion of the proximolateral surface.

In anterior view (Fig. 13k), and along the proximal third of the shaft, the surface of the fibula bears a conspicuous and proximodistally elongated iliofibular tubercle (attachment site for the m. iliofibularis) that resembles the condition found in other ceratosaurs, such as *Ceratosaurs*, *Skorpiovenator*, *Aucasaurus* and *Xenotarsosaurus*. The iliofibularis tubercle has a rugose surface and is oval in outline, merging into the posterolateral surface of the fibular shaft. In posterior view (Fig. 13l), a portion of the lateral fossa is exposed. The shaft is straight, turning laterally concave in the distal portion due to a lateral inclination of the articular surface. There is a separate contact between the fibula and the ascending process of the astragalus as in many ceratosaurs, whereas they are fused together in *Aucasaurus*, *Xenotarsosaurus*, *Afromimus* and *Masiakasaurus*, possibly related to ontogeny. The distal end of the fibular is slightly expanded anteroposteriorly but much less so than the proximal end (Fig. 13m). The distal articular surface is D-shaped

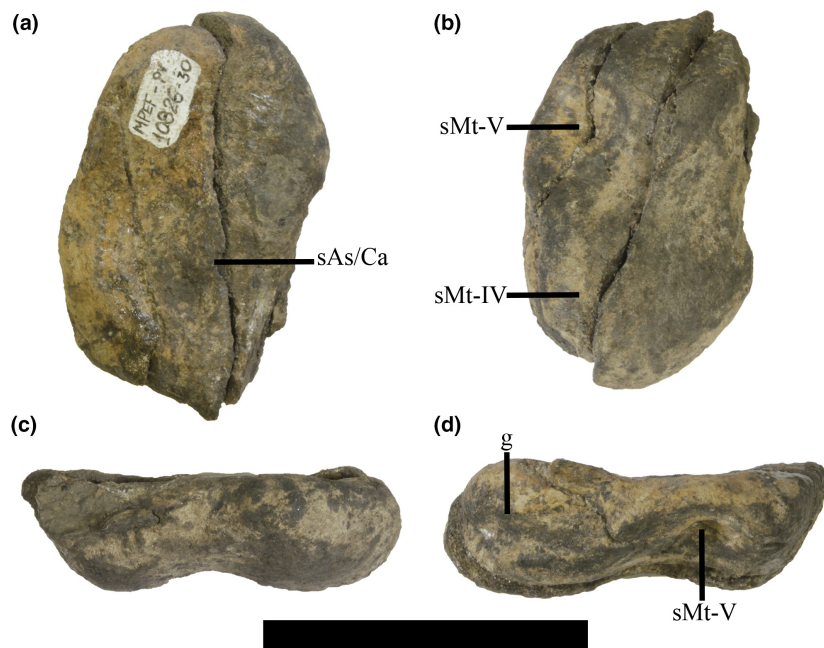


Fig. 14. Right IV distal tarsal of *Koleken inakayali* MPEF-PV 10826. In (a) proximal, (b) distal, (c) medial and (d) lateral views. g, groove; sAs/CA, contact surface for the astragalocalcaneum; sMt-IV/V contact surfaces for the metatarsal IV and V. Scale bar: 5 cm.

and well-preserved, lacking any signature of being fused to the tarsal complex (a condition present in *Xenotarsosaurus* and *Aucasaurus*).

Astragalus. Only part of the right astragalus has been preserved in *Koleken*. It was found separated from the tibia and fibula, lacking any sign of fusion with these hind limb bones. In proximal view (Fig. 13n), the bone has a kidney-like outline. There are two major areas for the contact with the distal tibia. The ascending process is not preserved, so we cannot know its overall morphology (Fig. 13n,o). The distal condyles are orientated anteroventrally as in other ceratosaurs, except *Elaphrosaurus* where they are ventrally-orientated. The astragalus has a pronounced

horizontal groove across the anterior face of the distal condyles as in other ceratosaurs, except in *Elaphrosaurus* which has a weakly developed groove.

Distal tarsals. *Koleken* preserves the third (DT-III) and fourth (DT-IV) distal tarsals (Figs 14a–d and 15a–e), the former is articulated and fused with metatarsal-III (MT-III) (Fig. 15a–e), whereas the latter is completely disarticulated (Fig. 14a–d). DT-III is positioned on the posterior half of the proximal surface of MT-III and has a sub-rectangular contour and a proximal surface slightly convex as in *Sinraptor*, *Dilophosaurus*, *Saltriovenator*, *Elemgasem*, *Eoabelisaurus* and *Aucasaurus*. DT-IV is a bean-shaped bone, different from the P-shaped element present in *Allosaurus*,



Fig. 15. Right metatarsus of *Koleken inakayali* MPEF-PV 10826. In (a) proximal, (b) anterior, (c) posterior, (d) medial, (e) lateral and (f) distal views. bu, bulge; clp, collateral ligament pit; Dt-III, distal tarsal III; ef, extensor fossa; gs, scar for the m. gastrocnemius; is, intercondylar sulcus; Mt-I/IV, metatarsal I to IV; r, ridge. Scale bar: 5 cm.

Sinraptor, *Ceratosaurus*, *Dilophosaurus* and *Saltriovenator*. Its proximal surface is slightly concave, whereas the distal surface is sinusoidal with a concave central portion (Fig. 14a,b). The latter surface snugly articulates with a large pit in the dorsal surface of metatarsal-IV (MT-IV) via a large rounded posterolateral condyle that occupies roughly half the anteroposterior length of the distal tarsal (Fig. 14b,c). The smaller anterior condyle has a pinched lateral margin created by a circular posteriorly positioned ventral fossa and would have articulated with MT-V (Fig. 14b,d). The posterior portion of the lateral surface of the distal tarsal bears a longitudinal groove that roughly extends to the midline of the element (Fig. 14d). The dorsal surface of the distal tarsal is weakly concave and would have sat horizontally as in other theropods. A similar distal tarsal is preserved in *Aucasaurus*, although in *Koleken* the posterior edge appears to be more steeply inclined and the groove separating the ventral condyles appears to be more pronounced than in *Aucasaurus*.

Metatarsal I. Its whole morphology resembles metatarsal I (MT-I) of some tetanuran theropods (e.g. Hattori, 2016) (Fig. 15a–f). The proximal end of MT-I is narrow and tapers rapidly to a pointed proximal end (Fig. 15b,c), whereas in *Aucasaurus* it is proportionately longer and does not taper as markedly. The distal end is highly asymmetrical, as in most theropods, with the lateral condyle being much larger and dorsally elevated relative to the shaft compared to the medial condyle. The distal end of the metatarsal has a large, circular and deep collateral ligament pit on the lateral condyle but a much shallower and irregular shaped collateral ligament pit associated with the medial condyle (Fig. 15d,e). The development of the distal end of the metatarsal as well as the depth of the collateral pits is larger than in other abelisaurids in which this element is known, such as *Aucasaurus*. The intercondylar groove of the distal end is very shallow (Fig. 15f) as in *Spectrovenator* (Zaher et al., 2020), but different from other theropods such as *Aucasaurus*, *Allosaurus*, *Citipati*, *Deinonychus*, *Sinraptor* and *Tarbosaurus*.

Metatarsal II. Both metatarsals are preserved in *Koleken*. This element shows an intermediate condition between the extremely slender metatarsal observed in noasaurids and the robust metatarsal of most theropods (Fig. 15a–f), including the abelisaurids *Majungasaurus* and *Rahiolisaurus*. The proximal articular facet is subtriangular with a broader dorsal surface and a slightly pointed ventral end (Fig. 15a) as in *Aucasaurus*, *Majungasaurus* and *Skorpiovenator*. The shaft of metatarsal II (MT-II) is almost straight with a slightly convex lateral surface (that fits on the medial surface of the metatarsal III) and a slightly concave medial surface

(Fig. 15b). The dorsal margin of the proximal surface is dorsally elevated relative to the dorsal surface of the shaft. The dorsal surface of the shaft of MT-II gradually expands lateromedially towards the distal end, whereas the ventral surface is narrow, so that the metatarsal shaft is subtriangular in cross section (Fig. 15b,c). The distal end has a faintly marked extensor fossa in which the distal margin is much less developed than in other abelisaurids (e.g. *Eoabelisaurus*, *Aucasaurus*, *Majungasaurus*, *Masiakasaurus* and *Skorpiovenator*), but resembling the condition in *Elemgasem*.

The lateral margin of the distal half of the shaft is raised as a convex rugose ridge creating an increase in the dorsoventral depth of the metatarsal at the distal end of the shaft. This ridge is also present in *Aucasaurus*, *Eoabelisaurus*, *Majungasaurus* and *Skorpiovenator*. The distal ventral surface has a less-developed scar for the m. gastrocnemius pars medialis when compared with other abelisaurids (Fig. 15c). A broad and shallow intercondylar groove is only developed on the ventral end of this metatarsal, so that in distal view the condyles slightly flares towards the ventral end.

The medial condyle is narrower and dorsoventrally shallower than the lateral condyle (Fig. 15d,e). The medial condyle also has a pointed ventral corner whereas the lateral condyle has an evenly rounded ventral surface (Fig. 15e) as in *Aucasaurus* and *Elemgasem*. In distal view, the condyles are asymmetrical, with the lateral one being transversely wider and more distally projected than the medial one (Fig. 15f).

Metatarsal III. Metatarsal III (MT-III) is much more robust than the other metatarsals (>50% broader at the midshaft than metatarsal II) (Fig. 15a–f). The proximal articular surface is hourglass-shaped with a slightly obliquely directed long axis (Fig. 15a). The lateroventral corner of the proximal articular surface is poorly developed as in *Majungasaurus*, but differing from the condition of *Aucasaurus* or *Elaphrosaurus* that have a well-developed lateroventral flange that extends under the proximal end of metatarsal IV. The posterior portion of the proximal articular surface is covered by the DT-III that in turn rises proximally as in *Aucasaurus*, *Eoabelisaurus* and *Skorpiovenator*.

In dorsal view (Fig. 15b), the shaft is straight and the surface is flat along most of its length except for the distal region where the extensor fossa is located. The lateral margin of the shaft is not as concave as in *Aucasaurus*, whereas the medial margin has a noticeable flange along the distal third of the shaft (for MT-II) as in other abelisaurids such as *Aucasaurus*, *Majungasaurus* and *Skorpiovenator*. The ventral surface lacks rugosities for the m. gastrocnemius pars medialis and lateralis, which contrasts with the well-marked rugosities of *Eoabelisaurus*, *Skorpiovenator*

and *Aucasaurus* (Fig. 15c). The extensor fossa is shallower than in other abelisaurids. This fossa is laterally bounded by a ridge that bears a small bump as in other theropods (e.g. *Aucasaurus*, *Elemgasem* and *Sinraptor*).

The dorsal margin of the proximal end is remarkably elevated with respect to the dorsal surface of the shaft, creating a high step visible in lateral or medial view (Fig. 15d,e). This bulged proximodorsal area can be interpreted as an outgrowth (pathological?) of this metatarsal or conversely it may represent a partially ossified cartilage cap. Irrespective of the origin of this feature, a similar step is present in *Elemgasem*, while in *Eoabelisaurus*, *Skorpiovenator* and *Aucasaurus* it is faint. The distal condyles are broader and ventrally deeper than the shaft. The medial condyle bears a much larger collateral ligament pit than the lateral condyle (Fig. 15d,e). Although the medial condyle is slightly higher dorsoventrally than the lateral condyle, the articular surface is subrectangular in distal view as in other abelisaurids (*Skorpiovenator*, *Aucasaurus*, *Majungasaurus*) (Fig. 15f). The intercondylar groove is barely marked across the entire condyle, except for a shallow and narrow concavity on the ventral surface. In *Aucasaurus* the ventral surface bears a much broader intercondylar groove.

Metatarsal IV. Metatarsal IV (MT-IV) is slightly shorter than metatarsal II and its shaft curves laterally (Fig. 15a–f), as in *Majungasaurus* and to a higher degree than in noasaurids and the abelisaurids *Aucasaurus* and *Skorpiovenator*. The proximal end is subtriangular with a broadly convex dorsolateral margin, a sigmoid medial margin resembling that of *Aucasaurus* but contrasting with the flat shape in *Majungasaurus*, and a slightly concave lateroventral margin (Fig. 15a). The proximal articular surface has elevated dorsal and lateral rims, and a depressed central region (area for the articulation of the DT-IV), which is in sharp contrast with the flat proximal articular surface of most theropods (but not in others, such as *Pandoravenator*; Rauhut and Pol, 2017). This elevated rim actually has a visible sutural line that separates it from the rest of the metatarsal (visible especially in lateral view). This suture suggests that the elevated rim may represent a partially ossified cartilage cap.

The shaft has convex lateral and dorsal surfaces and flat ventral and medial surfaces. In dorsal view (Fig. 15b), the shaft has a convex medial rim and a concave lateral rim. The medial rim of the dorsal surface lacks the distinct rugose crest separating it from the medial surfaces of the shaft. The flat ventral surface is defined by two well-developed lateroventral and medioventral edges of the metatarsal shaft. The ventral surface of MT-IV also bears an oblique faint ridge that runs from medioproximally to laterodistally along

the distal half of the shaft, marking the attachment site for the m. gastrocnemius pars lateralis (which is much more rugose in *Aucasaurus* and *Skorpiovenator*) (Fig. 15c). The flat medial surface of the shaft of MT-IV probably only contacted MT-III along their proximal half (Fig. 15d). The length of this contact resembles that of *Majungasaurus* but seems to be shorter than in *Aucasaurus*, *Skorpiovenator* and all noasaurids where it is known.

The distal articular region is well-preserved except for the ventral end of the lateral condyle (Fig. 15b–f). The dorsal surface lacks the extensor fossa. The distal end has strongly asymmetrical condyles, with the medial condyle being much broader and more distally expanded than the lateral condyle, as in other abelisaurids (Fig. 15d–f). The medial condyle is rounded and merges gradually on the dorsal surface of the metatarsal shaft. The medial collateral pit has sharp margins, it is small, shallow and ventrally displaced, which differs from that of *Aucasaurus* in which it is diffuse and centrally-positioned (Fig. 15d). The lateral collateral pit is badly preserved, but it seems to have an oval outline and is more anteriorly displaced than the medial one (Fig. 15e). In distal view, the articular surface is considerably higher dorsoventrally than wide mediolaterally. Moreover, the medial condyle is more projected ventrally and distally than the lateral one (Fig. 15f). The intercondylar sulcus is faint, turning deeper ventrally.

Phalanges. Digit I is represented by the left and right first phalanx. Digit II is represented by the right first phalanx, left and right second phalanx and right ungual phalanx. Digit III is represented by the left and right first phalanx, the right second phalanx and the left ungual phalanx. Digit IV is represented by the right ungual phalanx (Fig. 16a–f).

Phalanx I-1. This phalanx is slightly curved medially along its shaft and is proportionately more robust than in *Aucasaurus* (Fig. 16a–f). The proximal articular surface is a single ovoid concavity with a straighter medial margin and a more convex lateral margin, resembling the condition of *Aucasaurus* but differing from the more evenly rounded outline of the articular surface of *Skorpiovenator*. The ventral end of the proximal surface of the phalanx bears a poorly developed process as in *Skorpiovenator*, but different from a conspicuous one present in *Aucasaurus*. However, a rugose area is present on the proximal portion. The lateral and medial condyles are subequal to each other in both height and width. The medial collateral ligament pit has an oval contour, is dorsally positioned, and is smaller in size relative to its lateral counterpart. The lateral pit is deep, has a tear-shaped outline, and occupies the dorsal half of the lateral surface of the distal end of the phalanx. The two

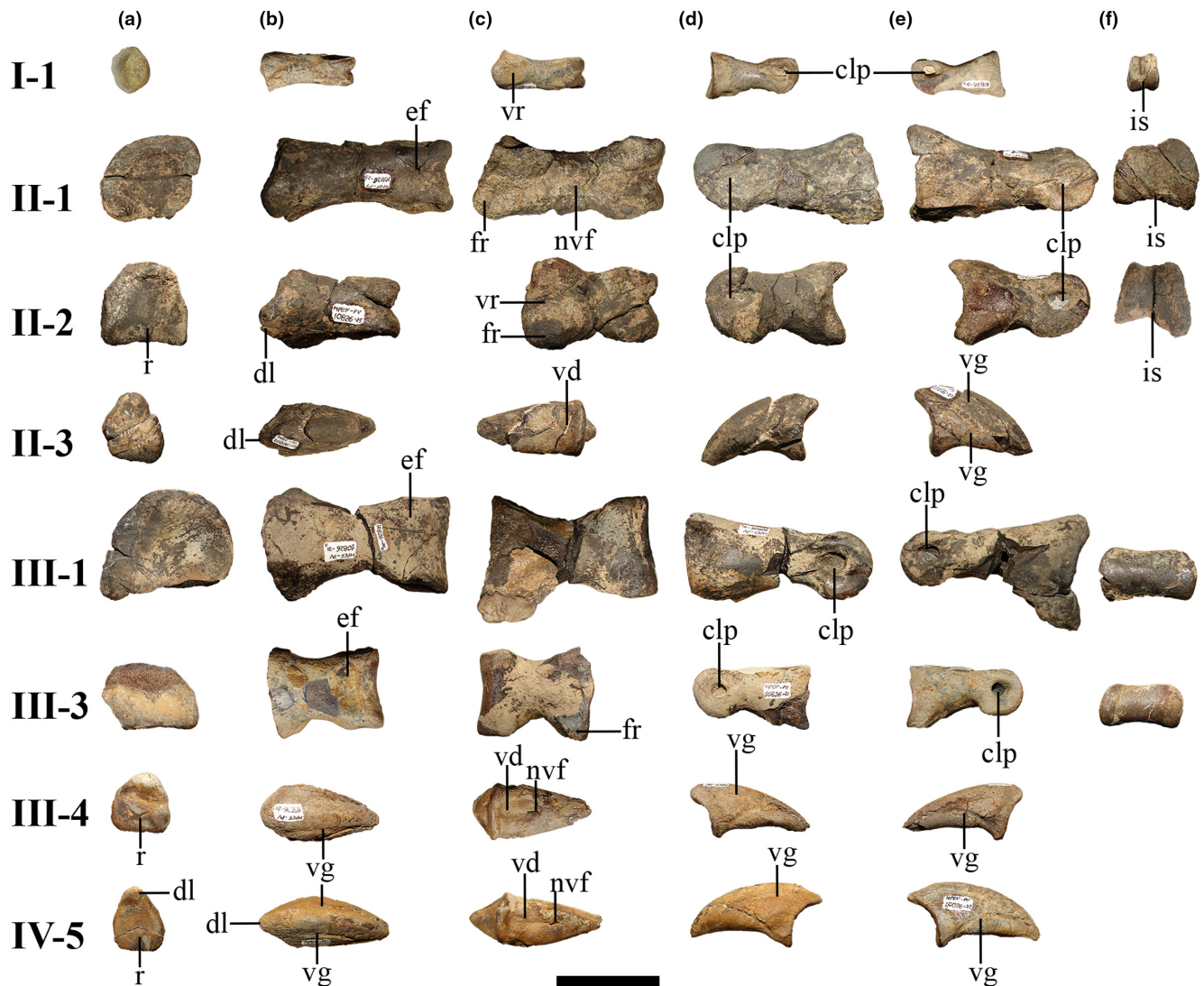


Fig. 16. Selected pedal phalanges of *Koleken inakayali* MPEF-PV 10826. In (a) proximal, (b) dorsal, (c) ventral, (d) medial, (e) lateral and (f) distal views. I-1, III-1 and III-4, left pedal phalanges. II-1/2/3, III-3 and IV-5, right pedal phalanges. clp, collateral ligament pit; dl, dorsal lip; ef, extensor fossa; fr, flexor ridge; is, intercondylar sulcus; nvf, neurovascular foramen; r, ridge; vd, ventral depression; vg, vascular groove; vr, ventral rugosity. Scale bar: 5 cm.

condyles are separated by a deep intercondylar groove. The distal articular condyles are barely expanded relative to the width of the shaft and their dorsal ends are slightly narrower than their ventral ends. A sulcus separates the two distal condyles.

Phalanx II-1. This phalanx is robust and almost twice the length of phalanx II-2 (Fig. 16a–f). The proximal articular surface lacks a middle vertical ridge. The single and ovoid proximal articular surface has evenly convex medial and lateral margins and more acute dorsal and ventral ends. The shaft is poorly constricted relative to its proximal and distal ends. A well-developed flexor ridge is present on the ventral surface of the medial edge, but the presence of a similar ridge on the lateral end

cannot be confirmed because this phalanx is damaged. *Aucasaurus* and *Skorpiovenator* have well-developed medial and lateral ridges. On the ventral surface, there is a marked rugosity near the medial flexor tubercle. A neurovascular foramen is present on the middle of the ventral surface. The extensor fossa on the dorsal surface of the distal end is relatively shallow in comparison with those of *Eoabelisaurus*, *Aucasaurus* and *Majungasaurus*. The distal condyles are narrower dorsally than ventrally such that in distal view the articular condyles flare ventrally. The medial collateral ligament pit is small and dorsally displaced, whereas the lateral one is larger, deeper and more centrally located. There is a deep intercondylar groove running all along the distal articular surface.

Phalanx II-2. This phalanx is short, being two thirds of the length of phalanx II-1 (Fig. 16a–f). The proximal articular surface has two well-defined articular facets, the medial one being lower and subtriangularly shaped, and the lateral one higher and kidney-shaped. These two facets are separated by a faint vertical ridge that runs obliquely (laterodorsally to medioventrally). In dorsal view, this phalanx is trapezoidal in shape, with a broader proximal end and a narrower distal end. There is a well-developed dorsoproximal lip that is more prominent than in *Aucasaurus*, and resembling the condition observed in *Skorpiovenator*. The ventral surface of the proximal end bears well-developed medial and lateral flexor ridges separated by a small and shallow rugose concavity. The shaft of this phalanx is constricted, especially in ventral view, as in *Eoabelisaurus* but different from *Aucasaurus* and *Skorpiovenator* that are only slightly constricted. The lateral and medial distal condyles are well-separated by the deep intercondylar groove and flare ventrally more than in *Aucasaurus*. Both collateral ligament pits are well-developed but the medial one is larger and more centrally located. The lateral collateral ligament pit is dorsally shifted on the lateral surface of the distal region of this phalanx.

Phalanx III-1. This phalanx is mostly represented (Fig. 16a–f), with the right phalanx preserving most of its proximal and distal end. The proximal articular surface is a broad D-shaped facet, with the convexity occupying the entire dorsal margin and with a straight ventral margin. The shape of this facet resembles that of *Eoabelisaurus* and *Majungasaurus*, but in *Aucasaurus* and *Skorpiovenator* there are distinct lateral, dorsal and medial margins, such that this articular facet has a more pentagonal outline in proximal view. The proximal articular facet is evenly concave and lacks any subdivision. In dorsal view, this element has an hourglass-shaped outline. The extensor fossa is shallow and transversely broad, different from a slightly deeper fossa in *Eoabelisaurus*, *Aucasaurus* and *Majungasaurus*. The collateral ligament pits are deep with a drop-like outline, well-defined and centred on the lateral and medial surfaces of the distal end. In lateral or medial view, the ventral end of the articular condyles seem to be flush with the ventral surface of the shaft, rather than being ventrally offset as in *Aucasaurus*. The lateral and medial distal articular condyles are subequal in width and height, contrasting with the more asymmetrical condition of *Aucasaurus*. Between the distal condyles there is no evidence of an intercondylar sulcus.

Phalanx III-3. This phalanx is almost completely preserved (Fig. 16a–f), with the exception of part of the rims of the proximal articular facet. The proximal

articular facet has a pentagonal outline, as in *Eoabelisaurus*, *Aucasaurus* and *Skorpiovenator*. The shaft is mediolaterally constricted relative to the proximal and distal ends, which is especially noticeable in ventral view. The distal end has a well-developed extensor fossa with a conspicuous anterior rim, as in other abelisaurids. The ventral surface has a well-developed lateral flexor ridge and a shallow concavity on its central portion, close to the proximal end. There are deep and well-defined collateral ligament pits that are centred on the medial and lateral surfaces. The oval medial and lateral condyles are subequal to each other and lack an intercondylar groove separating them. The lateral and medial condyles only slightly flare ventrally so that in distal view, the articular surface has a subrectangular shape.

Pedal unguals. The three preserved pedal unguals (II–IV) are stout (Fig. 16a–f), mediolaterally asymmetrical (although the ungual phalanx of the digit-III is slightly more symmetrical) and have dorsolateral, ventrolateral, dorsomedial and ventromedial claw grooves, which converge distally, as in other abelisauroids. As in other abelisauroids, the ventral surface of the pedal unguals possess a ventral depression on its proximal end that is connected with the ventrolateral and ventromedial grooves, and lack a flexor tubercle. The proximal surface of the pedal unguals has a vertical ridge that connects the dorsal lip to the ventral rim. The ventral surfaces of these elements hold neurovascular foramina.

Results and discussion

Histological analysis

The tibial shaft is formed by a thick cortex surrounding a free medullary cavity (Fig. 17a,b). The compacta is almost entirely formed by primary bone, which predominantly consists of parallel-fibred bone, with characteristic mass birefringence and flattened osteocyte lacunae (Fig. 17c). Vascular canals are abundant in the whole compacta. Six irregularly spaced LAGs (four single and two double) are recorded in the compacta (Fig. 17b). A very thin layer of secondarily formed lamellar bone tissue, here interpreted as an inner circumferential layer (ICL) partially lines the perimedullary margin of the cortex (Fig. 17d).

Ontogenetic stage and minimum age

Bone histological results preserve records of relevant events in the life history of vertebrates (Chinsamy Turan, 2005; Erickson, 2014; de Buffrénil and Quilhac, 2021). This is because noticeable histological

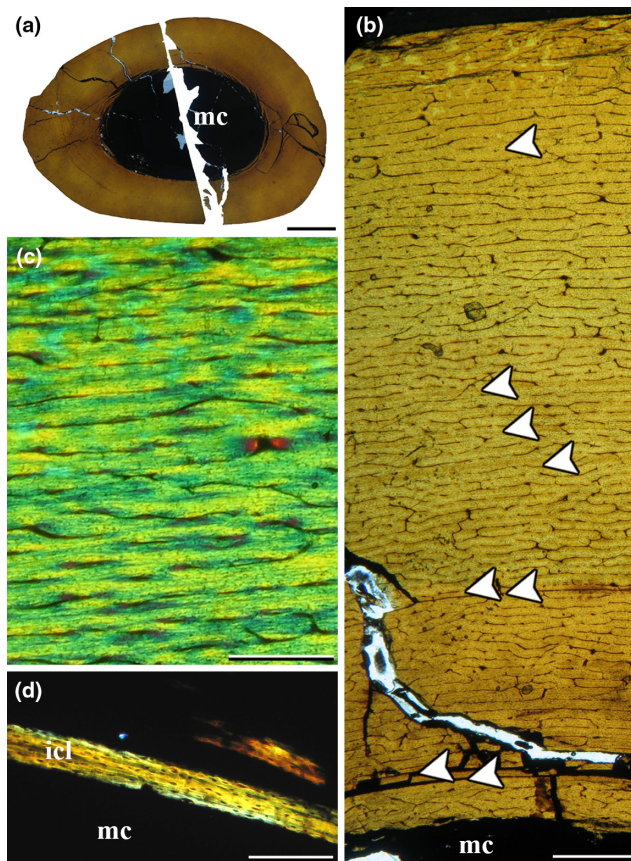


Fig. 17. Bone histological analysis of *Koleken inakayali* MPEF PV 10826 tibia. Lines of arrested growth (LAGs) are indicated with white arrowheads. (a) General view of the complete section. (b) General view of the compacta showing the position of the lines of arrested growth. (c) Primary bone tissue formed by well-vascularized parallel-fibred bone. (d) Detail of the perimedullary region showing a thin inner circumferential layer. (a, b) Plane polarized light; (c) cross polarized light with lambda compensator; (d) cross polarized light. icl: inner circumferential layer; mc: medullary cavity. Scale bars: 10 mm (a); 1 mm (b); 0.5 mm (c); 0.2 mm (d).

changes occur when individuals reach both somatic (i.e. asymptotic growth) and sexual maturity (Chinsamy Turan, 2005; Erickson, 2014). The attainment of somatic maturity is commonly inferred on the basis of the presence of an external fundamental system (EFS, also referred as an outer circumferential layer, OCL) in the subperiosteal cortex (Horner et al., 1999; Chinsamy Turan, 2005; Erickson, 2014). An EFS is a histological structure that, when present, is formed in the subperiosteal cortex, particularly within long bones. The EFS consist of a layer of poorly vascularized (or avascular) parallel-fibred or lamellar tissue which usually exhibits very closely spaced LAGs (Chinsamy Turan, 2005; Woodward et al., 2011). In the case of the sexual maturity attainment, it is generally assumed that the same occurred well before somatic maturity in non-avian dinosaurs (e.g. Sander, 2000; Erickson et al., 2007; Lee and Werning, 2008). Sexual maturity

is usually inferred on the basis of a distinct change in the spatial arrangement of intrinsic collagenous fibres (from disorganized to well-organized) and/or a clear reduction in the spacing between successive LAGs (e.g. Castanet and Baez, 1991; Khonsue et al., 2010). These changes are related to a decrease in the apposition bone growth rate originating from the allocation of more resources for reproduction rather than growth (Sander, 2000; Klein and Sander, 2008). The absence of a distinct EFS in the tibia of MPEF-PV 10826 indicates that the individual died before the attainment of somatic maturity. Furthermore, because a clear decrease in the bone apposition rate is not evident in the cortical bone, sexual maturity also appears to not have been reached by the individual. This subadult stage is supported by the presence of a very thin and incomplete ICL, attesting to medullary cavity expansion that had just ceased. Regarding growth cycle counting, we estimate a minimum age of 6 years for the specimen.

Taxonomic status and ontogenetic stage of Koleken

The description of *Koleken* involved comparisons with over 20 abelisauroid species, of which five species have published histology-based assessments of maturity (Pol and Rauhut, 2012; Lee and O'Connor, 2013; Aranciaga Rolando et al., 2021; Baiano et al., 2022; Baiano and Cerda, 2023). The holotype of *Koleken* has a comparable minimum age as that of *Niebla* (6 vs. 9 years old; Aranciaga Rolando et al., 2021), whereas others are represented by more mature individuals. Histological data of MPEF-PV 1826 agree with some osteological evidence that suggest this specimen was not fully grown. In the postcranium of *Koleken*, the presence of a neurocentral suture line in the dorsals is an indication of immaturity (Brochu, 1996). In its skull, the unfused nasals might suggest immaturity, although in abelisaurids such a straightforward inference is not possible, as the holotype of *Aucasaurus* is a sexually and somatically mature individual (11 years) that also lacks nasal fusion.

Nevertheless, all of the rostral and orbital bones known in the type of *Koleken* have well-developed rugosities and ornamentation on their surface, a feature that appears late in crocodylian ontogeny (Vickaryous and Hall, 2008; Clarac et al., 2015; de Buffrénil et al., 2015). This criterion was applied to justify the maturity of different tyrannosaurids among theropods (e.g. Carr et al., 2017), although at the moment we lack clade-specific criteria based on ontogenetic series of dinosaurian species (see Griffin et al., 2021). Moreover, some sutural contacts, such as the postorbital-frontal suture, are markedly interdigitated. In crocodylians the degree of interdigitation increases through ontogeny, playing a key role in cranial stress accommodation (Bailleul et al., 2016). These observations

are also compatible with the 6 years of minimum age based on histological data, as together they indicate that the specimen has acquired some osteological maturity, despite not being fully grown.

The intermediate ontogenetic stage of MPEF-PV 10826 provides some guidance in interpreting the anatomical differences from other abelisaurids, in particular the only other abelisaurid known from the La Colonia Formation (*Carnotaurus sastrei*; Bonaparte, 1985). Features known to be variable during late ontogeny for other archosaur taxa should be taken with caution if they are found (like the fusion of skull bones, or the visible neurocentral suture). However, features that are not known to vary in late ontogeny in other taxa can be more confidently interpreted as anatomical differences not related to ontogeny. Several of the differences described above between *Koleken* and *Carnotaurus* fall into this latter category. For example, the proximal tip of the lesser trochanter ends proximally to the ventral margin of the femoral head, whereas it ends below in *Carnotaurus*, *Ekrixinosaurus* and *Aucasaurus*. In addition, the autapomorphic dorsal neural spines of *Koleken* bearing an elevated rim along the anterior, dorsal and posterior margins in lateral view are not observed in other theropods in general. In fact, it would be unexpected to find more extensive bone deposition along rims or crests in early ontogenetic stages that are absent in later ontogenetic stages.

The skull bones of *Koleken*, in particular the nasal, frontal and postorbital, show differences from those of *Carnotaurus* that we consider highly unlikely to be the product of ontogenetic variation. The nasal in these two taxa has a different type of ornamentation on its dorsal surface: *Koleken* has a rugose lateral crest and a flat medial region covered with broad circular pits, whereas *Carnotaurus* has an evenly convex dorsal surface devoid of crests and with a more irregular tuberculate ornamentation. Their ornamentation is well-developed in both cases and different from each other rather than being less developed in *Koleken* than in *Carnotaurus*. The postorbital of *Koleken* has a remarkably low anterior process that has a height-to-length ratio that is 0.4, whereas this ratio is >0.8 in *Carnotaurus*. The dorsal surface of the postorbital of *Koleken* is lateromedially broad, ornamented and dorsally convex, but in *Carnotaurus* the posterior process has a narrow crest along its dorsal surface. These differences, in particular the latter, are hard to reconcile as an ontogenetic trajectory. Finally, the frontal of *Koleken* lacks the massive frontal horn that characterizes each frontal of *Carnotaurus* but instead has a gently convex dorsal surface with small tubercle ornamentation. Although horns appear early in other dinosaurian taxa (Horner and Goodwin, 2006), data from different specimens of the abelisaurid *Majungasaurus* indicate that there is variability (possibly both individual and ontogenetic)

in the development of the median eminence of the frontal in this taxon (Sampson and Witmer, 2007). At the moment, we lack additional data to evaluate variability among frontal eminences in abelisaurids given that almost all species are only known from their holotype. Thus, while some anatomical differences conveyed might be potentially ontogenetic, we consider that the set of anatomical features noted above is more likely to be the result of taxonomic differences rather than ontogenetic change.

Finally, given the most remarkable difference between *Koleken* and *Carnotaurus* is the presence of the remarkable horns of the latter, we need to consider the hypothesis of sexual dimorphism. To date, presence or absence of horns have not been documented as a case of sexual dimorphism in archosaurs, either extinct or extant (Padian and Horner, 2011; Hone et al., 2012), and have only been reported in a Triassic archosauromorph (Sengupta et al., 2017). More specifically, no dinosaur has been determined to exhibit sexual dimorphism under rigorous analysis (Mallon, 2017). Body size has been reported as a feature showing sexual dimorphism, but Hone and Mallon (2017) suggested that a minimum of 60 animals were needed to detect this difference in alligators. Thus, data from other dinosaurs (and more generally, archosaurs) do not suggest sexual dimorphism as a likely scenario, although with only two specimens at hand we are unable to rigorously test this hypothesis. Moreover, the differences found between the type of *Koleken* and *Carnotaurus* are not restricted to the frontal horns but extend to multiple other bones, including the postorbital, nasal, dorsal vertebrae, and femur. Therefore, at the moment we consider it more conservative to recognize these as taxonomic differences between two closely related abelisaurid species that lived during the Maastrichtian in central Patagonia.

Phylogenetic analyses without chronostratigraphic information

Parsimony. The parsimony analysis recovered $>100\,000$ MPTs (see the *mptsNEX.tre* file in [Supplementary Data](#)) with a length of 558 steps, a consistency index of 0.530 and a retention index of 0.769. The strict consensus (Fig. S1) collapses the entire ceratosaurian ingroup into a single polytomy, which is caused by the following 15 unstable taxa detected by the IterPCR method: *Afromimus*, *Dahalokely*, *Elemgasem*, *Genusaurus*, *Huinculsaurus*, *Kryptops*, *Kurupi*, *Noasaurus*, *Pycnonemosaurus*, *Quilmesaurus*, *Rahiolisaurus*, *Thanos*, as well as the unnamed specimens MNN TIG6, MPCN PV 69 and MPM 99. Logistic regression revealed a strong and significant relationship between incompleteness (fraction of missing or inapplicable matrix entries) and

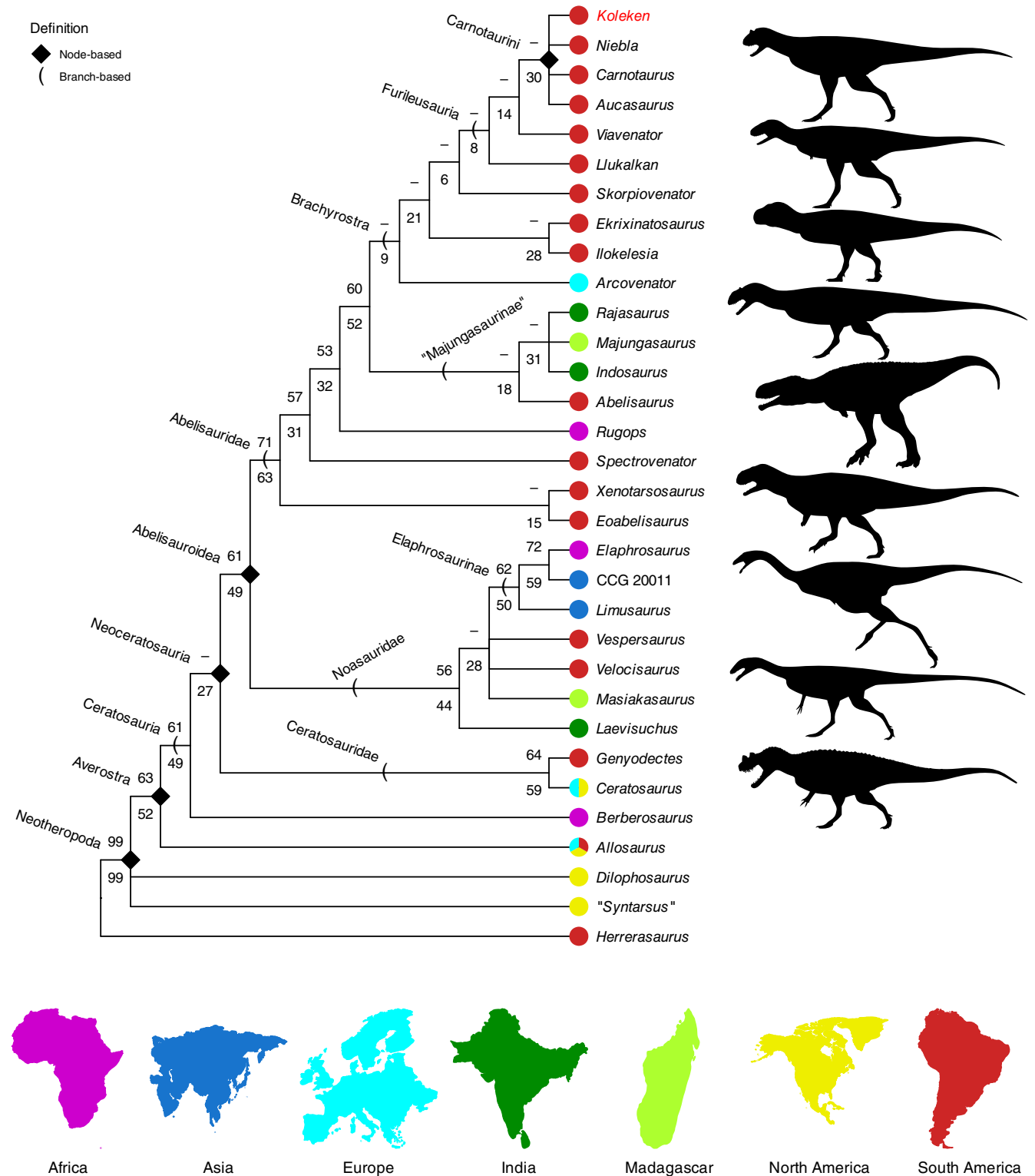


Fig. 18. Phylogenetic relationships of *Koleken inakayali* according to parsimony analysis. Reduced strict consensus of 100 000 most parsimonious trees after pruning the 15 unstable taxa detected using IterPCR. Node labels denote bootstrap support from 100 pseudoreplicates after disregarding the unstable taxa (top: absolute percentage if >50%, bottom: GC value). Ceratosaur silhouettes from PhyloPic (<http://phylopic.org>) courtesy of (from top to bottom): Scott Hartman (CC BY-NC-SA 3.0); Scott Hartman (CC BY-NC-SA 3.0); Jagged Fang Designs (CC0 1.0); Scott Hartman (CC BY-NC-SA 3.0); Tasman Dixon (CC BY 4.0); Iain Reid (CC BY 3.0); villesink (CC BY-NC-SA 3.0); Scott Hartman (CC BY-NC-SA 3.0); Scott Hartman (CC BY-NC-SA 3.0).

unstable status (McFadden's pseudo- $R^2 = 0.381$, $P = 0.009$). However, according to the IterPCR script, the only terminals that are unstable owing to lack of information are *Thanos*, MPCN PV 69, *Kryptops*, *Elemgasem* and *Genusaurus*. All other unstable taxa also exhibit character conflict that drives their alternative positions. When these unstable taxa are pruned from the trees, the reduced consensus shows a well-resolved topology with only three polytomies among derived noosaurids, 'majungasaurines' and within Carnotaurini (Fig. 18). Support values are markedly low across the tree (average BS = 17.3%, only three nodes with BS > 70%; see also Fig. S2). Well-supported nodes were identified using the *perjak* script, an exploratory analysis finding taxa that decrease nodal support (Fig. S3).

As in several previously published phylogenies (Baiano et al., 2021, 2022; Cerroni et al., 2022), there are several terminal taxa that form the basal branches of Abelisauridae (*Eoabelisaurus*, *Rugops*, *Spectrovenator*) and two major clades: Brachyrostra and 'Majungasaurinae' (Fig. 18). Brachyrostra includes derived Late Cretaceous forms from South America and possibly Europe, whereas 'Majungasaurinae' includes abelisaurids from India and Madagascar. Interestingly, *Abelisaurus* is recovered as a 'majungasaurine', rendering Majungasaurinae Tortosa et al., 2014 a junior synonym of Abelisaurinae Bonaparte and Novas, 1985 (ICZN, 1999: Articles 23.1, 36.1; see also Longrich et al., 2017; Baiano et al., 2021). However, the close affinities of *Abelisaurus* with 'majungasaurines' are weakly supported (Fig. 18) and it can be placed with brachyrostrans with two extra steps (see also Baiano et al., 2022). The retrieved topology may have nomenclatural consequences for the use of Majungasaurinae/Abelisaurinae but requires a detailed reevaluation of the affinities of *Abelisaurus*. Here, we provisionally continue to refer to 'majungasaurines' given the frequent use of this name in recent literature. Another difference is the position of *Arcovenator* within brachyrostrans rather than 'majungasaurines' as in the original analysis (Tortosa et al., 2014); however, this position is more robust as it takes four extra steps in our dataset to place *Arcovenator* in the original position.

Koleken is retrieved deeply nested within furileusaurian abelisaurids, forming a polytomy with *Carnotaurus*, *Aucasaurus* and *Niebla*. This node is unambiguously diagnosed by the presence of skull roof ornamentation along the lateral side (ch. 24–2), a medial fossa ventral to occipital condyle (ch. 67–0; unknown in the new taxon) and strongly dorsally (>50°) orientated transverse processes in anterior caudal vertebrae (ch. 243–3). *Koleken* and *Carnotaurus* are known from the same formation and are found as sister taxa in some MPTs, based on the following derived features: (i) the presence of 12 maxillary teeth or fewer (ch. 88–1; this

condition is shared with *Dilophosaurus* and noosaurids); and (ii) the absence of a groove on the ventral surface of the anterior caudal vertebrae (ch. 140–1; a condition shared with several abelisaurids). However, the parsimony analysis also places the new taxon in other positions as it is scored differently than *Carnotaurus* for several anatomical characters, such as: (i) the absence of a knob-like projection on the parietals (ch. 28–0; a condition similar to early branching averostrans as *Allosaurus*, *Ceratosaurus* and *Eoabelisaurus*) of *Koleken*, whereas in *Carnotaurus* there is a conspicuous protuberance in correspondence of the union of these bones; (ii) *Koleken* lacks the typical striations of the parietal plates (ch. 90–0; a condition present in early diverging theropods and several ceratosaurs such as *Ceratosaurus*, *Genyodectes*, *Rahiolisaurus*, *Spectrovenator* and noosaurids) observed in *Carnotaurus* and other abelisaurids; and (iii) *Koleken* also lacks an infrapopliteal ridge (ch. 206–0; a condition also present in several abelisaurids and noosaurids), which is present in *Carnotaurus*.

Bayesian analysis. The topology of the MCC summary tree obtained from the nonclock Bayesian analysis of all 47 taxa is poorly supported, with posterior probabilities (PPs) exceeding 0.95 for only three nodes, two of which are located outside the ingroup (Fig. S4). The relationships are generally similar to those recovered by the parsimony analysis (normalized polytomy-corrected RF distance from the reduced consensus tree: 0.302). Common features of both topologies include the placement of *Koleken* as a close relative of *Niebla* and *Aucasaurus*, although this clade has maximal support (PP = 1) in the Bayesian analysis, indicating that in contrast to the parsimony analysis, trees uniting *Koleken* with *Carnotaurus* were never sampled. The stratigraphically incongruous sister-group relationship between the Middle Jurassic *Eoabelisaurus* and the Late Cretaceous *Xenotarsosaurus* recovered by parsimony persists in the MCC tree. Using both methods, this relationship is very weakly supported (Bayesian PP = 0.57 and parsimony jackknife = 23%) but in the Bayesian analysis it is placed outside rather than within Abelisauroida (in contrast to the parsimony results).

Table 1
Bayes factor (BF) comparison of the two relaxed clock models. The 2 log BF values are given relative to the worst-fit model, and interpreted following the guidelines of Kass and Raftery (1995)

Clock model	Log marginal likelihood	2 log BF	Support
Linked across partitions	–1546.548	0	—
Unlinked across partitions	–1540.391	12.314	Very strong

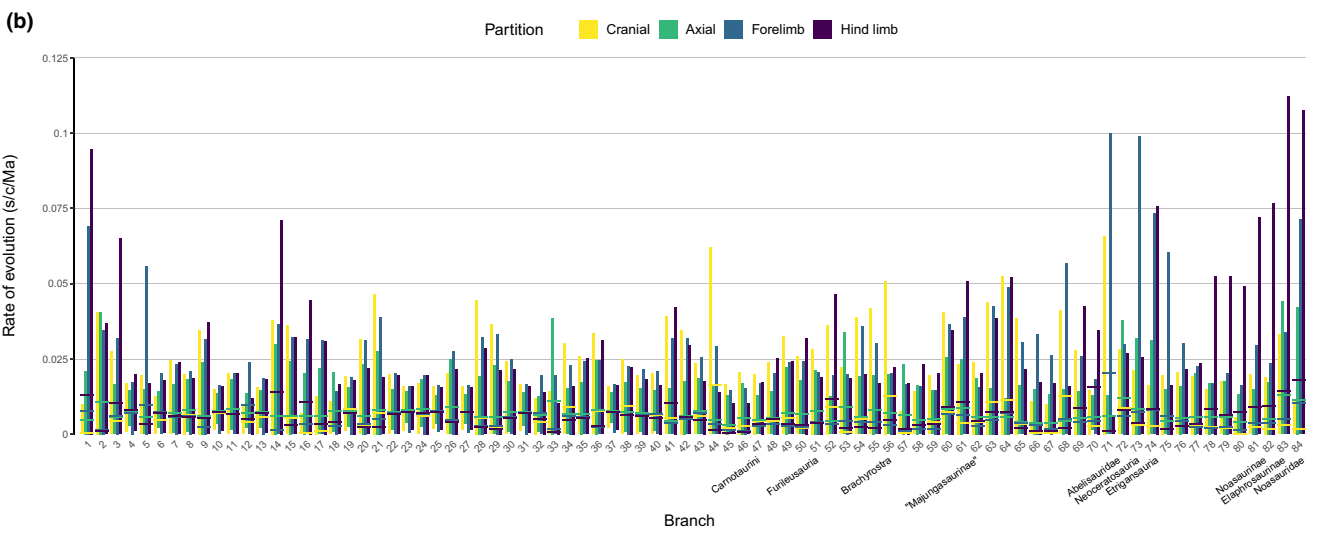
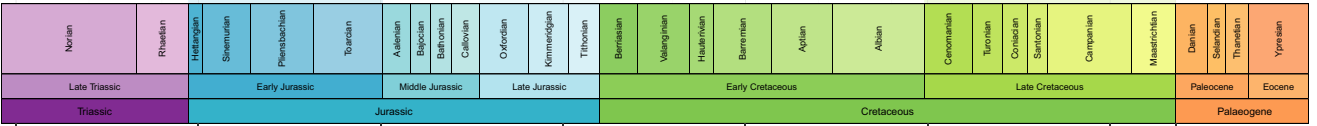
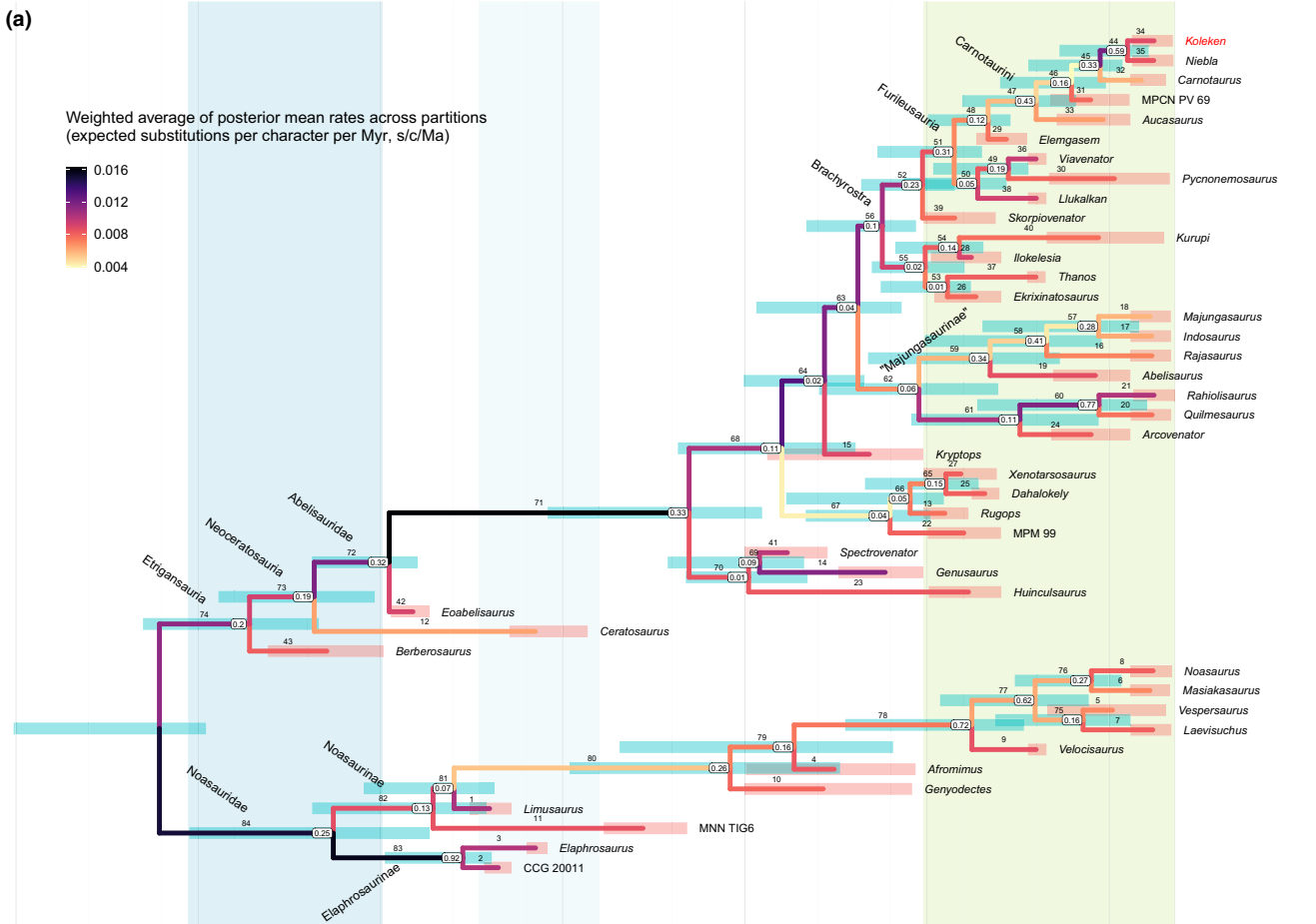


Fig. 19. Results of the Bayesian tip-dating analysis: (a) the maximum clade credibility (MCC) tree with posterior median node heights and (b) the partition-specific rates of morphological evolution estimated for its branches. In (a), the numbers next to individual nodes represent clade posterior probabilities, the blue bars indicate the 95% credibility intervals (CIs) for the ages of internal nodes, and the red bars denote the 95% CIs for the ages of individual tips. The branches are coloured by the average of partition-specific posterior mean rates of morphological evolution, weighted by the number of characters in each partition. The offset of the tree from the present is set to the posterior median age of the youngest tip. In (b), the horizontal lines represent the posterior median estimates of partition-specific branch rates, whereas the vertical bars denote the corresponding 95% CIs. Ordering along the horizontal axis follows the branch indices in panel (a).

Tip-dating analyses

The Bayes factor model comparison yielded a 2 log BF value of 12.314 in favour of the unlinked clock model (Table 1), corresponding to decisive support *sensu* Jeffreys (1961) or very strong support *sensu* Kass and Raftery (1995). The analysis performed under this favoured model yielded a MCC tree that differed substantially from both the parsimony estimate (normalized polytomy-corrected RF distance: 0.478) and the nonclock Bayesian MCC tree (normalized RF distance: 0.825) with respect to its topology (Fig. 19a). The split between the lineage leading to Abelisauridae (Etrigansauria *sensu* Delcourt, 2018) and the one leading to Noasauridae was recovered as the earliest divergence within Ceratosauria, in agreement with one previous dataset (Wang et al., 2017; see also Delcourt, 2018; Baiano et al., 2020). Three early branching taxa that had been consistently identified as non-abelisauroid ceratosaurs by almost all previous analyses are placed by the tip-dating analysis along the abelisaurid lineage (*Berberosaurus*, *Ceratosaurus*) or along the noosaurid lineage (*Genyodectes*). Another difference from the parsimony results is that *Xenotarsosaurus* is allied with other Cretaceous taxa rather than with *Eoabelisaurus* (Fig. 19a). These relationships contradict both the results obtained from the time-free methods (parsimony and nonclock Bayesian inference) as well as from all previous iterations of this dataset (Carrano and Sampson, 2008; Pol and Rauhut, 2012; Rauhut and Carrano, 2016; Baiano et al., 2021, 2022; Ibiricu et al., 2021; Cerroni et al., 2022). However, the unorthodox placements of the taxa mentioned above are very weakly supported in the tip-dating analysis (with $PP \leq 0.26$; Fig. 19a) and there is a considerable topological uncertainty across the whole tree (average $PP = 0.237$; Fig. 20). *Koleken* is recovered as the sister-group of *Niebla*, with the resulting clade being moderately supported as one of the few nodes whose posterior probability exceeded 0.5 (Figs 19a and 20). As in the other analyses, these two taxa are deeply nested within Furileusauria and closely allied with *Carnotaurus* and *Aucasaurus*.

Estimating divergence times in Ceratosauria

These results suggest that the inclusion of stratigraphic age information did little to increase

confidence in ceratosaur phylogenetic relationships, although it certainly affected the phylogenetic placement of certain taxa as noted above. The differences between the parsimony and tip-dating analyses also concern divergence times because these are estimated in different ways by the two methods. The *evolrates* script produces time trees using a step-wise approach. Trees are first inferred based on morphological characters in a parsimony analysis (ignoring stratigraphic information) and subsequently time-scaled based on maximum ages for each terminal taxon. In this approach, age and character data are used for different purposes: character data places taxa in the tree and age data places nodes along the geological time-scale. By contrast, Bayesian tip-dating simultaneously employs both character data and stratigraphic information to co-infer tree topology and node ages, averaging the topology estimates over the uncertainty in divergence times and the divergence time estimates over the uncertainty in topology. In tip-dating inference, branches with a larger amount of character change are, on average, more likely to have longer durations, potentially extending the history of certain clades well beyond their first appearance in the fossil record (which is used for the *evolrates* estimates). In some cases, the resulting discrepancies between the two methods are notable and cross important chronostratigraphic boundaries.

The first divergence among ceratosaurs is dated by the tip-dating analysis back to the latest Triassic (before the Triassic–Jurassic mass extinction event) with a posterior median age of 207.2 Ma (Fig. 19) and a 95% credible interval (CI) extending from the early Norian to the early Sinemurian (225.3–198.9 Ma). These values reflect the root age prior, which was based on the age of *Saltriovenator*, the oldest putative ceratosaurian (Dal Sasso et al., 2018). The calibration employing the maximum age of the oldest taxon places the origin of Ceratosauria close to the Sinemurian–Pliensbachian boundary (Fig. 21; 190.8 Ma) based on the age of *Berberosaurus*, the oldest ceratosaurian included in our dataset and likely the oldest uncontroversial member of the clade (Allain et al., 2007). Tip-dating estimates the earliest splits within both Noosauridae and Etrigansauria to be Early Jurassic in age, but for the latter clade, the older end of the 95% CI (207.6 Ma) also crosses the Triassic–Jurassic boundary. By contrast, the divergence time of Noosauridae in the

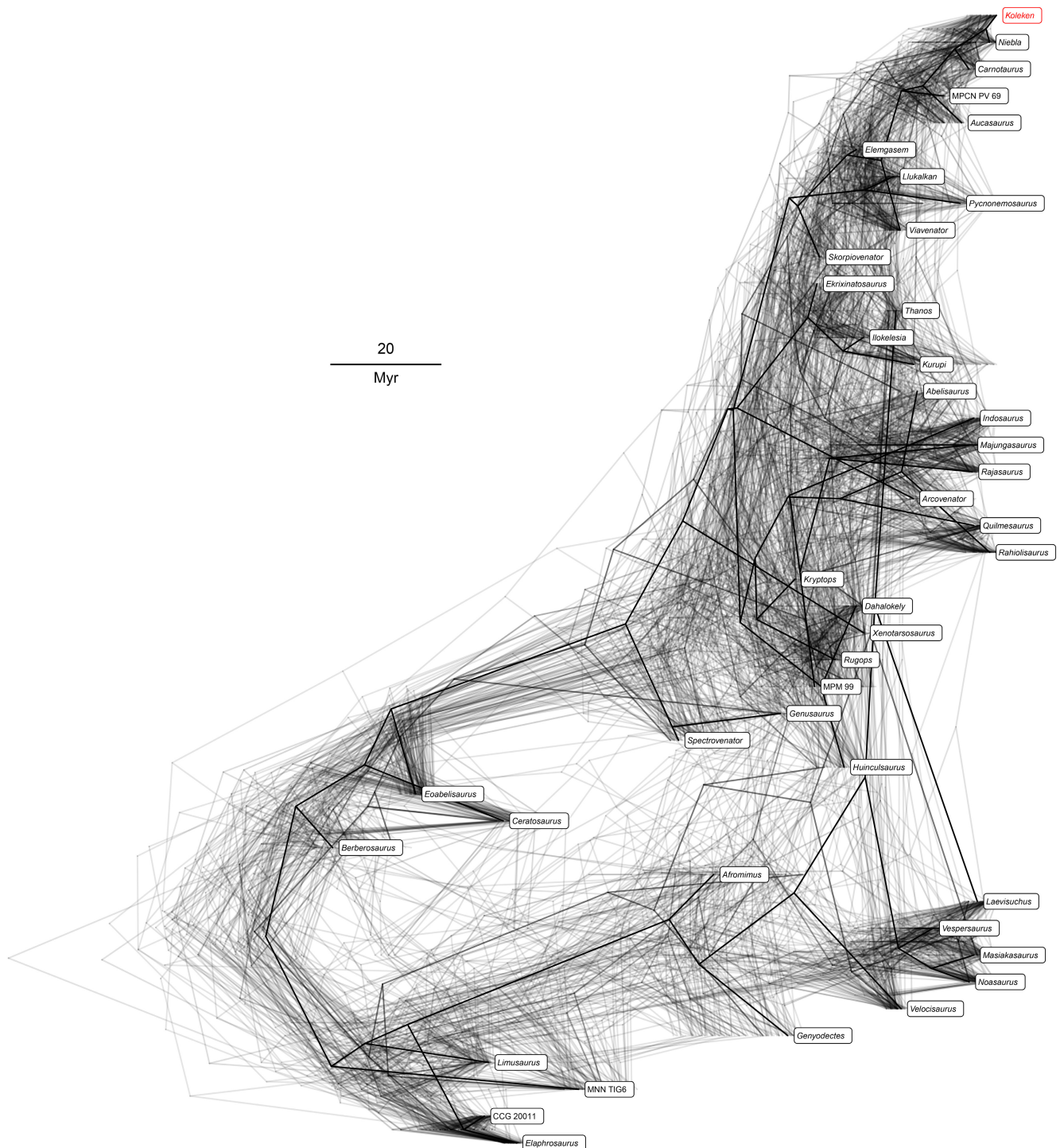


Fig. 20. DensiTree (Bouckaert, 2010) representation of 101 trees yielded by the FBD tip-dating analysis, ordered by their posterior density (highest = most opaque, lowest = most transparent). The trees depicted represent 2.5% of the pooled posterior sample from all four replicates.

parsimony trees calibrated with maximum ages is dated close to the Middle–Late Jurassic boundary (163.5 Ma) given the age of the oldest noasaurid (*Limosaurus*; Xu et al., 2009). Etrigansauria is not recovered in the parsimony tree but *evolrates* would

date this clade at the Sinemurian–Pliensbachian boundary given *Berberosaurus* is its oldest sampled member (see above).

Furileusauria, the clade within which *Koleken inakayali* is included, has been noted (Coria and

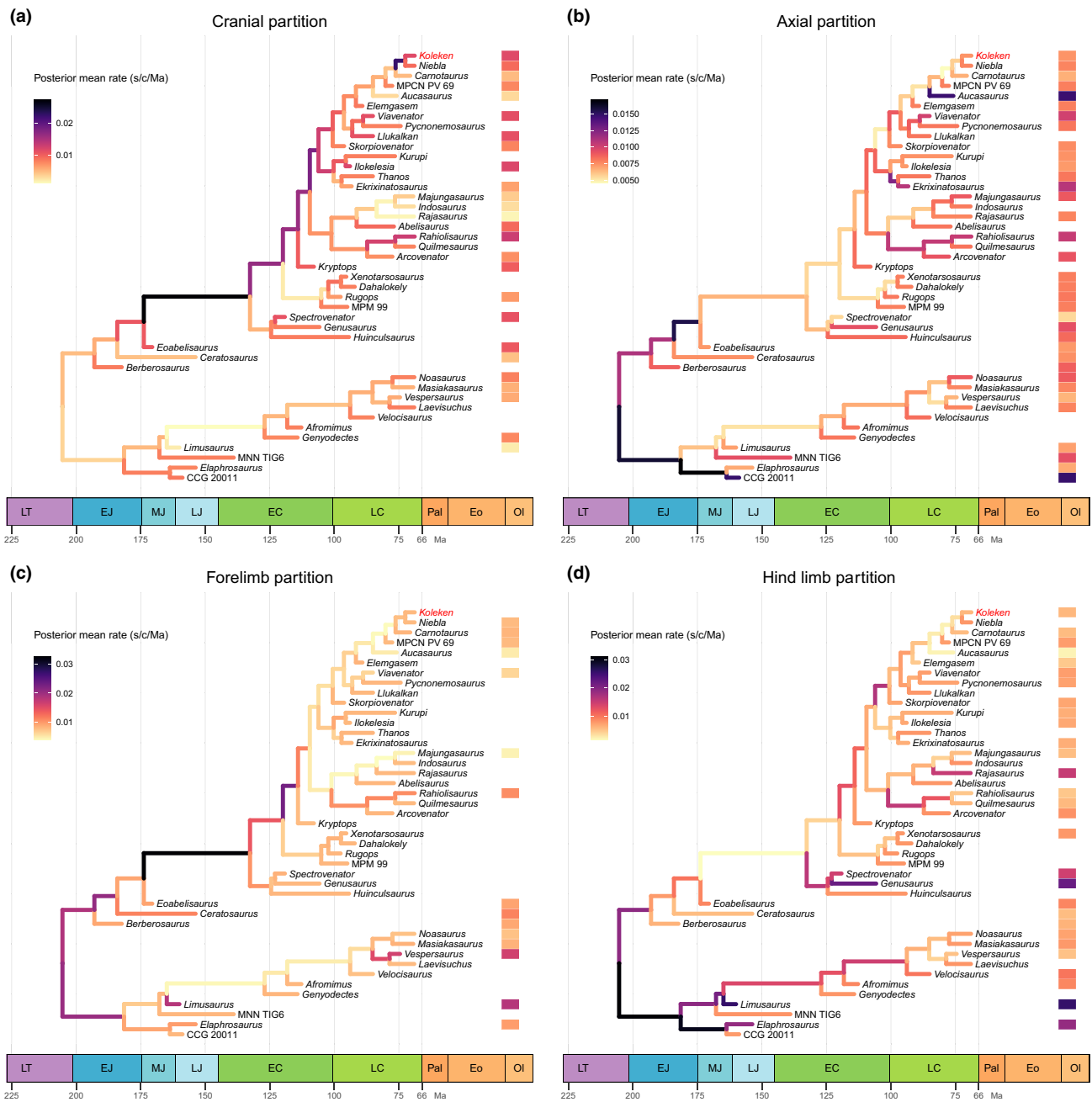


Fig. 21. Absolute rates of morphological evolution estimated for the (a) cranial, (b) axial, (c) forelimb and (d) hind limb partitions, plotted on the MCC tree from Fig. 19. Branch colours and scale bars denote posterior mean rates in units of expected substitutions per character per Myr. Boxes to the right of each tree indicate the presence or absence of character data for a given tip, and are coloured according to the mean posterior rate for tips with nonmissing data.

Salgado, 2005; Novas et al., 2005; Baiano et al., 2022) to diversify after a major faunal turnover among South American dinosaurs around the Cenomanian–Turonian boundary (93.9 Ma). A similar turnover event has also been reported among vertebrate and invertebrate lineages (Elder, 1987; Apesteguía, 2002), and extinction levels have been estimated to reach 30% among

marine organisms (Hut et al., 1987; Sepkoski, 1996). This is, in fact, the age estimated in the parsimony trees calibrated with maximum ages given the age of *Elmgasem*, its oldest member (Baiano et al., 2022). The Bayesian tip-dating analysis places the origin of Furileusauria before this event, in the Cenomanian (98.6 Ma), but its 95% CI (106.8–92.4 Ma) extends to

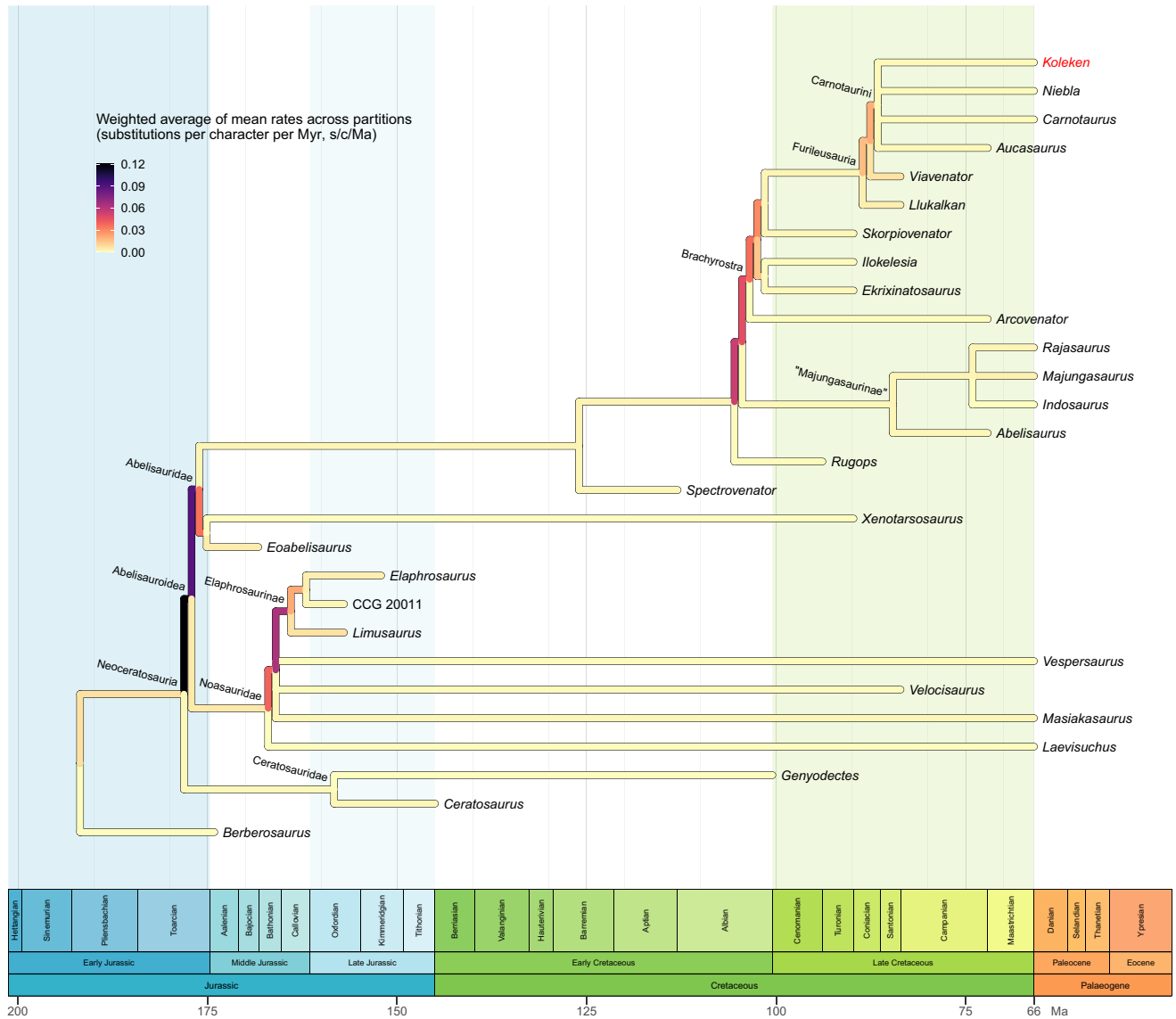


Fig. 22. Results of the parsimony analysis calibrated against geological time. The branches are coloured by the average of partition-specific mean rates of morphological evolution, weighted by the number of characters in each partition. Rates of morphological change were calculated on the MPTs but plotted on the reduced consensus tree from Fig. 18.

the base of the Turonian. In the tip-dated analysis, the average 95% CI width is 19.7 Ma for the ages of internal nodes and 8.9 Ma for the tip ages. The tip-dating results have a better stratigraphic fit (MCC tree: $MSM^* = 0.36$, $GER = 0.93$, $P = 0.001$; all trees: $MSM^* = 0.22–0.52$, $GER = 0.87–0.96$) than the parsimony trees. This is expected, as tip-dating utilizes stratigraphic age information for the inference of tree topology. The MPTs have stratigraphic fit ranges ($MSM^* = 0.11–0.16$, $GER = 0.69–0.80$) that are nonetheless significantly better ($P = 0.001$) than a random assignment of observed ages to the terminal taxa.

Evolutionary rates in Ceratosauria

Overall rates. Both the parsimony-based and Bayesian analyses show that the highest evolutionary rates among ceratosaurs occurred during their initial radiation in the Jurassic (Figs 19 and 22). Although direct comparisons between the two methods are hindered by differences between the topologies on which the rates were estimated (Figs 19 and 22), both infer high rates of morphological evolution in basal branches of Noasauridae, which diverged from each other in the Early to Middle Jurassic. Both methods

coincide in inferring high rates for the branch subtending Elaphrosaurinae, dated to the Early to Middle Jurassic by tip-dating and to the Middle Jurassic by the time-scaled parsimony tree. In the parsimony-based analysis, this inference may have been influenced by the highly distinctive body plan of *Limusaurus* (Xu et al., 2009). However, the elaphrosaurine rates are still estimated to be very high even by the Bayesian analysis, which recovers *Limusaurus* in Noasaurinae rather than Elaphrosaurinae, in contrast to most recent studies (e.g. Rauhut and Carrano, 2016; but see Dal Sasso et al., 2018).

Both analyses also agree in inferring high rates of evolution either at the origin of Abelisauridae (parsimony; Fig. 22) or very close to it (tip-dating; Fig. 19). These are likely to reflect the establishment of many characteristic abelisaurid features (e.g. low neural arches with epiprezygapophyseal lamina, wide spinoprezygapophyseal fossa, frontoparietal fusion), which have been recognized since the group was first described (Bonaparte, 1985; Bonaparte and Novas, 1985; Bonaparte et al., 1990). Within Abelisauridae, both methods infer a second pulse with moderately high evolutionary rates of evolution for the branches associated with the Early Cretaceous radiation of the clade (Figs 19 and 22), including the origin and earliest evolution of Brachyrostra. The relatively high evolutionary rate sustained through this time is likely to have resulted in the distinctive appearance of Cretaceous abelisaurids (e.g. skull with short and high rostrum, presence or ornamentation on dermal skull bones, short cervical vertebrae, reduction of forelimb length, and low and elongated ilium). Both the parsimony-based and Bayesian analyses find that the rate of overall evolutionary change gradually decreases during the Late Cretaceous (Figs 19 and 22), albeit with the exception of some ‘majungasaurine’ branches in Bayesian tip-dating (Fig. 19). Interestingly, the tip-dating analysis infers a fairly high rate of evolution for the putative clade uniting *Koleken* and *Niebla* (Fig. 19), a clade that is not unambiguously supported in the parsimony analysis.

The rates inferred for terminal branches also show disparate results between the two methods. The rates estimated in the parsimony-based analysis for the terminal branches are uniformly low (0–0.0070 s/c/Ma), reflecting their long average temporal duration (28.55 Ma) in the trees calibrated by maximum ages. In the tip-dated tree, terminal branches are much shorter on average (9.13 Ma), resulting in faster rates (range 0.0058–0.0116 s/c/Ma). This is a consequence of both topological differences and the treatment of tip ages, which are drawn from the uncertainty ranges of the corresponding taxa by tip-dating but always extended to the younger end of such ranges by *evolrates*.

Partition-specific rates. In addition to calculating rates for the entire dataset, we also conducted partitioned rate analyses for four different anatomical regions (skull, axial skeleton, forelimb and hind limb). Although there are differences between the two methods, both analyses agree that there is no branch whose evolution is uniformly accelerated across all four anatomical regions (Figs 21 and 23). The high evolutionary rates mentioned above for Elaphrosaurinae are predominantly caused by changes in the axial and hind limb skeleton (Figs 21b,d and 23b,d). In fact, in the tip-dating analysis, the rates of hind limb evolution along the branches subtending Elaphrosaurinae and Noasauridae represent some of the highest rates inferred by this study (with the 95% CI containing values >0.1 s/c/Ma).

Within Abelisauridae, the evolutionary rates of cranial characters generally exceed the three postcranial partitions according to both parsimony-based and Bayesian analyses (Figs 21 and 23). The Early Cretaceous diversification of abelisaurids shows consistently high rates of evolution in the cranial partition as estimated by both methods. During the Early Cretaceous abelisaurid radiation, postcranial characters generally exhibit low evolutionary rates (Fig. 21, 23 and S8), except for a small number of branches in the forelimb partition according to the tip-dating analysis (Fig. 21) and the axial partition according to the parsimony-based analysis (Fig. 23). For instance, the forelimb partition shows high rates for the basal branches of abelisaurids above *Eoabelisaurus* that extend through the Late Jurassic and Early Cretaceous (Fig. 21c). This is likely to accommodate the large morphological difference in the forelimb anatomy between *Eoabelisaurus* and Late Cretaceous abelisaurids. The tip-dating analysis infers especially high rates (with the 95% CI including values >0.1 s/c/Ma) for the first branch above *Eoabelisaurus* that spans over 40 Myr (from the Middle Jurassic to the Early Cretaceous), and moderately high rates for the three subsequent basal branches of abelisaurids the jointly extend through the last 20 Myr of the Early Cretaceous. This pattern of a longer and more accelerated basal branch and decreasing rates inferred along the three subsequent shorter branches is intriguing given the fact that none of the abelisaurids known from the Middle–Late Jurassic and Early Cretaceous have known forelimb elements.

During the Late Cretaceous, both methods agree on a general pattern: rates of cranial evolution are moderately high in the Late Cretaceous close to the base of Brachyrostra, but noticeably lower across the rest of the lineage in the Late Cretaceous (Figs 19a, 23a and S8). This suggests that at least for the cranium, the establishment of the abelisaurid body plan during the Early Cretaceous was followed by sustained high rates of evolution, echoing a pattern recently inferred

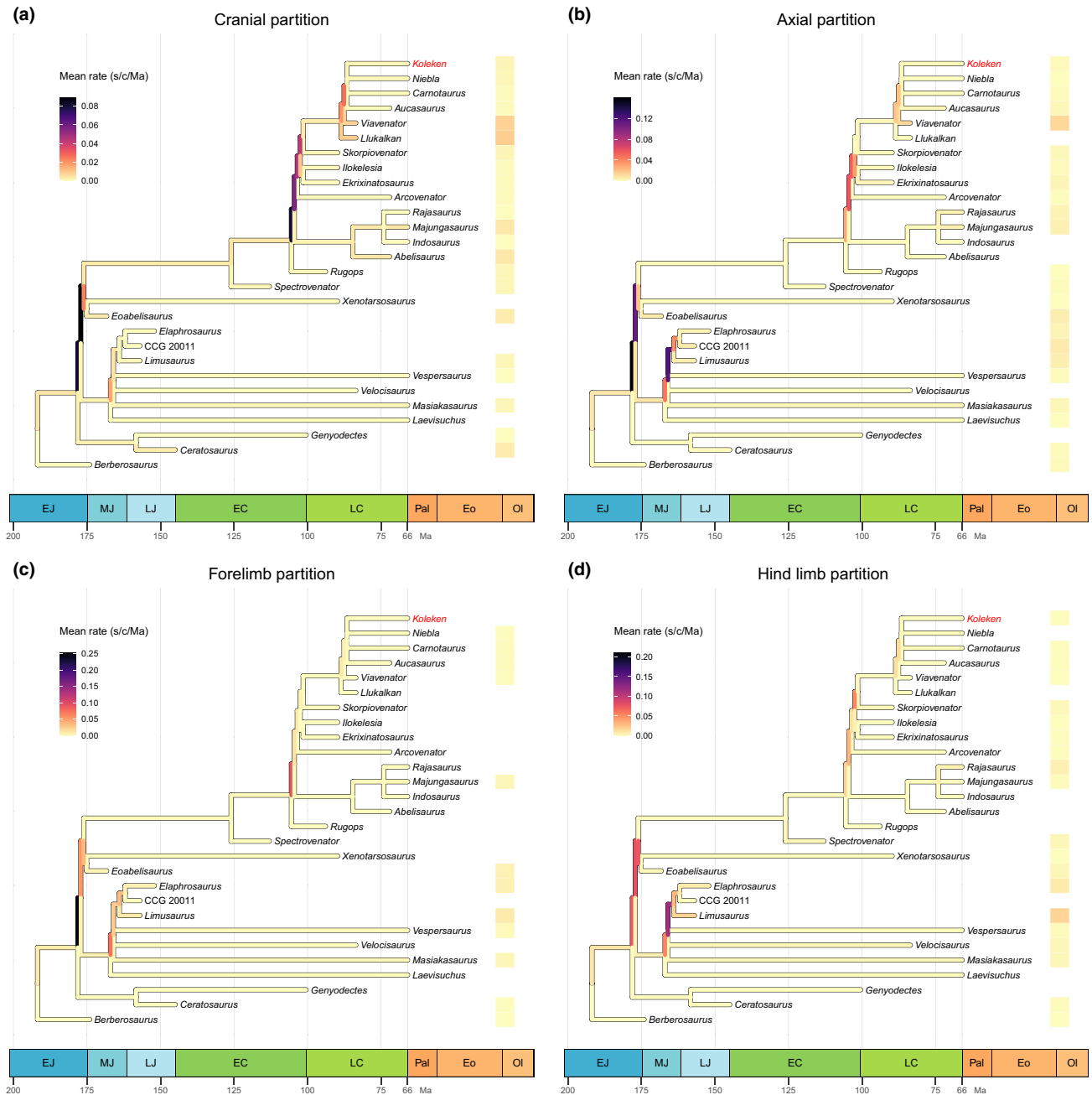


Fig. 23. Rates of morphological evolution estimated by the parsimony analysis for the (a) cranial, (b) axial, (c) forelimb and (d) hind limb partitions, calculated based on the MPTs but plotted on the consensus tree from Fig. 18. Branch colours and scale bars denote mean rates in units of substitutions per character per Myr. Boxes to the right of each tree indicate the presence or absence of character data for a given tip, and are coloured according to the mean rate for tips with nonmissing data.

at the origin of birds (Brusatte et al., 2014). All character partitions show moderate-to-low rates in nearly all abelisaurids in the parsimony-based analysis (Fig. 23). This is in general agreement with the tip-dating analysis, which infers overall lower rates except for relatively high rates of evolution in some branches and partitions, such as for the axial skeleton in

Aucasaurus (Fig. 20b). Another difference between the two rate estimation approaches in this part of the tree is found in the clade uniting *Koleken* and *Niebla* (Fig. 21), which is characterized by a high rate of evolution in the tip-dating analysis. The partitioned analysis shows it was the skull that drove the high overall rates estimated by the tip-dating analysis for this clade,

which exhibits one of the highest rates of cranial evolution in the tree (Figs 19b and 21a; posterior mean cranial rate: 0.022 s/c/Ma). This case may exemplify how differently the two methods perform in the presence of uncertainty owing to the high amount of missing data, because the overlap between these two taxa is limited to five characters: three in the cranial partition and two in the axial skeleton. The parsimony-based inference is influenced by optimization uncertainties and by the lack of resolution among these two abelisaurids and other latest Cretaceous taxa (e.g. *Carnotaurus*, *Aucasaurus*), and yields low average rate values for all these branches (Fig. 23).

Despite the above-noted differences in parts of the tree, the two methods agree that for most partitions ceratosaurian theropods had an “early burst”-like pattern of evolution (Simpson, 1944; Harmon et al., 2010), with rates of evolution slowing down as the clade diversified. As noted above, there are differences in the details of this early accelerated evolution as reconstructed by the two methods and it remains to be tested if this is a genuine pattern, or how much it is influenced by the paucity and/or incompleteness of abelisaurid taxa from the Jurassic and earliest Cretaceous.

The differences noted above for the two methods can be important for understanding some stages in ceratosaurian evolution and may be due to a number of reasons. These include topological differences between the parsimony and tip-dating analyses, as well as the distinct ways in which the two methods estimate the amount of character change, date the tree and handle missing data. Parsimony minimizes the overall amount of character change along branches, whereas tip-dating uses an evolutionary model to correct for multiple hits (Huelsenbeck et al., 2001; Swofford et al., 2001) so that it will generally infer greater amounts of change along branches (i.e. longer branches in terms of expected changes per character). Accordingly, tip-dating may be expected to estimate higher branch rates. However, the rate of a given branch is a function of both its length and its duration, and the latter quantity varies in a less straightforward manner between the two approaches.

When the same taxon represents the oldest known descendant of two nested nodes, *evolrates* will estimate the branch connecting these two nodes to have a duration of zero, and artificially expand it to a small arbitrary value (here set to 1 Ma). This leads to a clustering of very short internal branches in the time-scaled parsimony tree (Figs 22 and 23). In the tip-dating approach, the durations of internal branches are not set to a fixed value. As a result, tip-dating often estimates longer durations for internal branches (tip-dating mean: 9.66 Ma; *evolrates* mean: 8.21 Ma) (cf. Figs 19 and 22). These longer branch durations

can, in turn, be expected to favour slower branch rates, which is borne out by comparing the corresponding total (tip-dating: 0.0039–0.0162 s/c/Ma; *evolrates*: 0.0012–0.1205 s/c/Ma) and interquartile (tip-dating: 0.0070–0.0092 s/c/Ma; *evolrates*: 0.0025–0.0395 s/c/Ma) ranges.

Finally, both methods also differ in their treatment of missing data in terminal taxa. To minimize the length of the tree, parsimony assumes no change in terminal branches for characters scored with missing entries, skewing the overall distribution of branch rates downward. In the tip-dating approach, the rates of branches without data are instead drawn from a prior distribution, whose shape is affected by hyperpriors and estimated from the character matrix as a whole. In effect, tip-dating samples rates for taxa with missing data from what was determined to be a plausible range based on the data present in the remaining taxa.

Irrespective of the differences of two methods, both of them also agree that noosaurids and abelisaurids may have been characterized by fundamentally different modes of morphological evolution. Both methods agree that noosaurid evolution was primarily characterized by early high rates in the axial and hind limb skeleton (although more data on the skull of noosaurids are needed to rigorously test this hypothesis). However, the two methods differ in their inferences about abelisaurid evolution. Bayesian tip-dating infers comparatively slow morphological change in the Early Jurassic followed by a pulse of accelerated skull and forelimb evolution in the Late Jurassic–Early Cretaceous, whereas parsimony methods reconstruct high evolutionary rates in the skull and axial skeleton in the Early Jurassic and a second pulse during the Early Cretaceous. Whereas the two analytical methods coincide in many patterns, especially when fossil diversity is more densely sampled (e.g. Late Cretaceous abelisaurids), there are important differences in areas of the tree or periods of time in which fossils are scarce (e.g. Late Jurassic, earliest Cretaceous) and missing data are more abundant (e.g. forelimb anatomy). Further evidence will be necessary to determine the so-far obscure early period of ceratosaurian evolution where alternative methods provide disparate answers.

Acknowledgements

We thank the Secretaría de Cultura of the Chubut Province for granting the permits to conduct fieldwork in the La Colonia Formation. We thank the successive teams of La Colonia field expeditions that contributed to the development of this project, particularly to Pablo Puerta who has played a pivotal role in the field logistics of this project and José O’Gorman who found this specimen. We thank the personnel of the prep lab

at the Museo Paleontológico Egidio Feruglio that prepared this specimen, especially to Mariano Caffa and Ariel Aresti who prepared most of the materials here described. We thank Maria Agostinho for taking the photographs. Recent exploration efforts for the La Colonia field project have been possible thanks to funding by the National Geographic Society (92822R-22 to DP) and the School of Life Sciences of The Chinese University of Hong Kong (to MP). MP's participation in this project was also supported by the School of Life Sciences of The Chinese University of Hong Kong. Rumayl Irfan Mangi is thanked for his help preparing the specimen figures as part of an undergraduate research placement in MP's laboratory. Joseph Stiegler is thanked for his comments on the specimen. DČ thanks Ben Redelings, Sebastian Höhna, Joëlle Barido-Sottani and Jiansi Gao for their help with RevBayes, including bug fixes that proved essential to the analyses described in this paper, and to Alessio Capobianco, Sebastian Höhna, Rachel Warnock and April Wright for stimulating discussions about Bayesian morphological phylogenetics. All Bayesian phylogenetic analyses were performed on the Midway3 Research Computing Cluster at the University of Chicago. All parsimony analyses were conducted in TNT and The Willi Hennig Society is thanked for subsidizing this software and making it freely available. Finally, we thank Mauricio Cerroni, Christophe Hendrickx and Oliver Rauhut for their constructive reviews that greatly improved the quality of the manuscript.

Author contributions

DP, MAB and MP described the specimen and ran the parsimony analysis. DČ ran the Bayesian phylogenetic analyses. DP and DČ ran the parsimony-based and Bayesian evolutionary rate analyses, respectively. IAC conducted the histological analysis. DP, MAB, DČ, IAC and MP wrote the discussion and methods sections. DP, MAB, DČ, FEN, IAC and MP edited and approved the final version of the manuscript.

Conflict of interest

None declared.

Data availability statement

Data is available in full between this manuscript (and its [Supporting Information](#)) and [Supplementary Data](#) archived as a permanent digital record in the

CUHK Research Data Repository at this URL: <https://doi.org/10.48668/X53LJM>. This published work and the nomenclatural acts it contains have been registered in ZooBank. Publication LSID urn:lsid:zoo-bank.org:pub:C2725A43-7C4A-448A-A11D-DD5D33AFC31A. Genus LSID urn:lsid:zoo-bank.org:act:8E384B7B-6731-40DF-B65B-035AD7DB753B. Species LSID urn:lsid:zoo-bank.org:act:A147BAD3-87F0-403F-A1C0-2067D0B11169.

References

- Accarie, H., Beaudoin, B., Dejax, J., Friès, G., Michard, J.G. and Taquet, P., 1995. Discovery of a new theropod dinosaur *Genusaurus sisteronis* ng, n. sp. in the marine Albian of Sisteron (Alpes de haute-Provence, France) and the extension into the Lower Cretaceous of the Ceratosaur lineage. *Comptes rendus-academie des sciences Paris serie 2 sciences de la terre et des planetes fascicule A*, 320, 327.
- Agnolín, F.L., Powell, J.E., Novas, F.E. and Kundrát, M., 2012. New alvarezsaurid (Dinosauria, Theropoda) from uppermost Cretaceous of north-western Patagonia with associated eggs. *Cretac. Res.* 35, 33–56.
- Agnolín, F.L., Cerroni, M.A., Scanferla, A., Goswami, A., Paulina-Carabajal, A., Halliday, T., Cuff, A.R. and Reuil, S., 2021. First definitive abelisaurid theropod from the Late Cretaceous of northwestern Argentina. *J. Vertebr. Paleontol.* 41, e2002348.
- Albino, A.M., 2000. New record of snakes from the Cretaceous of Patagonia (Argentina). *Geodiversitas* 22, 247–253.
- Allain, R., Tykoski, R., Aquesbi, N., Jalil, N.E., Monbaron, M., Russell, D. and Taquet, P., 2007. An abelisauroid (Dinosauria: Theropoda) from the Early Jurassic of the high Atlas Mountains, Morocco, and the radiation of ceratosaurids. *J. Vertebr. Paleontol.* 27, 610–624.
- Allman, E.S., Holder, M.T. and Rhodes, J.A., 2010. Estimating trees from filtered data: identifiability of models for morphological phylogenetics. *J. Theor. Biol.* 263, 108–119.
- Apesteeguía, S., 2002. Successional structure in continental tetrapod faunas from Argentina along the Cretaceous. *Boletim do VI Simposio sobre o Cretaceo do Brasil-II, Abstracts book*, 135–141.
- Apesteeguía, S., Agnolín, F. and Claeson, K., 2007. Review of Cretaceous dipnoans from Argentina (Sarcopterygii: Dipnoi) with descriptions of new species. *Rev. Mus. Argent. Cienc. Nat., n.s.* 9, 27–40.
- Apesteeguía, S., Luzuriaga, J.E.S., Gallina, P.A., Granda, J.T. and Jaramillo, G.A.G., 2020. The first dinosaur remains from the Cretaceous of Ecuador. *Cretac. Res.* 108, 104345.
- Aranciaga Rolando, M., Cerroni, M.A., Marsà, J.A.G., Motta, M.J., Rozadilla, S., Eglí, F.B. and Novas, F.E., 2021. A new medium-sized abelisaurid (Theropoda, Dinosauria) from the Late Cretaceous (Maastrichtian) Allen Formation of northern Patagonia, Argentina. *J. S. Am. Earth Sci.* 105, 102915.
- Aranciaga Rolando, A.M., Motta, M.J., Agnolín, F.L., Manabe, M., Tsuihiji, T. and Novas, F.E., 2022. A large Megaraptoridae (Theropoda: Coelurosauria) from Upper Cretaceous (Maastrichtian) of Patagonia, Argentina. *Sci. Rep.* 12, 6318.
- Baiano, M.A. and Cerda, I.A., 2023. Osteohistology of *Aucasaurus garridoi* (Dinosauria, Theropoda, Abelisauridae): inferences on lifestyle and growth strategy. *Hist. Biol.* 35, 693–704.
- Baiano, M.A. and Filippi, L.S., 2022. New allosauroid (Theropoda, Tetanurae) remains from the Sierra Barrosa Formation (middle Coniacian, Upper Cretaceous), Patagonia, Argentina. *Publ. Electron. Assoc. Paleontol. Argent.* 22, 1–10.
- Baiano, M.A., Coria, R.A. and Cau, A., 2020. A new abelisauroid (Dinosauria: Theropoda) from the Huincul Formation (lower Upper Cretaceous, Neuquén Basin) of Patagonia, Argentina. *Cretac. Res.* 110, 104408.

- Baiano, M.A., Coria, R.A., Canale, J.I. and Gianechini, F.A., 2021. New abelisaurid material from the Anacleto Formation (Campanian, Upper Cretaceous) of Patagonia, Argentina, shed light on the diagnosis of the Abelisauridae (Theropoda, Ceratosauria). *J. S. Am. Earth Sci.* 110, 103402.
- Baiano, M.A., Pol, D., Bellardini, F., Windholz, G.J., Cerda, I.A., Garrido, A.C. and Coria, R.A., 2022. *Elemgasem nubilus*: a new brachyrostran abelisaurid (Theropoda, Ceratosauria) from the Portezuelo Formation (Upper Cretaceous) of Patagonia, Argentina. *Pap. Palaeontol.* 8, e1462.
- Baiano, M.A., Coria, R., Chiappe, L.M., Zurriaguz, V. and Coria, L., 2023. Osteology of the axial skeleton of *Aucasaurus garridoi*: phylogenetic and paleobiological inferences. *PeerJ* 11, e16236.
- Bailleul, A.M., Scannella, J.B., Horner, J.R. and Evans, D.C., 2016. Fusion patterns in the skulls of modern archosaurs reveal that sutures are ambiguous maturity indicators for the Dinosauria. *PLoS One* 11, e0147687.
- Barido-Sottani, J., Aguirre-Fernández, G., Hopkins, M.J., Stadler, T. and Warnock, R.C.M., 2019. Ignoring stratigraphic age uncertainty leads to erroneous estimates of species divergence times under the fossilized birth–death process. *Proc. R. Soc. B Biol. Sci.* 286, 20190685.
- Bellardini, F., Windholz, G.J., Baiano, M.A., Garrido, A.C. and Filippi, L.S., 2021. New titanosaur remains from the Portezuelo Formation (Turonian–Coniacian) and their implications for the sauropod faunal diversity of the southern Neuquén Basin, Patagonia, Argentina. *J. S. Am. Earth Sci.* 111, 103457.
- Bonaparte, J.F., 1985. A horned Cretaceous carnosaur from Patagonia. *Natl. Geogr. Res.* 1, 140–151.
- Bonaparte, J.F., 1991. Los vertebrados fósiles de la Formación Río Colorado, de la ciudad de Neuquén y cercanías, Cretácico Superior, Argentina. *Rev. Mus. Argent. Cienc. Nat., n.s.* 4, 15–123.
- Bonaparte, J.F., 1996. Cretaceous tetrapods of Argentina. *Münchener Geowiss. Abh.* 30, 73–130.
- Bonaparte, J.F. and Coria, R.A., 1993. Un nuevo y gigantesco saurópodo titanosaurio de la Formación Río Limay (Albiano-Cenomaniano) de la Provincia del Neuquén, Argentina. *Ameghiniana* 30, 271–282.
- Bonaparte, J.F. and Novas, F.E., 1985. *Abelisaurus comahuensis*, n. g., n. sp., Carnosauria from the Late Cretaceous of Patagonia. *Ameghiniana* 21, 259–265.
- Bonaparte, J.F., Franchi, M.R., Powell, J.E. and Sepulveda, E.G., 1984. La Formación Los Alamitos (Campaniano–Maastrichtiano) del sudeste de Río Negro, con descripción de *Kritosaurus australis* n. sp. (Hadrosauridae). Significado paleobiogeográfico de los vertebrados. *Rev. Asoc. Geol. Argent.* 39, 284–299.
- Bonaparte, J.F., Novas, F.E. and Coria, R.A., 1990. *Carnotaurus sastrei* Bonaparte, the horned, lightly built carnosaur from the Middle Cretaceous of Patagonia. *Contributions in Science, Natural History Museum of Los Angeles County*, 416, 1–42.
- Bonaparte, J.F. and Powell, J.E., 1980. A continental assemblage of tetrapods from the Upper Cretaceous beds of El Brete, northwestern Argentina (Sauropoda–Coelurosauria–Carnosauria–Aves). *Mém. Soc. géol. Fr., n.s.* 139, 19–28.
- Borel, C.M., Guler, M.V., Navarro, E.L. and Astini, R.A., 2016. Ancient coastal environments in a Maastrichtian–?Paleocene Atlantic shoreline: A phytoplankton approach. *Publ. Electrón. Asoc. Paleontol. Argent.* 16, 76–87.
- Bouckaert, R.R., 2010. DensiTree: making sense of sets of phylogenetic trees. *Bioinformatics* 26, 1372–1373.
- Bouckaert, R.R., Vaughan, T.G., Barido-Sottani, J., Duchêne, S., Fourment, M., Gavryushkina, A., Heled, J., Jones, G., Kühnert, D., De Maio, N., Matschiner, M., Mendes, F.K., Müller, N.F., Ogilvie, H.A., du Plessis, L., Poppinga, A., Rambaut, A., Rasmussen, D., Siveroni, I., Suchard, M.A., Wu, C.-H., Xie, D., Zhang, C., Stadler, T. and Drummond, A.J., 2019. BEAST 2.5: an advanced software platform for Bayesian evolutionary analysis. *PLoS Comput. Biol.* 15, e1006650.
- Brochu, C.A., 1996. Closure of neurocentral sutures during crocodylian ontogeny: implications for maturity assessment in fossil archosaurs. *J. Vertebr. Paleontol.* 16, 49–62.
- Brum, A.S., Pegas, R.V., Bandeira, K.L., Souza, L.G., Campos, D.A. and Kellner, A.W., 2021. A new unenlagiine (Theropoda, Dromaeosauridae) from the Upper Cretaceous of Brazil. *Pap. Palaeontol.* 7, 2075–2099.
- Brusatte, S.L., Lloyd, G.T., Wang, S.C. and Norell, M.A., 2014. Gradual assembly of avian body plan culminated in rapid rates of evolution across the dinosaur–bird transition. *Curr. Biol.* 24, 2386–2392.
- de Buffrénil, V. and Quilhac, A., 2021. Bone tissue types: a brief account of currently used categories. In: de Buffrénil, V., Zylberberg, L., Padian, K. and de Ricqlès, A. (Eds.), *Comparative skeletal histology and palaeohistology*. CRC Press, Boca Raton, FL, pp. 147–190.
- de Buffrénil, V., Clarac, F., Fau, M., Martin, S., Martin, B., Pellé, E. and Laurin, M., 2015. Differentiation and growth of bone ornamentation in vertebrates: a comparative histological study among the Crocodylomorpha. *J. Morphol.* 276, 425–445.
- Calvo, J.O. and Bonaparte, J.F., 1991. *Andesaurus delgadoi* gen. et sp. nov. (Saurischia–Sauropoda), titanosaurid dinosaur from the Río Limay Formation (Albian–Cenomanian), Neuquén, Argentina. *Ameghiniana* 28, 303–310.
- Calvo, J.O., Porfiri, J.D. and Kellner, A.W., 2004. On a new maniraptoran dinosaur (Theropoda) from the Upper Cretaceous of Neuquén, Patagonia, Argentina. *Arq. Mus. Nacional. Rio de Janeiro* 62, 549–566.
- Canale, J.I., Scanferla, C.A., Agnolín, F.L. and Novas, F.E., 2009. New carnivorous dinosaur from the Late Cretaceous of NW Patagonia and the evolution of abelisaurid theropods. *Naturwissenschaften* 96, 409–414.
- Canale, J.I., Apesteguía, S., Gallina, P.A., Mitchell, J., Smith, N.D., Cullen, T.M., Shinya, A., Haluza, A., Gianechini, F.A. and Makovicky, P.J., 2022. New giant carnivorous dinosaur reveals convergent evolutionary trends in theropod arm reduction. *Curr. Biol.* 32, 3195–3202.
- Carr, T.D., Varricchio, D.J., Sedlmayr, J.C., Roberts, E.M. and Moore, J.R., 2017. A new tyrannosaur with evidence for anagenesis and crocodile-like facial sensory system. *Sci. Rep.* 7, 44942.
- Carrano, M.T. and Hutchinson, J.R., 2002. Pelvic and hindlimb musculature of *Tyrannosaurus rex* (Dinosauria: Theropoda). *J. Morphol.* 253, 207–228.
- Carrano, M.T. and Sampson, S.D., 2008. The phylogeny of Ceratosauria (Dinosauria: Theropoda). *J. Syst. Palaeontol.* 6, 183–236.
- Carrano, M.T., Sampson, S.D. and Forster, C.A., 2002. The osteology of *Masiakasaurus knopfleri*, a small abelisauroid (Dinosauria: Theropoda) from the Late Cretaceous of Madagascar. *J. Vertebr. Paleontol.* 22, 510–534.
- Carrano, M.T., Loewen, M.A. and Sertich, J.J., 2011. New materials of *Masiakasaurus knopfleri* Sampson, Carrano, and Forster, 2001, and implications for the morphology of the Noosauridae (Theropoda: Ceratosauria). *Smithson. Contrib. Paleobiol.* 95, 1–53.
- Carrano, M.T., Benson, R.B. and Sampson, S.D., 2012. The phylogeny of Tetanurae (Dinosauria: Theropoda). *J. Syst. Palaeontol.* 10, 211–300.
- Castanet, J. and Baez, M., 1991. Adaptation and evolution in *Gallotia* lizards from the Canary Islands: age, growth, maturity and longevity. *Amphibia-Reptilia* 12, 81–102.
- Cerda, I.A., Pereyra, M.E., Garrone, M., Ponce, D., Navarro, T.G., Gonzalez, R., Militello, M., Luna, C.A. and Jannello, J.M., 2020. A basic guide for sampling and preparation of extant and fossil bones for histological studies. *Publ. Electrón. Asoc. Paleontol. Argent.* 20, 15–28.
- Černý, D., Madzia, D. and Slater, G.J., 2022. Empirical and methodological challenges to the model-based inference of diversification rates in extinct clades. *Syst. Biol.* 71, 153–171.

- Cerroni, M.A., Motta, M.J., Agnolín, F.L., Rolando, A.A., Egli, F.B. and Novas, F.E., 2020. A new abelisaurid from the Huincul Formation (Cenomanian-Turonian; Upper Cretaceous) of Río Negro province, Argentina. *J. S. Am. Earth Sci.* 98, 102445.
- Cerroni, M.A., Canale, J.I. and Novas, F.E., 2021. The skull of *Carnotaurus sastrei* Bonaparte 1985 revisited: Insights from craniofacial bones, palate and lower jaw. *Hist. Biol.* 33, 2444–2485.
- Cerroni, M.A., Baiano, M.A., Canale, J.I., Agnolín, F.L., Otero, A. and Novas, F.E., 2022. Appendicular osteology of *Skorpiovenator bustingorryi* (Theropoda, Abelisauridae) with comments on phylogenetic features of abelisaurids. *J. Syst. Palaeontol.* 20, 1–32.
- Chinsamy Turan, A., 2005. The Microstructure of Dinosaur Bones: Deciphering Biology Through Fine Scale Techniques. The Johns Hopkins University Press, Baltimore, 224 pp.
- Clarac, F., Souter, T., Cornette, R., Cubo, J. and de Buffrenil, V., 2015. A quantitative assessment of bone area increase due to ornamentation in the Crocodylia. *J. Morphol.* 276, 1183–1192.
- Clyde, W.C., Krause, J.M., De Benedetti, F., Ramezani, J., Cúneo, N.R., Gandolfo, M.A., Haber, P., Whelan, C. and Smith, T., 2021. New South American record of the Cretaceous–Paleogene boundary interval (La Colonia Formation, Patagonia, Argentina). *Cretac. Res.* 126, 104889.
- Coria, R.A., 2001. A new theropod from the Late Cretaceous of Patagonia. In: Tanke, D.H. and Carpenter, K. (Eds.), *Mesozoic Vertebrate Life*. Indiana University Press, Bloomington, IN, pp. 3–9.
- Coria, R.A. and Currie, P.J., 2006. A new carcharodontosaurid (Dinosauria, Theropoda) from the Upper Cretaceous of Argentina. *Geodiversitas* 28, 71–118.
- Coria, R.A. and Currie, P.J., 2016. A new megaraptoran dinosaur (Dinosauria, Theropoda, Megaraptoridae) from the Late Cretaceous of Patagonia. *PLoS One* 11, e0157973.
- Coria, R.A. and Salgado, L., 1995. A new giant carnivorous dinosaur from the Cretaceous of Patagonia. *Nature* 377, 224–226.
- Coria, R.A. and Salgado, L., 1996. A basal iguanodontian (Ornithischia: Ornithopoda) from the Late Cretaceous of South America. *J. Vertebr. Paleontol.* 16, 445–457.
- Coria, R.A. and Salgado, L., 2000. A basal Abelisauria Novas, 1992 (Theropoda-Ceratosauria) from the Cretaceous of Patagonia, Argentina. *Gaia* 15, 89–102.
- Coria, R.A. and Salgado, L., 2005. Mid-Cretaceous turnover of saurischian dinosaur communities: evidence from the Neuquen Basin. In: Veiga, G.D., Spalletti, L.A., Howell, J.A. and Schwarz, E. (Eds.), *The Neuquen Basin, Argentina: A Case Study in Sequence Stratigraphy and Basin Dynamics*. Geological Society of London, Special Publication, 252. Geological Society, London, UK, pp. 317–327.
- Coria, R.A., Chiappe, L.M. and Dingus, L., 2002. A new close relative of *Carnotaurus sastrei* Bonaparte 1985 (Theropoda: Abelisauridae) from the Late Cretaceous of Patagonia. *J. Vertebr. Paleontol.* 22, 460–465.
- Cruzado-Caballero, P., Gasca, J.M., Filippi, L.S., Cerda, I.A. and Garrido, A.C., 2019. A new ornithopod dinosaur from the Santonian of northern Patagonia (Rincón de los Sauces, Argentina). *Cretac. Res.* 98, 211–229.
- Cruzado-Caballero, P. and Powell, J., 2017. *Bonapartesaurus rionegrensis*, a new hadrosaurine dinosaur from South America: implications for phylogenetic and biogeographic relations with North America. *J. Vertebr. Paleontol.* 37, e1289381.
- Cúneo, N.R., Hermsen, E.J. and Gandolfo, M.A., 2013. *Regnellidium* (Salvinales, Marsileaceae) macrofossils and associated spores from the Late Cretaceous of South America. *Int. J. Plant Sci.* 174, 340–349.
- Cúneo, N.R., Gandolfo, M.A., Zamaloa, M.C. and Hermsen, E., 2014. Late Cretaceous aquatic plant world in Patagonia, Argentina. *PLoS One* 9, e104749.
- Currie, P.J. and Zhao, X.J., 1993. A new carnosaur (Dinosauria, Theropoda) from the Jurassic of Xinjiang, People's Republic of China. *Can. J. Earth Sci.* 30, 2037–2081.
- Dal Sasso, C., Maganuco, S. and Cau, A., 2018. The oldest ceratosaurian (Dinosauria: Theropoda), from the Lower Jurassic of Italy, sheds light on the evolution of the three-fingered hand of birds. *PeerJ* 6, e5976.
- De Benedetti, F., Zamaloa, M.D.C., Gandolfo, M.A. and Cúneo, N.R., 2018. Heterosporous ferns from Patagonia: the case of *Azolla*. In: Krings, M., Harper, C.J., Cúneo, N.R. and Rothwell, G.W. (Eds.), *Transformative Paleobotany*. Academic Press, Cambridge, MA, pp. 361–373.
- Delcourt, R., 2017. Revised morphology of *Pycnonemosaurus nevesi* Kellner & Campos, 2002 (Theropoda: Abelisauridae) and its phylogenetic relationships. *Zootaxa* 4276, 1–45.
- Delcourt, R., 2018. Ceratosaur palaeobiology: new insights on evolution and ecology of the southern rulers. *Sci. Rep.* 8, 9730.
- Elder, W.P., 1987. The paleoecology of the Cenomanian-Turonian (Cretaceous) stage boundary extinctions at Black Mesa, Arizona. *PALAIOS* 2, 24–40.
- Erickson, G.M., 2014. On dinosaur growth. *Annu. Rev. Earth Planet. Sci.* 42, 675–697.
- Erickson, G.M., Curry Rogers, K., Varricchio, D.J., Norell, M.A. and Xu, X., 2007. Growth patterns in brooding dinosaurs reveals the timing of sexual maturity in non-avian dinosaurs and genesis of the avian condition. *Biol. Lett.* 3, 558–561.
- Ezcurra, M.D. and Agnolín, F.L., 2012. A new global palaeobiogeographical model for the late Mesozoic and early Tertiary. *Syst. Biol.* 61, 553–566.
- Fabreti, L.G. and Höhna, S., 2021. Convergence assessment for Bayesian phylogenetic analysis using MCMC simulation. *Methods Ecol. Evol.* 13, 77–90.
- Farke, A.A. and Sertich, J.J., 2013. An abelisauroid theropod dinosaur from the Turonian of Madagascar. *PLoS One* 8, e62047.
- Filippi, L.S., Méndez, A.H., Valieri, R.D.J. and Garrido, A.C., 2016. A new brachyrostran with hypertrophied axial structures reveals an unexpected radiation of latest Cretaceous abelisaurids. *Cretac. Res.* 61, 209–219.
- Filippi, L.S., Méndez, A.H., Gianechini, F.A., Valieri, R.D.J. and Garrido, A.C., 2018. Osteology of *Viavenator exxoni* (Abelisauridae; Furileusauria) from the Bajo de la Carpa Formation, NW Patagonia, Argentina. *Cretac. Res.* 83, 95–119.
- Francillon-Vieillot, H., de Buffrenil, V., Castanet, J., Geraudie, J., Meunier, F.J., Sire, J.Y., Zylberberg, L. and Ricqlès, A., 1990. Skeletal biomineralization: patterns, processes and evolutionary trends. In: Carter, J.G. (Ed.), *Microstructure and Mineralization of Vertebrate Skeletal Tissues* (Vol. 1). Van Nostrand Reinhold, New York, USA, pp. 471–548.
- Gallego, J., Gandolfo, M.A., Cúneo, N.R. and Zamaloa, M.C., 2014. Fossil Araceae from the Upper Cretaceous of Patagonia, Argentina, with implications on the origin of free-floating aquatic aroids. *Rev. Palaeobot. Palynol.* 211, 78–86.
- Gallina, P. and Apesteguía, S., 2005. *Cathartesaura anaerobica* gen. et sp. nov., a new rebbachisaurid (Dinosauria, Sauropoda) from the Huincul Formation (Upper Cretaceous), Río Negro, Argentina. *Rev. Mus. Argent. Cienc. Nat., n.s.* 7, 153–166.
- Gandolfo, M.A., Cúneo, N.R. and Hermsen, E.J., 2014. Reporte preliminar sobre la paleoflora de la Formación La Colonia (Campaniano-Maastrichtiano, Cretácico Tardío), Chubut, Patagonia, Argentina. *Bol. Soc. Geol. Mex.* 66, 11–23.
- Gasparini, Z., Sterli, J., Parras, A., O'Gorman, J.P., Salgado, L., Varela, J. and Pol, D., 2015. Late Cretaceous reptilian biota of the La Colonia Formation, central Patagonia, Argentina: Occurrences, preservation and paleoenvironments. *Cretac. Res.* 54, 154–168.
- Gavryushkina, A., Welch, D., Stadler, T. and Drummond, A.J., 2014. Bayesian inference of sampled ancestor trees for epidemiology and fossil calibration. *PLoS Comput. Biol.* 10, e1003919.
- Gianechini, F.A., Méndez, A.H., Filippi, L.S., Paulina-Carabajal, A., Juárez-Valieri, R.D. and Garrido, A.C., 2020. A new furileusaurian abelisaurid from La Invernada (Upper Cretaceous, Santonian, Bajo de la Carpa Formation), northern Patagonia, Argentina. *J. Vertebr. Paleontol.* 40, e1877151.

- Goloboff, P.A., 2022. From Observations to Optimal Phylogenetic Trees: Phylogenetic Analysis of Morphological Data: Volume 1. CRC Press, Boca Raton, FL, USA.
- Goloboff, P.A. and Morales, M.E., 2023. TNT version 1.6, with a graphical interface for MacOS and Linux, including new routines in parallel. *Cladistics* 39, 144–153.
- Goloboff, P.A. and Szumik, C.A., 2015. Identifying unstable taxa: efficient implementation of triplet-based measures of stability, and comparison with Phyutility and RogueNaRok. *Mol. Phylogenet. Evol.* 88, 93–104.
- Goloboff, P.A., Farris, J.S. and Nixon, K.C., 2008. TNT, a free program for phylogenetic analysis. *Cladistics* 24, 774–786.
- Gómez, R.O., Garberoglio, F.F. and Rougier, G.W., 2019. A new Late Cretaceous snake from Patagonia: phylogeny and trends in body size evolution of madtsoiid snakes. *C. R. Palevol* 18, 771–781.
- González Riga, B.J., Lamanna, M.C., Ortiz David, L.D., Calvo, J.O. and Coria, J.P., 2016. A gigantic new dinosaur from Argentina and the evolution of the sauropod hind foot. *Sci. Rep.* 6, 19165.
- Griffin, C.T., Stocker, M.R., Colleary, C., Stefanic, C.M., Lessner, E.J., Riegler, M., Formos, K., Koeller, K. and Nesbitt, S.J., 2021. Assessing ontogenetic maturity in extinct saurian reptiles. *Biol. Rev.* 96, 470–525.
- Guler, M.V., Borel, C.M., Brinkhuis, H., Navarro, E. and Astini, R., 2014. Brackish to freshwater dinoflagellate cyst assemblages from the La Colonia Formation (Paleocene?), northeastern Patagonia, Argentina. *Ameghiniana* 51, 141–153.
- Harmon, L.J., Losos, J.B., Davies, J., Gillespie, R.G., Gittleman, J.L., Jennings, W.B., Kozak, K.H., McPeck, M.A., Moreno-Roark, F., Near, T.J., Purvis, A., Ricklefs, R.E., Schluter, D., Schulte, J.A., Seehausen, O., Sidlauskas, B.L., Torres-Carvajal, O., Weir, J.T. and Mooers, A.Ø., 2010. Early bursts of body size and shape evolution are rare in comparative data. *Evolution* 64, 2385–2396.
- Harper, T., Parras, A. and Rougier, G.W., 2019. *Reigitherium* (Meridiolestida, Mesungulatoidea) an enigmatic Late Cretaceous mammal from Patagonia, Argentina: Morphology, affinities, and dental evolution. *J. Mamm. Evol.* 26, 447–478.
- Hattori, S., 2016. Evolution of the hallux in non-avian theropod dinosaurs. *J. Vertebr. Paleontol.* 36, e1116995.
- Heath, T.A., Huelsenbeck, J.P. and Stadler, T., 2014. The fossilized birth–death process for coherent calibration of divergence-time estimates. *Proc. Natl Acad. Sci. USA* 111, E2957–E2966.
- Hendrickx, C. and Mateus, O., 2014a. *Torvosaurus gurneyi* n. sp., the largest terrestrial predator from Europe, and a proposed terminology of the maxilla anatomy in nonavian theropods. *PLoS One* 9, e88905.
- Hendrickx, C. and Mateus, O., 2014b. Abelisauridae (Dinosauria: Theropoda) from the Late Jurassic of Portugal and dentition-based phylogeny as a contribution for the identification of isolated theropod teeth. *Zootaxa* 3759, 1–74.
- Hendrickx, C., Tschopp, E. and Ezcurra, M., 2020. Taxonomic identification of isolated theropod teeth: the case of the shed tooth crown associated with *Aerosteon* (Theropoda: Megaraptora) and the dentition of Abelisauridae. *Cretac. Res.* 108, 104312.
- Höhna, S., Landis, M.J., Heath, T.A., Boussau, B., Lartillot, N., Moore, B.R., Huelsenbeck, J.P. and Ronquist, F., 2016. RevBayes: Bayesian phylogenetic inference using graphical models and an interactive model-specification language. *Syst. Biol.* 65, 726–736.
- Höhna, S., Landis, M.J. and Huelsenbeck, J.P., 2021. Parallel power posterior analyses for fast computation of marginal likelihoods in phylogenetics. *PeerJ* 9, e12438.
- Hone, D.W.E. and Mallon, J.C., 2017. Protracted growth impedes the detection of sexual dimorphism in non-avian dinosaurs. *Palaeontology* 60, 535–545.
- Hone, D.W.E., Naish, D. and Cuthill, I.C., 2012. Does mutual sexual selection explain the evolution of head crests in pterosaurs and dinosaurs? *Lethaia* 45, 139–156.
- Horner, J.R. and Goodwin, M.B., 2006. Major cranial changes during *Triceratops* ontogeny. *Proc. R. Soc. B Biol. Sci.* 273, 2757–2761.
- Horner, J.R., de Ricqlès, A. and Padian, K., 1999. Variation in dinosaur skeletochronology indicators: implications for age assessment and physiology. *Paleobiology* 25, 295–304.
- Huelsenbeck, J.P., Ronquist, F., Nielsen, R. and Bollback, J.P., 2001. Bayesian inference of phylogeny and its impact on evolutionary biology. *Science* 294, 2310–2314.
- Huerta-Cepas, J., Serra, F. and Bork, P., 2016. ETE 3: reconstruction, analysis, and visualization of phylogenomic data. *Mol. Biol. Evol.* 33, 1635–1638.
- Hut, P., Alvarez, W., Elder, W.P., Hansen, T., Kauffman, E.G., Keller, G., Shoemaker, E.M. and Weissman, P.R., 1987. Comet showers as a cause of mass extinctions. *Nature* 329, 118–126.
- Ibiricu, L.M., Casal, G.A., Martínez, R.D., Lamanna, M.C., Luna, M. and Salgado, L., 2013. *Katpensaurus goicoecheai*, gen. et sp. nov., a Late Cretaceous rebbachisaurid (Sauropoda, Diplodocoidea) from central Patagonia, Argentina. *J. Vertebr. Paleontol.* 33, 1351–1366.
- Ibiricu, L.M., Baiano, M.A., Martínez, R.D., Alvarez, B.N., Lamanna, M.C. and Casal, G.A., 2021. A detailed osteological description of *Xenotarsosaurus bonapartei* (Theropoda: Abelisauridae): implications for abelisauroid phylogeny. *Cretac. Res.* 124, 104829.
- ICZN [International Commission on Zoological Nomenclature], 1999. International Code of Zoological Nomenclature, 4th edition. International Trust for Zoological Nomenclature, London, UK.
- Iori, F.V., de Araújo-Júnior, H.I., Tavares, S.A.S., da Silva Marinho, T. and Martinelli, A.G., 2021. New theropod dinosaur from the Late Cretaceous of Brazil improves abelisauroid diversity. *J. S. Am. Earth Sci.* 112, 103551.
- Irmis, R.B., Mundil, R., Martz, J.W. and Parker, W.G., 2011. High-resolution U–Pb ages from the Upper Triassic Chinle Formation (New Mexico, USA) support a diachronous rise of dinosaurs. *Earth Planet. Sci. Lett.* 309, 258–267.
- Jeffreys, H., 1961. Theory of Probability, 3rd edition. Oxford University Press, Oxford, UK.
- Kass, R.E. and Raftery, A.E., 1995. Bayes factors. *J. Am. Stat. Assoc.* 90, 773–795.
- Kellner, A.W.A. and Campos, D.D.A., 2002. On a theropod dinosaur (Abelisauria) from the continental Cretaceous of Brazil. *Arq. Mus. Nac.* 60, 163–170.
- Kellner, A.W.A., Campos, D.D.A. and Trotta, M.N., 2005. Description of a titanosaurid caudal series from the Bauru Group, Late Cretaceous of Brazil. *Arq. Mus. Nac.* 63, 529–564.
- Kellner, A.W.A., Azevedo, S.A., Machado, E.B., Carvalho, L.B.D. and Henriques, D.D., 2011. A new dinosaur (Theropoda, Spinosauridae) from the Cretaceous (Cenomanian) Alcântara Formation, Cajual Island, Brazil. *An. Acad. Bras. Cienc.* 83, 99–108.
- Khonsue, W., Chaiananporn, T. and Pomchote, P., 2010. Skeletochronological assessment of age in the Himalayan crocodile newt, *Tylostotriton verrucosus* (Anderson, 1871) from Thailand. *Trop. Nat. Hist.* 10, 181–188.
- Klein, N. and Sander, M., 2008. Ontogenetic stages in the long bone histology of sauropod dinosaurs. *Paleobiology* 34, 247–263.
- Krause, D.W., Sampson, S.D., Carrano, M.T. and O'Connor, P.M., 2007. Overview of the history of discovery, taxonomy, phylogeny, and biogeography of *Majungasaurus crenatissimus* (Theropoda: Abelisauridae) from the Late Cretaceous of Madagascar. *J. Vertebr. Paleontol.* 27(S2), 1–20.
- Lanfear, R., Hua, X. and Warren, D.L., 2016. Estimating the effective sample size of tree topologies from Bayesian phylogenetic analyses. *Genome Biol. Evol.* 8, 2319–2332.
- Langer, M.C., de Oliveira Martins, N., Manzig, P.C., de Souza Ferreira, G., de Almeida Marsola, J.C., Fortes, E., Lima, R., Sant'ana, L.C.F., da Silva Vidal, L., da Silva Lorençato, R.H. and Ezcurra, M.D., 2019. A new desert-dwelling dinosaur

- (Theropoda, Noasaurinae) from the Cretaceous of south Brazil. *Sci. Rep.* 9, 9379.
- Lawver, D.R., Debee, A.M., Clarke, J.A. and Rougier, G.W., 2011. A new enantiornithine bird from the Upper Cretaceous La Colonia Formation of Patagonia, Argentina. *Ann. Carnegie Museum* 80, 35–42.
- Lee, A.H. and O'Connor, P.M., 2013. Bone histology confirms determinate growth and small body size in the noosaurid theropod *Masiakasaurus knopfleri*. *J. Vertebr. Paleontol.* 33, 865–876.
- Lee, A.H. and Werning, S., 2008. Sexual maturity in growing dinosaurs does not fit reptilian growth models. *Proc. Natl Acad. Sci. USA* 105, 582–587.
- Lepage, T., Bryant, D., Philippe, H. and Lartillot, N., 2007. A general comparison of relaxed molecular clock models. *Mol. Biol. Evol.* 24, 2669–2680.
- Lewis, P.O., 2001. A likelihood approach to estimating phylogeny from discrete morphological character data. *Syst. Biol.* 50, 913–925.
- Longrich, N.R., Pereda-Superbiola, X., Jalil, N.-E., Khaldoune, F. and Jourani, E., 2017. An abelisaurid from the latest Cretaceous (late Maastrichtian) of Morocco, North Africa. *Cretac. Res.* 76, 40–52.
- Longrich, N.R., Isasmendi, E., Pereda-Superbiola, X. and Jalil, N.-E., 2023. New fossils of Abelisauridae (Dinosauria: Theropoda) from the upper Maastrichtian of Morocco, North Africa. *Cretac. Res.* 152, 105677.
- Madsen, J.H., Jr., 1976. *Allosaurus fragilis*: a revised osteology. *Utah Geol. Mineral. Surv. Bull.* 109, 1–163.
- Madsen, J.H., Jr. and Welles, S.P., 2000. *Ceratosaurus* (Dinosauria, Theropoda): a revised osteology. *Utah Geol. Surv. Mis. Publ.* 00-2, 1–80.
- Makovicky, P.J., Apesteguía, S. and Agnolín, F.L., 2005. The earliest dromaeosaurid theropod from South America. *Nature* 437, 1007–1011.
- Makovicky, P.J., Apesteguía, S. and Gianechini, F.A., 2012. A new coelurosaurian theropod from the La Buitrera fossil locality of Río Negro, Argentina. *Fieldiana Life Earth Sci.* 2012, 90–98.
- Mallon, J.C., 2017. Recognizing sexual dimorphism in the fossil record: lessons from nonavian dinosaurs. *Paleobiology* 43, 495–507.
- Marshall, C.R., 2017. Five palaeobiological laws needed to understand the evolution of the living biota. *Nat. Ecol. Evol.* 1, 0165.
- Martínez, R., Giménez, O., Rodríguez, J. and Bochaty, G., 1986. *Xenotarsosaurus bonapartei* nov. gen. et sp. (Carnosauria, Abelisauridae), un nuevo Theropoda de la Formación Bajo Barreal, Chubut, Argentina. *IV Congreso Argentino de Paleontología y Biostratigrafía*, 2, 23–31.
- Matzke, N.J. and Irmis, R.B., 2018. Including autapomorphies is important for paleontological tip-dating with clocklike data, but not with non-clock data. *PeerJ* 6, e4553.
- Méndez, A.H., 2012. The caudal vertebral series in abelisaurid dinosaurs. *Acta Palaeontol. Pol.* 59, 99–107.
- Meso, J.G., Hendrickx, C., Baiano, M.A., Canale, J.I., Salgado, L. and Díaz-Martínez, I., 2021. Isolated theropod teeth associated with a sauropod skeleton from the Late Cretaceous Allen Formation of Río Negro, Patagonia, Argentina. *Acta Palaeontol. Pol.* 66, 409–423.
- Novas, F.E., 1996. Alvarezsauridae, Cretaceous basal birds from Patagonia and Mongolia. *Mem. Queensl. Mus.* 39, 675–702.
- Novas, F.E., 1998. *Megaraptor namunhuaiquii*, gen. et sp. nov., a large-clawed, Late Cretaceous theropod from Patagonia. *J. Vertebr. Paleontol.* 18, 4–9.
- Novas, F.E. and Pol, D., 2005. New evidence on deinonychosaurian dinosaurs from the Late Cretaceous of Patagonia. *Nature* 433, 858–861.
- Novas, F.E. and Puerta, P.F., 1997. New evidence concerning avian origins from the Late Cretaceous of Patagonia. *Nature* 387, 390–392.
- Novas, F.E., Cambiaso, A.V. and Ambrosio, A., 2004. A new basal iguanodontian (Dinosauria, Ornithischia) from the Upper Cretaceous of Patagonia. *Ameghiniana* 41, 75–82.
- Novas, F.E., De Valais, S., Vickers-Rich, P. and Rich, T., 2005. A large Cretaceous theropod from Patagonia, Argentina, and the evolution of carcharodontosaurids. *Sci. Nat.* 92, 226–230.
- Novas, F.E., Pol, D., Canale, J.I., Porfiri, J.D. and Calvo, J.O., 2009. A bizarre Cretaceous theropod dinosaur from Patagonia and the evolution of Gondwanan dromaeosaurids. *Proc. R. Soc. B Biol. Sci.* 276, 1101–1107.
- Novas, F.E., Chatterjee, S., Rudra, D.K. and Datta, P.M., 2010. *Rahiolisaurus gujaratensis*, n. gen. n. sp., a new abelisaurid theropod from the Late Cretaceous of India. In: Bandyopadhyay, S. (Ed.), *New Aspects of Mesozoic Biodiversity*. Springer, Berlin Heidelberg, Germany, pp. 45–62.
- Novas, F.E., Agnolín, F.L., Ezcurra, M.D., Porfiri, J. and Canale, J.I., 2013. Evolution of the carnivorous dinosaurs during the Cretaceous: the evidence from Patagonia. *Cretac. Res.* 45, 174–215.
- O'Connor, P.M., 2007. The postcranial axial skeleton of *Majungasaurus crenatissimus* (Theropoda: Abelisauridae) from the Late Cretaceous of Madagascar. *J. Vertebr. Paleontol.* 27 (S2), 127–163.
- O'Gorman, J.P., Salgado, L., Cerda, I.A. and Gasparini, Z., 2013a. First record of gastroliths associated with elasmosaur remains from La Colonia Formation (Campanian–Maastrichtian), Chubut, Patagonia Argentina, with comments on the probable depositional palaeoenvironment of the source of the gastroliths. *Cretac. Res.* 40, 212–217.
- O'Gorman, J.P., Salgado, L., Varela, J. and Parras, A., 2013b. Elasmosaurs (Sauropterygia, Plesiosauria) from the La Colonia Formation (Campanian–Maastrichtian), Argentina. *Alcheringa* 37, 259–267.
- Oriozabala, C., Sterli, J. and de la Fuente, M.S., 2020. New species of the long-necked chelid *Yaminuechelys* from the Upper Cretaceous (Campanian–Maastrichtian) of Chubut, Argentina. *Cretac. Res.* 106, 104197.
- Padian, K. and Horner, J.R., 2011. The evolution of 'bizarre structures': biomechanics, sexual selection, social selection or species recognition? *J. Zool.* 283, 3–17.
- Pascual, R., Goin, F.J., González, P., Ardolino, A. and Puerta, P.F., 2000. A highly derived docodont from the Patagonian Late Cretaceous: evolutionary implications for Gondwanan mammals. *Geodiversitas* 22, 395–414.
- Pérez-Moreno, A., Salgado, L., Carballido, J.L., Otero, A. and Pol, D., 2024. A new titanosaur from the La Colonia Formation (Campanian–Maastrichtian), Chubut Province, Argentina. *Hist. Biol.* 1–20. <https://doi.org/10.1080/08912963.2024.2332997>.
- Pol, D. and Escapa, I.H., 2009. Unstable taxa in cladistic analysis: identification and the assessment of relevant characters. *Cladistics* 25, 515–527.
- Pol, D. and Goloboff, P.A., 2020. The impact of unstable taxa in coelurosaurian phylogeny and resampling support measures for parsimony analyses. *Bull. Am. Mus. Nat. Hist.* 440, 97–115.
- Pol, D. and Norell, M.A., 2001. Comments on the Manhattan Stratigraphic Measure. *Cladistics* 17, 285–289.
- Pol, D. and Rauhut, O.W., 2012. A Middle Jurassic abelisaurid from Patagonia and the early diversification of theropod dinosaurs. *Proc. R. Soc. B Biol. Sci.* 279, 3170–3175.
- Porfiri, J.D., Calvo, J.O. and Santos, D.D., 2011. A new small deinonychosaur (Dinosauria: Theropoda) from the Late Cretaceous of Patagonia, Argentina. *An. Acad. Bras. Cienc.* 83, 109–116.
- Porfiri, J.D., Valieri, R.D.J., Santos, D.D. and Lamanna, M.C., 2018. A new megaraptoran theropod dinosaur from the Upper Cretaceous Bajo de la Carpa Formation of northwestern Patagonia. *Cretac. Res.* 89, 302–319.
- Powell, J.E., 1990. *Epachthosaurus sciutoi*, un dinosaurio saurópodo del Cretácico de Patagonia (Provincia de Chubut, Argentina). *V Congreso Argentino de Paleontología y Biostratigrafía, Tucumán, Actas*, 1, 123–128.

- Powell, J.E., 1992. Osteología de *Saltasaurus loricatus* (Sauropoda-Titanosauridae) del Cretácico Superior del noroeste Argentino. In: Sanz, J.L. and Buscalioni, A.D. (Eds.), *Los Dinosaurios y Su Entorno Biótico: Actas del Segundo Curso de Paleontología en Cuenca*. Instituto Juan de Valdés, Cuenca, Spain, pp. 165–230.
- R Core Team, 2022. R: A Language and Environment for Statistical Computing. R Foundation for Statistical Computing, Vienna, Austria. Available from: <https://www.r-project.org/>.
- Rambaut, A., Drummond, A.J., Xie, D., Baele, G. and Suchard, M.A., 2018. Posterior summarization in Bayesian phylogenetics using Tracer 1.7. *Syst. Biol.* 67, 901–904.
- Rannala, B., Zhu, T. and Yang, Z., 2012. Tail paradox, partial identifiability, and influential priors in Bayesian branch length inference. *Mol. Biol. Evol.* 29, 325–335.
- Rauhut, O.W. and Carrano, M.T., 2016. The theropod dinosaur *Elaphrosaurus bambergi*, from the Late Jurassic of Tendaguru, Tanzania. *Zool. J. Linnean Soc.* 178, 546–610.
- Rauhut, O.W. and Pol, D., 2017. A theropod dinosaur from the Late Jurassic Cañadón Calcáreo Formation of central Patagonia, and the evolution of the theropod tarsus. *Ameghiniana* 54, 539–566.
- Rauhut, O.W., Cladera, G., Vickers-Rich, P. and Rich, T.H., 2003. Dinosaur remains from the Lower Cretaceous of the Chubut group, Argentina. *Cretac. Res.* 24, 487–497.
- Riguetti, F.J., Apesteguía, S. and Pereda-Suberbiola, X., 2022. A new Cretaceous thyreophoran from Patagonia supports a South American lineage of armoured dinosaurs. *Sci. Rep.* 12, 11621.
- Robinson, D.F. and Foulds, L.R., 1981. Comparison of phylogenetic trees. *Math. Biosci.* 53, 131–147.
- Ronquist, F., Klopfstein, S., Vilhelmsen, L., Schulmeister, S., Murray, D.L. and Rasnitsyn, A.P., 2012a. A total-evidence approach to dating with fossils, applied to the early radiation of the Hymenoptera. *Syst. Biol.* 61, 973–999.
- Ronquist, F., Teslenko, M., van der Mark, P., Ayres, D.L., Darling, A., Höhna, S., Larget, B., Liu, L., Suchard, M.A. and Huelsenbeck, J.P., 2012b. MrBayes 3.2: efficient Bayesian phylogenetic inference and model choice across a large model space. *Syst. Biol.* 61, 539–542.
- Rougier, G.W., Forasiepi, A.M., Hill, R.V. and Novacek, M., 2009. New mammalian remains from the Late Cretaceous La Colonia Formation, Patagonia, Argentina. *Acta Palaeontol. Pol.* 54, 195–212.
- Rougier, G.W., Turazzinni, G.F., Cardozo, M.S., Harper, T., Lires, A.I. and Canessa, L.A., 2021. New specimens of *Reigitherium bunodontum* from the Late Cretaceous La Colonia Formation, Patagonia, Argentina and meridiolestidan diversity in South America. *J. Mamm. Evol.* 28, 1051–1081.
- Rozadilla, S., Brissón-Egli, F., Agnolín, F.L., Aranciaga-Rolando, A.M. and Novas, F.E., 2021. A new hadrosaurid (Dinosauria: Ornithischia) from the Late Cretaceous of northern Patagonia and the radiation of South American hadrosaurids. *J. Syst. Palaeontol.* 19, 1207–1235.
- Rubilar-Rogers, D., Vargas, A.O., González Riga, B., Soto-Acuña, S., Alarcón-Muñoz, J., Iriarte-Dáz, J., Arévalo, C. and Gutstein, C.S., 2021. *Arackar licanantay* gen. et sp. nov. a new lithostrotian (Dinosauria, Sauropoda) from the Upper Cretaceous of the Atacama region, northern Chile. *Cretac. Res.* 124, 104802.
- Salgado, L., 1996. *Pellegrinisaurus powelli* nov. gen. et sp. (Sauropoda, Titanosauridae) from the Upper Cretaceous of Lago Pellegrini, northwestern Patagonia, Argentina. *Ameghiniana* 33, 355–365.
- Salgado, L. and Azpilicueta, C., 2000. Un nuevo saltasaurino (Sauropoda, Titanosauridae) de la provincia de Río Negro (Formación Allen, Cretácico Superior), Patagonia, Argentina. *Ameghiniana* 37, 259–264.
- Salgado, L. and de Souza Carvalho, I., 2008. *Uberabatitan ribeiroi*, a new titanosaur from the Marília Formation (Bauru Group, Upper Cretaceous), Minas Gerais, Brazil. *Palaeontology* 51, 881–901.
- Salgado, L. and Gasparini, Z., 2006. Reappraisal of an ankylosaurian dinosaur from the Upper Cretaceous of James Ross Island (Antarctica). *Geodiversitas* 28, 119–135.
- Salgado, L., Garrido, A., Cocca, S.E. and Cocca, J.R., 2004. Lower Cretaceous rebbachisaurid sauropods from Cerro Aguada del León (Lohan Cura Formation), Neuquén Province, northwestern Patagonia, Argentina. *J. Vertebr. Paleontol.* 24, 903–912.
- Sampson, S.D. and Witmer, L.M., 2007. Craniofacial anatomy of *Majungasaurus crenatissimus* (Theropoda: Abelisauridae) from the Late Cretaceous of Madagascar. *J. Vertebr. Paleontol.* 27, 32–104.
- Sampson, S.D., Witmer, L.M., Forster, C.A., Krause, D.W., O'Connor, P.M., Dodson, P. and Ravoavy, F., 1998. Predatory dinosaur remains from Madagascar: implications for the Cretaceous biogeography of Gondwana. *Science* 280, 1048–1051.
- Sander, P.M., 2000. Longbone histology of the Tendaguru sauropods: implications for growth and biology. *Paleobiology* 26, 466–488.
- Sengupta, S., Ezcurra, M.D. and Bandyopadhyay, S., 2017. A new horned and long-necked herbivorous stem-archosaur from the Middle Triassic of India. *Sci. Rep.* 7, 8366.
- Sepkoski, J.J., Jr., 1996. Patterns of Phanerozoic extinction: a perspective from global data bases. In: Walliser, O.H. (Ed.), *Global events and event stratigraphy in the Phanerozoic*. Springer, Heidelberg, Germany, pp. 35–51.
- Sereno, P.C., Martinez, R.N., Wilson, J.A., Varricchio, D.J., Alcobor, O.A. and Larsson, H.C., 2008. Evidence for avian intrathoracic air sacs in a new predatory dinosaur from Argentina. *PLoS One* 3, e3303.
- Simões, T.R., Caldwell, M.W. and Pierce, S.E., 2020. Sphenodontian phylogeny and the impact of model choice in Bayesian morphological clock estimates of divergence times and evolutionary rates. *BMC Biol.* 18, 191.
- Simpson, G.G., 1944. *Tempo and Mode in Evolution*. Columbia University Press, New York, USA.
- Smith, M.R., 2020. TreeDist: distances between phylogenetic trees. R package version 2.5.0. Comprehensive R Archive Network. <https://doi.org/10.5281/zenodo.7157309>.
- Soto-Acuña, S., Vargas, A.O., Kaluza, J., Leppe, M.A., Botelho, J.F., Palma-Liberona, J., Simon-Gutstein, C., Fernández, R.A., Ortiz, H., Milla, V., Aravena, B., Manríquez, L.M.E., Alarcón-Muñoz, J., Pino, J.P., Trevisan, C., Mansilla, H., Hinojosa, L.F., Muñoz-Walther, V. and Rubilar-Rogers, D., 2021. Bizarre tail weaponry in a transitional ankylosaur from subantarctic Chile. *Nature* 600, 259–263.
- Stadler, T., 2010. Sampling-through-time in birth–death trees. *J. Theor. Biol.* 267, 396–404.
- Steel, M.A. and Penny, D., 1993. Distributions of tree comparison metrics—some new results. *Syst. Biol.* 42, 126–141.
- Sterli, J. and de la Fuente, M.S., 2013. New evidence from the Palaeocene of Patagonia (Argentina) on the evolution and palaeo-biogeography of Meiolaniformes (Testudinata, new taxon name). *J. Syst. Palaeontol.* 11, 835–852.
- Sterli, J., Parras, A., Albino, A., Becerra, M.G., Carballido, J.L., Gouiric-Cavalli, S., Muzzopappa, P., Oriozabala, C., Panzeri, K.M., Pérez Moreno, A. and Salgado, L., 2021. Vertebrados continentales de la Formación La Colonia (Campaniano-Maastrichtiano). In *Relatorio XXI Congreso Geológico Argentino Puerto Madryn, Geología y Recursos Naturales de la Provincia del Chubut* (pp. 167–198).
- Swofford, D.L. and Maddison, W.P., 1987. Reconstructing ancestral character states under Wagner parsimony. *Math. Biosci.* 87, 199–229.
- Swofford, D.L., Waddell, P.J., Huelsenbeck, J.P., Foster, P.G., Lewis, P.O. and Rogers, J.S., 2001. Bias in phylogenetic estimation and its relevance to the choice between parsimony and likelihood methods. *Syst. Biol.* 50, 525–539.
- Szöllösi, G.J., Höhna, S., Williams, T.A., Schrempf, D., Daubin, V. and Boussau, B., 2022. Relative time constraints improve molecular dating. *Syst. Biol.* 71, 797–809.

- Tortosa, T., Buffetaut, E., Vialle, N., Dutour, Y., Turini, E. and Cheylan, G., 2014. A new abelisaurid dinosaur from the Late Cretaceous of southern France: palaeobiogeographical implications. *Ann. Paléontol.* 100, 63–86.
- Turelli, M., Cooper, B.S., Richardson, K.M., Ginsberg, P.S., Peckenpaugh, B., Antelope, C.X., Kim, K.J., May, M.R., Abrieux, A., Wilson, D.A., Bronski, M.J., Moore, B.R., Gao, J.-J., Eisen, M.B., Chiu, J.C., Conner, W.R. and Hoffmann, A.A., 2018. Rapid global spread of wRi-like *Wolbachia* across multiple *Drosophila*. *Curr. Biol.* 28, 963–971.
- Vickaryous, M.K. and Hall, B.K., 2008. Development of the dermal skeleton in *Alligator mississippiensis* (Archosauria, Crocodylia) with comments on the homology of osteoderms. *J. Morphol.* 269, 398–422.
- Wang, S., Stiegler, J., Amiot, R., Wang, X., Du, G.-H., Clark, J.M. and Xu, X., 2017. Extreme ontogenetic changes in a ceratosaurian theropod. *Curr. Biol.* 27, 144–148.
- Warren, D.L., Geneva, A.J. and Lanfear, R., 2017. RWTY (R we there yet): an R package for examining convergence of Bayesian phylogenetic analyses. *Mol. Biol. Evol.* 34, 1016–1020.
- Wills, M.A., 1999. Congruence between phylogeny and stratigraphy: randomization tests and the gap excess ratio. *Syst. Biol.* 48, 559–580.
- Wilson, J.A., 1999. A nomenclature for vertebral laminae in sauropods and other saurischian dinosaurs. *J. Vertebr. Paleontol.* 19, 639–653.
- Wilson, J.A., 2012. New vertebral laminae and patterns of serial variation in vertebral laminae of sauropod dinosaurs. *Contrib. Mus. Paleontol.* 32, 91–110.
- Wilson, J.A., Sereno, P.C., Srivastava, S., Bhatt, D.K., Khosla, A. and Shani, A., 2003. A new abelisaurid (Dinosauria, Theropoda) from the Lameta Formation (Cretaceous, Maastrichtian) of India. *Contrib. Mus. Paleontol.* 31, 1–42.
- Wilson, J.A., D’Emic, M.D., Ikejiri, T., Moacdieh, E.M. and Whitlock, J.A., 2011. A nomenclature for vertebral fossae in sauropods and other saurischian dinosaurs. *PLoS One* 6, e17114.
- Woodward, H.N., Horner, J.R. and Farlow, J.O., 2011. Osteohistological evidence for determinate growth in the American Alligator. *J. Herpetol.* 45, 339–342.
- Wright, A.M., Bapst, D.W., Barido-Sottani, J. and Warnock, R.C.M., 2022. Integrating fossil observations into phylogenetics using the fossilized birth–death model. *Annu. Rev. Ecol. Evol. Syst.* 53, 251–273.
- Xie, W., Lewis, P.O., Fan, Y., Kuo, L. and Chen, M.-H., 2011. Improving marginal likelihood estimation for Bayesian phylogenetic model selection. *Syst. Biol.* 60, 150–160.
- Xu, X., Clark, J.M., Mo, J., Choiniere, J., Forster, C.A., Erickson, G.M., Hone, D.W.E., Sullivan, C., Eberth, D.A., Nesbitt, S.J., Zhao, Q., Hernandez, R., Jia, C.-K., Han, F.-L. and Guo, Y., 2009. A Jurassic ceratosaur from China helps clarify avian digital homologies. *Nature* 459, 940–944.
- Yang, Z., 1994. Maximum likelihood phylogenetic estimation from DNA sequences with variable rates over sites: approximate methods. *J. Mol. Evol.* 39, 306–314.
- Zaher, H., Pol, D., Navarro, B.A., Delcourt, R. and Carvalho, A.B., 2020. An Early Cretaceous theropod dinosaur from Brazil sheds light on the cranial evolution of the Abelisauridae. *C. R. Palevol.* 19, 101–115.
- Zhang, C. and Wang, M., 2019. Bayesian tip dating reveals heterogeneous morphological clocks in Mesozoic birds. *R. Soc. Open Sci.* 6, 182062.
- Zhang, C., Rannala, B. and Yang, Z., 2012. Robustness of compound Dirichlet priors for Bayesian inference of branch lengths. *Syst. Biol.* 61, 779–784.

Supporting Information

Additional supporting information may be found online in the Supporting Information section at the end of the article.

Supplementary analyses. Description and results of additional analyses conducted in this study.

Table S1–S6. Supplementary tables.

Figure S1–S53. Supplementary figures.

List of characters. Morphological characters used for the phylogenetic analyses reported in this study.